DECLARATION

I declare that this dissertation is, to the best of my belief and knowledge, my own unassisted work. It is being submitted for the Master of Science in Engineering at the University of the Witwatersrand, Johannesburg.

It has never been submitted in part or whole for a degree in this or any other university.

Ronald Gunda

---------- day of ----------

ABSTRACT

The IsaMill is a recently developed process equipment , first commissioned on a large scale in the early 90s in an effort to help recover values from old mine dumps due to improvements in downstream extraction technologies which could further recover values from ores with fine particles, a technology which was not available before. Also due to depletion of easy-to-extract ores and prevalence of fine grained ores which cannot be economically liberated using the traditional mills like ball mills , there was need to develop a mill that could grind ore to sizes of the order of less than 20 micrometres; hence the evolution of the Isamill. As this is a recent technology, limited research has been done to fully characterise this mill, important to mineral processing economics as it is

Milling efficiency and operation of the plant can be improved if the degree of mixing in the mill can be reduced as that reduces overgrinding or under grinding. A clearer understanding of the mill dynamics will help in coming up with better understanding of mill operations which will assist in developing better mill design and control philosophies.

An M4 pilot IsaMill with overall length 393mm and internal diameter 135mm was used for the test work. Temperature measurements were used to identify the mixing process in the mill. Ten resistance temperature devices (RTDs) were inserted along the length of the mill from feed to discharge. Holes were drilled on the mill shell and insulated copper conductors were glued into the holes. The copper conductors had drilled holes into which the RTDs were inserted to pick the heat transferred by the copper from the mill. A 16-channel data logger was used to convert the measured temperatures into an analogue temperature signal that was displayed on a personal computer.

The following process parameters were varied during the test runs to observe their effect on the resulting temperature profile along the length of the mill from feed to discharge:
(i)Slurry flow rate (2 -3*l/min).*
(ii)Mill tip speed (1 500*rpm*- 2 000*rpm*).
(iii)Media load (1.5-2.5*l).*

A platinum ore, UG2, from Amandebult in South Africa was used for the test work at Anglo American Technical Solutions. A feed with F_{80} = 88µm was used for the tests.
The characteristic temperature profile from the feed point to the mill discharge indicated overall plug flow behaviour with some axial mixing superimposed on the plug flow behaviour. The recirculating media and coarse particles at feed point caused a step change in temperature of the slurry as it enters the mill. The greatest temperature change within the mill was observed to occur at the first compartment of the mill.

A predictive model was developed (through use of mass and energy balances) to correlate the mill variables, tip speed, feed flow rate and media load with the resulting mill temperatures. The mixing coefficients of the mill were calculated. The model can predict the degree of mixing in the mill and could be used to predict the temperature profile along the length of the mill as well, given any combination of the above three mill variables.

It has been shown that use of temperature data acquisition systems has potential to improve control and monitoring of the IsaMill both operationally and from a maintenance point of view as the condition of the mill can be monitored without actually having to stop the mill but by looking at variations from the signature temperature profile.

This MSc.Eng dissertation is dedicated to my family members: Wife , Daughter , Mother , Late Father , Brothers and Sisters.

Acknowledgements

The author of this work would like to express his utmost gratitude to the following, who, in their various capacities facilitated the planning, execution and completion of this work:

The author's supervisor, Professor Michael .H. Moys, for his patience, guidance and encouragement throughout the work from project conception to the final execution and the writing of this dissertation.

The Wits mineral processing research group for their useful inputs during the research work; The following are thanked: Dr Murray Bwalya, Mr Clayton Bhondayi, Dr. Augustine Makokha, Mr Pascal Simba, Mr Mischeck Kime and Dr Francois Katubilwa.The Wits workshop team, Mr Theo Parrisonos and the rest of the team members for their assistance in the mechanical design part of the experimental rig and for their efficiency in executing their work.

Dr Neville Plint , Head of Research , Anglo American Platinum , Mr Deryck de Vaux , Metallurgical Research Manager , Anglo American Technical Solutions, Mr Braam Durant , Technical Specialist , Anglo American Technical Solutions , Mr Bernard Oostendorp , Metallurgist , Anglo American Technical Solutions , The Anglo Technical Solutions workshop , David Mbuli , plant operator, Deborah Mokoena and the rest of the Anglo American Technical Solutions team that assisted during the test works.Mr Clever Banganayi, Group Metallurgist, Aberdare Cables for facilitating with the copper metal required in the design of the experimental set-up.

My family and friends for their understanding during the time the author was not available and busy with the studies.

Funding from National Research Foundation (NRF), Anglo Platinum and the University of the Witwatersrand which enabled successful execution of the work is acknowledged. Opinions expressed and conclusions arrived at , are those of the author, not necessarily attributed to the NRF or any of the funders.

Most important of all, the author would like to thank the Almighty Lord for keeping him alive and strong during the time of the work.

TABLE OF CONTENTS

ITEM **PAGE**

Declaration i

Abstract ii

Dedication iv

Acknowledgements v

Table of Contents vi

CHAPTER 1

INTRODUCTION

1.1 Background And Motivation 1

1.2 Research Objectives 3

1.3 Report Structure 3

CHAPTER 2

LITERATURE REVIEW

2.1 Comminution 6

2.2 IsaMill Technology 7

ITEM **PAGE**

CHAPTER 3

DESIGN, SELECTION AND SPECIFICATION OF TEMPERATURE PROBES

AND VALIDATION OF PROPOSED TEMPERATURE MEASUREMENT TECHNIQUE.

3.1 Introduction **12**

3.2 Principle Of Operation Of The PT100. **12**

3.3 Probe And Test-piece Design Theory **15**

3.4 Laboratory Experimental Procedure **21**

3.5 Summary **29**

CHAPTER 4

PILOT SCALE EXPERIMENTAL METHODS AND TEST EQUIPMENT

SET-UP

4.1 Introduction **30**

4.2 Experimental Procedure **30**

4.3 Resistance Temperature Device (RTD) Calibration **40**

4.4 Mill Start-up Procedure **47**

4.5 Mill Shutdown Procedure **51**

4.6 Summary **51**

ITEM **PAGE**

CHAPTER 5

RESULTS AND ANALYSIS OF RESULTS

5.1 Introduction **52**

5.2 Checking Data Integrity And Reproducibility **52**

5.3 Graphical Representation Of Test Results **56**

5.4 Effects Of Mill Variables On The Temperature Profiles And PSD **66**

5.5 Conclusion **70**

CHAPTER 6

MODEL DEVELOPMENT AND TESTING

6.1 Introduction **71**

6.2 Model Basis And Structure **71**

6.3 Model Development **76**

6.4 Model Validation And Results **88**

6.5 Summary **98**

ITEM **PAGE**

CHAPTER 7

CONCLUSIONS, RECOMMENDATIONS AND REFERENCES

7.1 Conclusions **98**

7.2 Recommendations **99**

7.3 References **101**

LIST OF TABLES

TABLE NUMBER **PAGE**

2.1: Comparison of various grinding technologies: Independent Laboratory Data 10

3.2.1: Comparison of the different types of temperature measuring devices 14

3.3.1: Thermal Conductivities of Common Materials 18

3.4.1: Test equipment list and specifications 28

4.2.1: Project test matrix 37

4.2.2: Experiments carried out at 1.5 litres media load (37.5% v/v). 38

4.2.3: Power draw and pressure inside the grinding chamber at different experimental conditions. 38

4.2.4: Experiments carried out at 2.0 litres media load. 39

4.2.5: Power draw and pressure inside the grinding chamber at different experimental conditions of 2.0 litres media load. 39

4.2.7: Experiments carried out at 2.5 litres media load (62.5% v/v). 39

4.2.8: Power draw and pressure inside the grinding chamber at different experimental conditions of 2.5 litres media load. 40

4.3.1: Measured Probe Temperature vs Standard Temperature. 45

5.1: Temperature measurements for experiments 12, 15 and 18 along mill length. 53

5.2: Summary of the normalised temperatures as well as the descriptive statistical inferences 54

5.5: Normalised data and analysis of normalised data. 55

LIST OF TABLES

TABLE NUMBER	**PAGE**
5.6: The effect of process variables on the temperature profile and particle size distribution(PSD).	70
6.1: Bulk mineralogical composition	82
6.2: Base metal sulphides: relative abundance	83
6.3: Mill data	85
6.4: Summary of the relative positions of the temperature sensors from the feed point to the mill discharge point as well as the heat transfer areas associated with each section of the mill.	86
6.5: Effect of flow rate on back-mixing coefficient, β	94

LIST OF FIGURES:

FIGURE NUMBER			PAGE
1	:	Diagrammatic representation of projected temperature profiles along the length of the mill	2
2.1:		Pictorial representation of the mill's internal structure and grinding mechanism	8
2.2:		Anglo Platinum's South African IsaMill Plant in operation (installed 2008)	9
3.3.1:		Schematic representation of the first trial laboratory run.	15
3.3.2:		Schematic of insulated copper conductor with specifications	16
3.3.3:		Schematic of the first trial laboratory run	20
3.4.1:		Temperature-time response with a 1.4mm copper conductor diameter at a water bath temperature of 82^{o}C.	22
3.4.2:		Modified test-piece with poly urethane lining on the sides.	23
3.4.3:		Illustration of the reviewed experimental set-up with two probes and two multi-meters to measure variation of temperature with time.	24
3.4.4:		Temperature-time response for 1.5mm and 4.5mm conductor diameters at a water bath temperature of 50.5^{o}C.	25
3.4.5:		Temperature-time response curve for a 6.7mm and 7.9mm conductor in a water bath at 44^{o}C.	26

LIST OF FIGURES:

FIGURE NUMBER	PAGE
3.4.6: Schematic representation of the temperature measuring equipment for the laboratory to pilot test work.	27
4.2.1: Ball mill supplying feed slurry to the IsaMill (Courtesy of Anglo American Technical Solutions).	31
4.2.2: Pictorial representation of the experimental set-up of the M4 test work (Courtesy of Anglo American Technical Solutions).	32
4.2.3: Process flow diagram of the test rig	33
4.2.4: Temperature probes inserted along the length of the IsaMill , from the feed of the mill to the discharge of the mill.	34
4.2.5: Pictorial representation of the relative positions of the grinding discs and the temperature sensors from first disc(left) to product separator(right).	35
4.2.6: Schematic representation of the temperature profiling equipment.	36
4.3.1: Plot of temperature vs time for temperature probe no.12 at standard temperature of -0.9^0C.	41
4.3.2: Plot of temperature vs time for temperature probe no.12 at standard temperature of 43.6^0C.	42
4.3.3: Plot of temperature vs time for temperature probe no.12 at standard temperature of 33^0C.	43

LIST OF FIGURES:

FIGURE NUMBER	PAGE
4.3.4: Plot of temperature vs time for temperature probe no.12 at standard temperature of 19.9^0C.	44
4.3.5: Plot of temperature vs time for temperature probe no.12 at standard temperature of 51.9^0C.	45
4.3.6: Calibration curve for RTD no.12.	46
4.3.7: Illustration of the data acquisition system.	47
4.4.1: Temperature time curve for experiment 16.	49
4.4.2:Temperature rise to a high temperature steady state conditions.	50
4.4.4: Temperature-Time response curves showing steady state attainment for experiment 16 for eight RTDs along the mill length.	50
5.1- 5.8 : Temperature-Displacement graphs for different experiments	56-61
5.9: Temperature-Displacement graph: Effect of Tip speed on temperature profiles.	62
5.10: Temperature-Displacement graph : Effect of media load on the temperature profile.	63
5.11: Temperature-displacement graph: Effect of media load on temperature profiles.	64
5.12: Effect of flow rate on the temperature profile.	65
5.13: Effect of flow rate on the temperature profile.	65
5.14: Effect of tip speed on PSD.	66
5.16: Effect of flow rate on the PSD.	67
5.17: Effect of media load on PSD.	68

LIST OF FIGURES:

FIGURE NUMBER	PAGE
6.1: Model flow diagram	72
6.2: Illustration of the mill mass and energy balance	74
6.3: Material and energy balance on cell 1	75
6.4 : Material and energy balance on cell 2	76
6.5 : Matrix representation of mill mass and energy balance equations	79
6.6: Expt. 67 Model Vs Experimental results.	87
6.7: Expt. 69. Model Vs measured results.	88
6.8: Expt. 66 Model vs measured results.	88
6.9: Expt. 73. Model vs measured results.	89
6.10: Expt. 75. Model vs measured results.	90
6.11: Expt. 14. Measured vs model results.	90
6.12: Expt. 15. Measured vs model results.	91
6.13: Effect of slurry flow rate on the back-mixing coefficient β.	92
6.14: Effect of tip speed on the back-mixing coefficient , β.	95
6.15: Effect of media load on tip speed as well as on PSD.	96
6.16: Effect of media load on PSD.	97

APPENDICES:

APPENDIX	TITLE	PAGE
A:	Summary table of all experimental results	103
B:	Charts of model vs measured temperatures along mill length	104
C:	Model matrix inversion programme	124

CHAPTER 1: INTRODUCTION

1.1 Background and Motivation

The IsaMill is an ultrafine grinding mill used widely in the platinum, lead, copper, nickel and zinc industries (http://www.xstratatechnology.com/EN/Publications/IsaMillbrochure.pdf: 2012). This process equipment is globally a recent process development , first commissioned in the early 90s in an effort to help recover values from old mine dumps due to improvements in downstream extraction technologies which could further recover values from ores with fine particles, a technology which was not available before(Burford and Clark, 2012). Also due to depletion of easy-to-extract ores and prevalence of fine grained ores which cannot be economically liberated using the traditional mills like ball mills, there was need to develop a mill that could grind ore to sizes of the order of less than 20 micrometers; hence the evolution of the Isamill. As this is a recent technology, limited research has been done to fully characterise this mill, important to mineral processing economics as it is (Jayasundara et al, 2006).

Milling efficiency and operation of the plant can be improved if the degree of axial mixing in the mill can be reduced as under grinding and overgrinding are minimised. A clearer understanding of the mill dynamics will help in coming up with a better understanding of mill operations which will assist in developing better mill design and control philosophies.

A lot of heat is emitted during the comminution process; more precise information about the milling process can be extracted by inserting temperature probes at appropriate points along the mill length. An energy balance can also assist in dynamic or steady state modeling of the process. This research has used the process engineer's industrial experience and pilot mill test work to address the requirements on the IsaMill. The temperature down the length of the mill is shown as a function of mixing conditions in the mill (see Figure 1).

If the load behaviour in the mill is such that the mill contents are well mixed, then temperatures measured on the mill liner will all be similar along the length of the mill, while if there is no mixing, then, a steady increase in temperature will be expected along the length of the mill from feed to discharge. The temperature profile, therefore, gives us detailed information about the

mixing process occurring in the mill. This is useful for design, control, maintenance and trouble-shooting purposes. For instance, should there be excessive wear on the discs or lining during mill operations, the temperature profile will indicate this without actually having to stop and strip the mill to inspect, hence there will be better operational control and trouble shooting of the mill.

Different mill designs can be tested by observing the resulting temperature profiles in pilot mill operations under different design orientations, thus assisting in making optimised mill design.

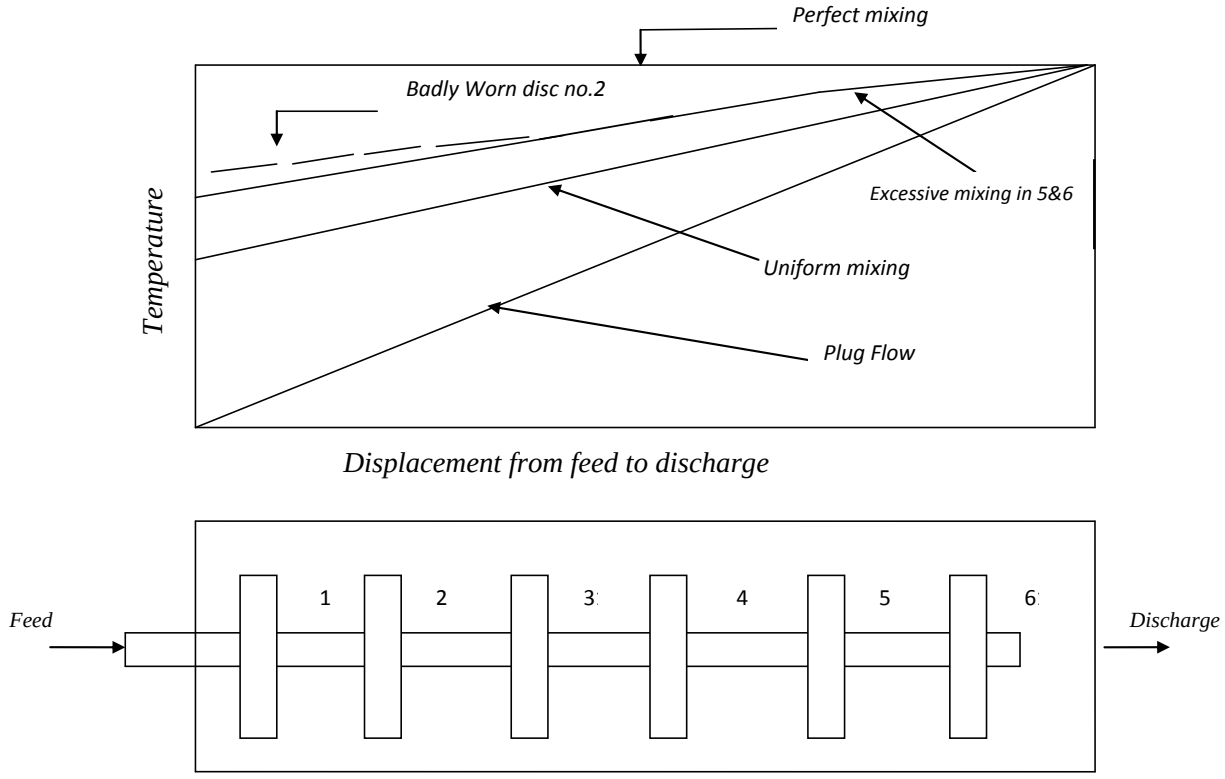

Fig.1 Diagrammatic representation of the projected temperature profiles along the length of the mill

1.2 Research Objectives

The objectives of the project were to:

- Investigate the behaviour of the IsaMill by use of temperature measurements to obtain information regarding the behaviour of the load in the mill (i.e to determine the nature of the flow in the mill whether it is plug flow, perfect mixing or different degrees of axial mixing).
- Develop models for the axial flow of slurry/media in the mill as driven by the impellors and by the classifier at the discharge end of the mill.
- Assess whether temperature measurements and the associated energy balance can be used for mill control.
- Compare results of the developed models with information obtained from the experimental temperature measurements.
- Determine the effect of the different mill operating variables on load behaviour inside the mill.

1.3 Dissertation Structure

This dissertation is divided into seven chapters with the remaining six chapters being divided into the following:

Chapter 2: Literature Review.

This chapter provides an overview of previous work that has been done to characterise slurry movement in IsaMills and other mills in general. It critically reviews existing literature and notes gaps in what has been published to-date regarding research in IsaMill operation, current practice and possibilities of exploring further to bring up new knowledge on possible techniques that can help maximise benefits from use of the IsaMill.

Areas of key importance in the review include possibilities of operationalizing current research outputs regarding the IsaMill, a maintenance view point to operation of the IsaMill, an overview of the fine to ultrafine milling process as well as exploring the possibilities of investigating this

mill in a typical continuous operating mode to enable recommendations which are industrially applicable.

Chapter 3: Design, Selection And Specification Of Temperature Probes And Validation Of The Proposed Temperature Measurement Technique.

This chapter describes the preliminary laboratory experimental work done to validate the proposed method of measuring temperature from the mill. It details the principle of operation of equipment to be used in the test work, the design and specification of the temperature sensors and the equipment set-up. Characteristic response behaviour of the proposed data acquisition technique is illustrated. It also gives typical response results and motivation to scale up to pilot scale operations at Anglo American Research.

Chapter 4: Pilot Scale Experimental Methods And Test Equipment Set-Up.

Details of the actual experimental work that was done on pilot facilities are given in this report. The experimental set-up is shown and the precautions taken in running the actual pilot work are detailed. A description of the mill commissioning process is given as well as details of the temperature sensor calibration process.

Chapter 5: Results And Analysis of Results.

This chapter contains sample extracts of the results that were obtained from the experimental test work, statistical checks that were done to check data reproducibility and integrity as well as general trends and profiles qualitatively obtained from the experimental results.

Qualitative relationships between mill operating variables and temperature profiles and product particle size distributions are shown together with a results summary sheet containing all details of Test No., Feed rate , Media load , Mill tip speed , Temperatures along the mill length, Average mill temperature differences for the different conditions from feed to discharge, The power draw , Feed and product size distribution.

Chapter 6: Model Development and Testing.

This chapter deals with the principles upon which the model to determine the axial load behaviour in the mill is based. It illustrates the tanks-in-series model (Makokha and Moys, 2011) which was adopted in this work as well as the fundamental mass and energy balances across the mill. The model constants were calculated and referenced. Parameter estimation on the model was done and model results were compared with experimental results from chapter 5 to see the extent to which the two correlate.

Chapter 7: Conclusions, Recommendations and References

In this chapter, the major outcomes of the research are outlined. Limitations encountered during the test work are highlighted and recommendations for future approaches to performing the work are made. Recommendations are also made on opportunities for further scope regarding the work in terms of scale-up possibilities.

CHAPTER 2: LITERATURE REVIEW

2.1 Comminution:

Comminution is a size reduction process commonly used in the mineral processing industry. It is an energy intensive and inefficient process. Typically about 40% of the direct operating costs of mineral processing plants is attributed to size reduction (Wills, 1992). The objective of size reduction is to liberate mineral values locked in ores and the more exposed the values are the more efficient the downstream processes like flotation and leaching become. Various technologies have been applied to effect the process of milling which takes place through three main mechanisms of attrition, abrasion and impact to effect particle breakage.

Attrition is the most commonly used method of size reduction. This breakage mechanism involves particles colliding together and with media in a mill to effect size reduction. Typically Ball mills, IsaMills and Rod mills use attrition breakage mechanism though they are primarily impact mills. Size reduction in the IsaMill is mainly by attrition due to high energy intensity of the mill. This mechanism is especially useful in large scale operations involving hard process materials. Attrition milling involves mainly wet milling.

Impact milling is applied in dry milling operations and involves particles impacting a harder surface thus causing particle breakage. Jet mills are typical impact mills and this particle breakage mechanism is typically applied when reducing size of brittle materials.

Size reduction by abrasion involves particles rubbing media surfaces under force, thus effecting particle breakage. This breakage mechanism is normally applied to particles with rough surfaces as this increases the coefficient of friction between the ore particles and the media particles assisting in effecting particle breakage.

Size reduction is divided into three main categories, that is primary, secondary and fine/ultrafine. The proposed research focuses on ultra-fine milling using the IsaMill. Ultrafine milling is mainly required in ores that are fine grained and have low grade. These ores can be ground to sizes of the order of less than twenty micro metres. Ultra-fine milling will assist in liberating the locked values under such circumstances.

2.2 IsaMill Technology

The IsaMill is a high speed stirred media mill used for main stream inert grinding (MIG) as well as for ultra-fine grinding (UFG). It has been primarily designed for ultrafine grinding and recent developments have resulted in it evolving as suitable mainstream inert grinding equipment. The IsaMill ranges in size from an M4 (4 litre pilot mill) to an M50 000 (46 000litre industrial mill) (http://www.xstratatechnology.com/EN/Publications/IsaMillbrochure.pdf:23 Dec 2012.).

It consists of a horizontal stationary chamber equipped with a grinding agitator which is a series of grinding discs mounted on a cantilever shaft to support the discs. The chamber is then filled with inert grinding media which rotates due to the motion of the rotating agitator. The particle size reduction mechanism is by attrition (Kwade and Schwedes, 2007).

This high speed stirred media mill is mainly used for high efficiency size reduction of concentrates and mineral ores (Yu et al, 2006). The high speed of rotation characterised by tip speeds of 21m/s creates an energy intensive environment that allows the mill to achieve the required high levels of size reduction. Feed slurry is pumped through a positive displacement pump from the feed end of the mill and it passes through a series of rotating discs inside the mill. These sections of the mill created by the discs have media within them. The media collides with the ore particles under the energy intense conditions resulting in particle breakage.

The IsaMill is able to operate with small media sizes of the order of 1.5mm to 6.0mm. The small media size increases the chances of media-particle collision making the IsaMill an energy efficient mill because of more media surface area than exists in other conventional grinding equipment.

The horizontal nature of the IsaMill and the slurry feed mechanism allow it to operate as a multi-stage size reduction unit. At the discharge end of the mill is a patented product separator that internally classifies the media and oversize particles before discharging the product. The product separator acts as a pump and classifier. The classified material oversize material is thrown back into the mill by the pumping action of the product separator. In so doing, the mill operates in open circuit with no need for external classification thus reducing the foot print of the equipment.

IsaMill technology is a recent technology developed by Xstrata Technology (then Mount Isa Mines) in collaboration with technology partners Netzsch and operator Anglo American Platinum. Full scale commercialization of IsaMill technology started in the early 90's and to-date little has been published to fully understand, characterise and optimise the mill. Research is still on-going to fully characterise the behaviour of this mill. The figure below is a pictorial representation of the IsaMill. The IsaMill is charecterised by high milling efficiency due to negligible short circuiting of the grinding zone as a result of having multiple grinding chambers in series. The IsaMill has outperformed other traditional mills as it operates with inert media, in open circuit, has a sharp product cut size minimizing generation of super fines due to low residence time and grinding mechanism which is mainly by attrition.

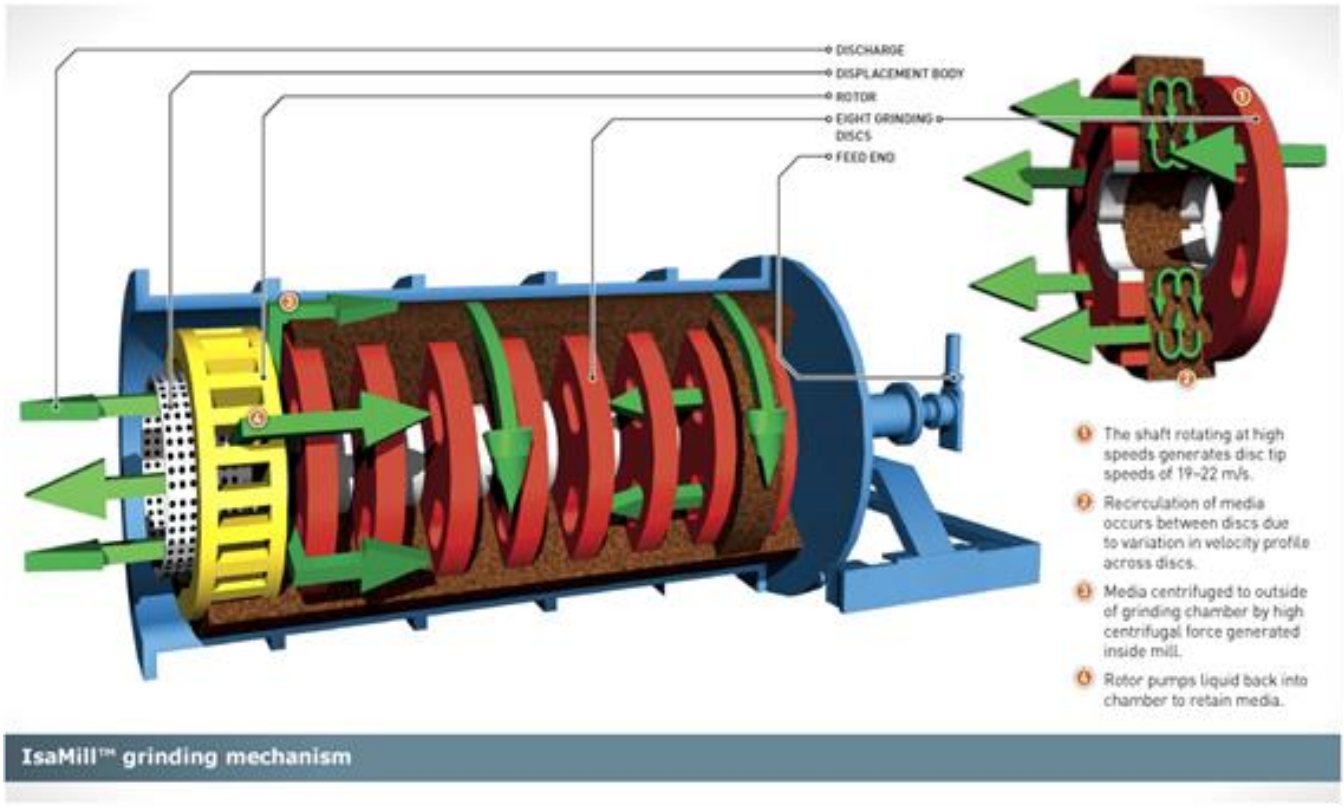

Figure 2.1: Pictorial representation of the mill's internal structure and grinding mechanism (Not to scale) (www.isamill.com : 18/04/2012).

Figure2.2 below is an installation of IsaMills at an Anglo Platinum concentrator in South Africa.

Figure 2.2: Anglo Platinum's South African IsaMill Plant in operation (installed 2008).

(Source:www.isamill.com: 21/04/2012).

There has been research on load behavior in mills in general but little has been done specifically on the IsaMill. The residence time distribution approach has been used to investigate load behavior in overflow discharge ball mills (Makokha, 2011), and the same approach could be used to investigate load behavior in an IsaMill.

Moys and van Nierop, 2001 have investigated the axial mixing of slurry in an autogeneous grinding mill and have applied the axial mixing model of Levenspiel (1999).

Most of the work that has been published (Jankovic ,2002) has been on projects to investigate the applications of the IsaMill to different mill requirements and comparing its performance with traditional tumbling mills like ball mills(Gao and Weller, 1993 ; Pease,et al, 2004) and little attention has been paid to the actual load behaviour inside the mill and to analytically

characterise its operation; hence the motivation for this research as it has already been established that the IsaMill has outperformed the traditional mills in secondary and tertiary milling operations (Gao and Weller, 1993). Table 2.1 below illustrates results compiled by Gao and Weller, 1993 in this respect.

Table 2.1: Comparison of various grinding technologies: Independent Laboratory Data (Gao and Weller, 1993).

Feature	Isa Mill	Tower Mills	Vertical Pin mills
Grinding Intensity (KW/L)	0.54	0.005	0.15-0.18
Residence Time to 15 µm (min)	0.6	154	7-9
Power Usage to 15µm (KWh/t)	17.4	59.6	37.5-39.0
Media Material	Various	Steel	Steel
Media size (mm)	0.8-1.6	9-12	6-8

The discrete element method (DEM) has been applied to simulation of the flow of grinding media in an IsaMill (Jayasundara, et al, 2006) as one of the pioneer researches into the investigation of the load behavior specifically as applied to this particular type of high intensity stirred media mill.

The cell model was proposed as describing the load behavior in an IsaMill with multiple stirrers (Kwade and Schwedes, 2007). In this model, in a stirred media mill with discs, the number of mixing cells is given by the number of discs plus one.

Farber, et al, 2011 have investigated the effect of media size and mechanical properties on milling efficiency and media consumption. Van der Westhuizen, et al, 2011 investigated IsaMill media movement using positron emission particle tracking using a batch IsaMill.

By looking at the geometry (stationary shell) of the IsaMill as well as its mode of operation and from a practical operability and scale up point of view, the author of this dissertation has proposed the use of temperature as a useful process control and monitoring measure. Use of temperature to investigate load behavior in the IsaMill was viewed as a method to investigate as

well as to help monitor operation of the mill under scaled-up conditions. Unlike sample collection for instance, involved in the use of the residence time distribution method, the use of temperature measurements was perceived to involve a once-off installation of equipment for monitoring temperatures. This information would be analysed by a programme that would display the mixing pattern and also help identify any malfunctioning in the mill, thus allowing corrective action to be taken. Most of the optimisation research on the IsaMill has been on batch mills or model mills. The proposal to use temperature to diagnose mixing in the IsaMill involves running the mill in a continuous operating mode as it operates continuously in industrial applications. Figure 1 illustrates the envisaged temperature profiles for different possible mill conditions as well as the different sections within the mill as has been described earlier.

CHAPTER 3.

DESIGN, SELECTION AND SPECIFICATION OF TEMPERATURE PROBES AND VALIDATION OF PROPOSED TEMPERATURE MEASUREMENT TECHNIQUE.

3.1 Introduction

This chapter details the preliminary laboratory work that was done to validate the proposed test method. It specifies the laboratory equipment used as well as the basis for motivation to scale up the work as described below. The optimum temperature measuring device was decided upon and its temperature-time response was characterised.

Table 3.2.1 below shows different types of thermometers and their characteristic features. The following factors were taken into account in determining the optimum temperature measuring device for the application:

(i) Cost.

(ii) Linearity of response between temperature and sensor property being measured.

(iii)Ease of handling under pilot plant operating conditions and suitability for pilot conditions.

(iv)Local availability of technical back-up and adaptability to data logging equipment.

(v)Repeatability.

From the information on the different types of temperature measuring devices and their characteristic features in Table 3.1.1 below, a resistance temperature device (RTD) was chosen to be the appropriate device for the application especially considering the diameter required for the application of at most 4mm for the temperature probe, a linear scale offered directly from the RTD together with high levels of repeatability. The PT100 resistance thermometer has been chosen for this application.

3.2 Principle of operation of the PT100.

This is a platinum resistance thermometer whose resistance at zero degrees Celsius is 100 Ohms. The PT100 resistance scale is linear in the temperature ranges of -200˚C to 640˚C. Thus, the variation of the temperature with resistance is linear in this range. The expected temperature

range for the proposed test work is 0^0C to 60^0C. The relationship between temperature (T) and resistance(R) is represented by the following equation which encompasses the fundamental interval of 0.385 Ohms increase in resistance from 100 Ohms in the platinum bead per every degree Celsius temperature rise:

$$T = \frac{R - 100}{0.385} \quad \text{----------} \quad 3.2.1$$

Table 3.2.1 Comparison of the different types of temperature measuring devices(www.peaksensors.co.uk/technicalinfo.html: 05 /07/2012)

PEAK SENSORS LTD temperature measurement & control	Thermocouple	Resistance Thermometer (RTD)	Thermistor	Infrared
Stability (Drift)	Reasonable for limited lifetime	Good	Good	Good
Repeatability	Reasonable	Good	Good	Good
Hysteresis	Excellent	Good	Good	Good
Vibration	Very Resistant	Less Resistant	Good	Tolerant
Measurement Area	Single Point	Whole RT Element	bead (Small)	Varies
Diameter	Small Sizes (to 0.25mm)	Larger (3.0mm min)	(0.5mm min)	Varies
Linearity	Not Linear	Reasonably Linear	Not Linear	Reasonably Linear
Reference Junction	Required	Not Required	Not Required	Not Required
Lead Wire Resistance	No Problem	Must be Considered	No Problem	Not Required
Contact Required	Yes	Yes	Yes	No
Response	Fast	Slower	Medium	Fast

3.3 Probe and Test-piece Design theory

Before a decision could be made on whether or not to use the RTD on a pilot scale, its temperature-time curve was plotted to have an indication of how fast the response of the measurement of the temperature of the mill is. The temperature-time response behaviour was investigated as below:

A laboratory scale approximate simulation of the actual mill shell was created as shown below.

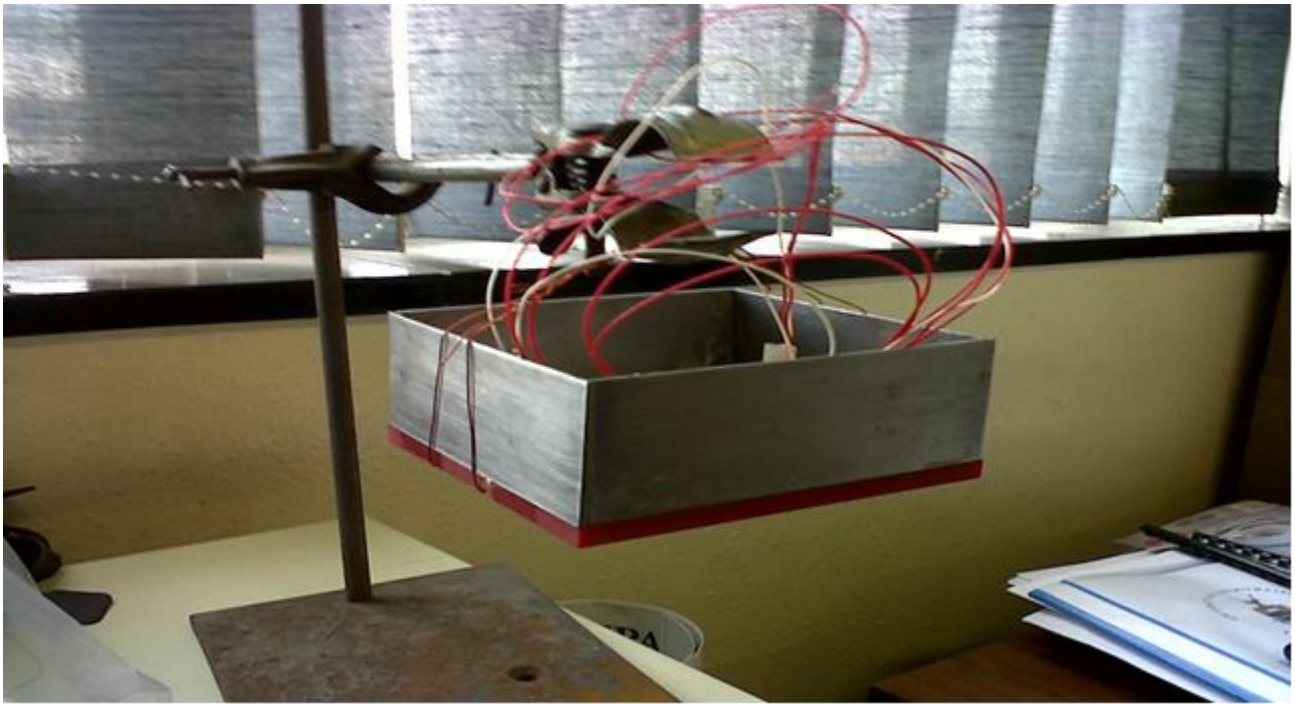

Figure 3.3.1: Simulated IsaMill shell

This was in the form of a hollow cube that was made up of steel sides and a steel base which was covered with polyurethane, low conductivity plastic material to prevent contact between the probe and steel and a polyurethane liner. The polyurethane liner of the stainless steel base simulates the rubber lining of the mill. The stainless steel base simulates the stainless steel shell of the mill. The thicknesses of the stainless steel base and the polyurethane lining were equal to the thickness of the actual pilot mill shell and liner respectively. The objective was to make the test piece as close as possible a simulation of the actual mill shell.

By the nature of the mill set-up, it would not be easy to directly pick the mill temperature when the mill is running, thus there was need to devise a way of measuring the mill temperature along the mill length without having to have the temperature sensor in direct contact with the mill slurry as wear during operation would cause damage to the probes.

An indirect method of measuring temperature would be to drill through the shell and then insert a high thermal conductivity and structurally strong material through the opening to plug the opening. The perimeter of the thermal conductor would be thermally insulated to prevent heat transfer from the conductor to the walls of the shell and thus minimise heat loss from the conductor and increase the fraction of heat transferred that will actually reach the temperature sensor.

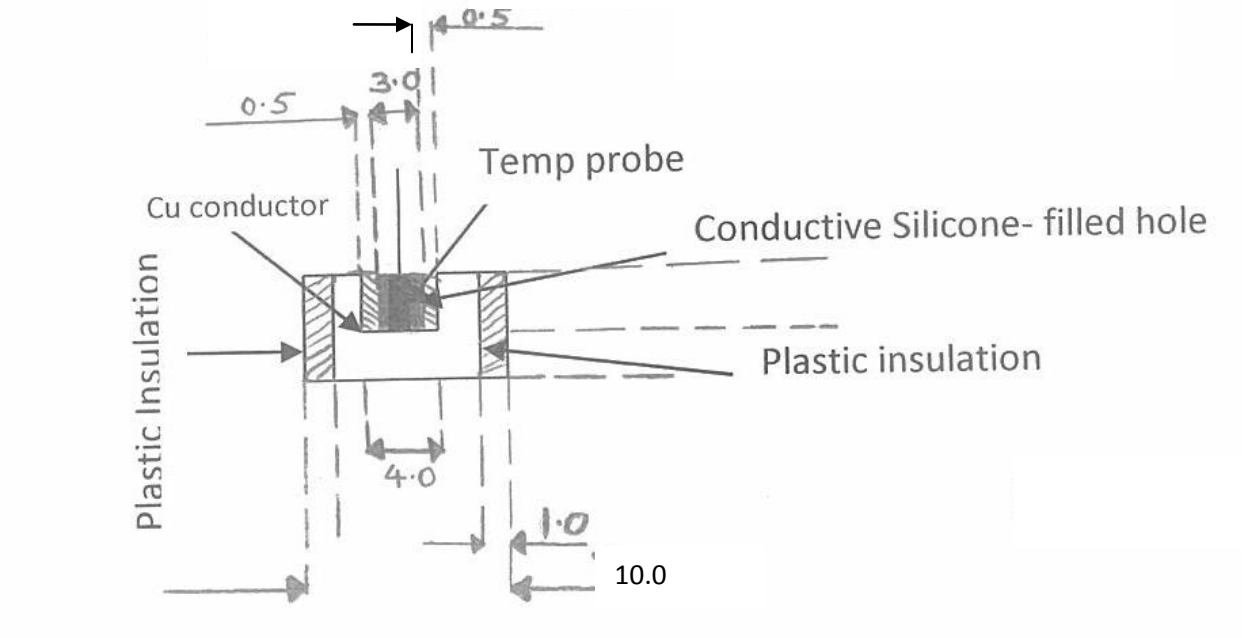

Figure 3.3.2 Schematic of insulated copper conductor with specifications.

The temperature sensor would be externally contacted with the high thermal conductivity conductor. Heat would then be transferred from the slurry inside the mill via the high thermal conductivity conductor to the temperature sensor. Care would be taken to ensure that the hole is sealed by use of glue to prevent slurry leaking through the drilled hole. The glue would have to withstand the temperatures of the operating environment. The temperature of the sensor would be expected to rise until it reached a steady value where there would be practically insignificant changes in temperature with time.

Fourier's law of heat transfer was used in the design,selection and specification process:

$$Q = \frac{kA\Delta T}{\Delta x} \quad \text{----------} \quad 3.2.1$$

Where Q is the rate of heat transfer (W), k is the thermal conductivity (W/m.K) of the conductor, ΔT is the expected temperature change as a result of the heat transfer (K or ^{o}C), A is the heat transfer area (m^2) and Δx is the thickness of the material through which heat is being transferred (m).

From the above equation, at a constant temperature change required for a process, the greatest amount of heat would be transferred through a conductor if a conductor has high thermal conductivity, large cross-sectional area and low thickness. From a feasibility and practical point of view, engineering judgment was used to limit the drilled holes through the shell to a maximum of 10 mm to safeguard the shell and also ensure tight sealing of the conductor plug against leakage from the shell as well as for the shell to be able to withstand pressure inside the mill during actual mill operations.

The conductor material had to be specified as a relatively cheap and locally available material without compromising on the above specifications.

Table 3.3.1 below is a list of different materials and their thermal conductivities.

Table 3.3.1 Thermal Conductivities of Common Materials

Material	Thermal conductivity (cal/sec)/(cm^2 C/cm)	Thermal conductivity (W/m K)*
Diamond	...	1000
Silver	1.01	406.0
Copper	0.99	385.0
Gold	...	314
Brass	...	109.0
Aluminum	0.50	205.0
Iron	0.163	79.5
Steel	...	50.2
Lead	0.083	34.7
Mercury	...	8.3
Ice	0.005	1.6
Glass,ordinary	0.0025	0.8
Concrete	0.002	0.8
Water at 20° C	0.0014	0.6
Asbestos	0.0004	0.08
Snow (dry)	0.00026	...
Fiberglass	0.00015	0.04
Brick,insulating	...	0.15
Brick, red	...	0.6
Cork board	0.00011	0.04
Wool felt	0.0001	0.04
Rock wool	...	0.04
Polystyrene (styrofoam)	...	0.033
Polyurethane(foam)	...	0.02
Wood	0.0001	0.12-0.04
Air at 0° C	0.000057	0.024
Helium (20°C)	...	0.138

Hydrogen(20°C)	...	0.172
Nitrogen(20°C)	...	0.0234
Oxygen(20°C)	...	0.0238
Silica aerogel	...	0.003

*Most from Young, Hugh D., University Physics, 7th Ed. Table 15-5. Values for diamond and silica aerogel from CRC Handbook of Chemistry and Physics. http://hyperphysics.phy-astr.gsu.edu/hbase/tables/thrcn.html: 07/07/2012

From the table above, copper was conveniently chosen as the thermally conducting material (k=385 W/m.K) that could be used for the heat transfer process. To prevent radial losses of heat from the copper, this copper would have its perimeter insulated with plastic. Plastic is a low-conducting material with thermal conductivities of the order of 0.03W/m.K (www.engineeringtoolbox.com/thermal-conductivity-d_429.html : 17/07/2012) vs 385W/m.K for copper .Thus minimum heat would be lost from the copper to the surroundings as copper is more than 12 800 times as conducting as the plastic lining. This would help improve the temperature response of the RTD as minimum heat would be lost elsewhere. The method adopted was semi-empirical as it involved several trials of copper diameters at laboratory scale to find the optimum experimental set-up that would give the highest possible rate of heat transfer together with a robust configuration for scale up to industrial pilot plant conditions.

To simulate the mill temperature environment, the set-up was inserted in a hot water bath and the variation between temperature and time was noted until the probe temperature recorded was almost constant. Two probes, each tied to a copper conductor of different diameters would be used for this and the probe with the faster response to the temperature would be chosen for the application.

The schematic diagram below represents the set-up of the first trial to find the optimum conductor diameter that would help pick the temperature being actually measured.

Figure 3.3.3 below is a schematic representation of the test piece.

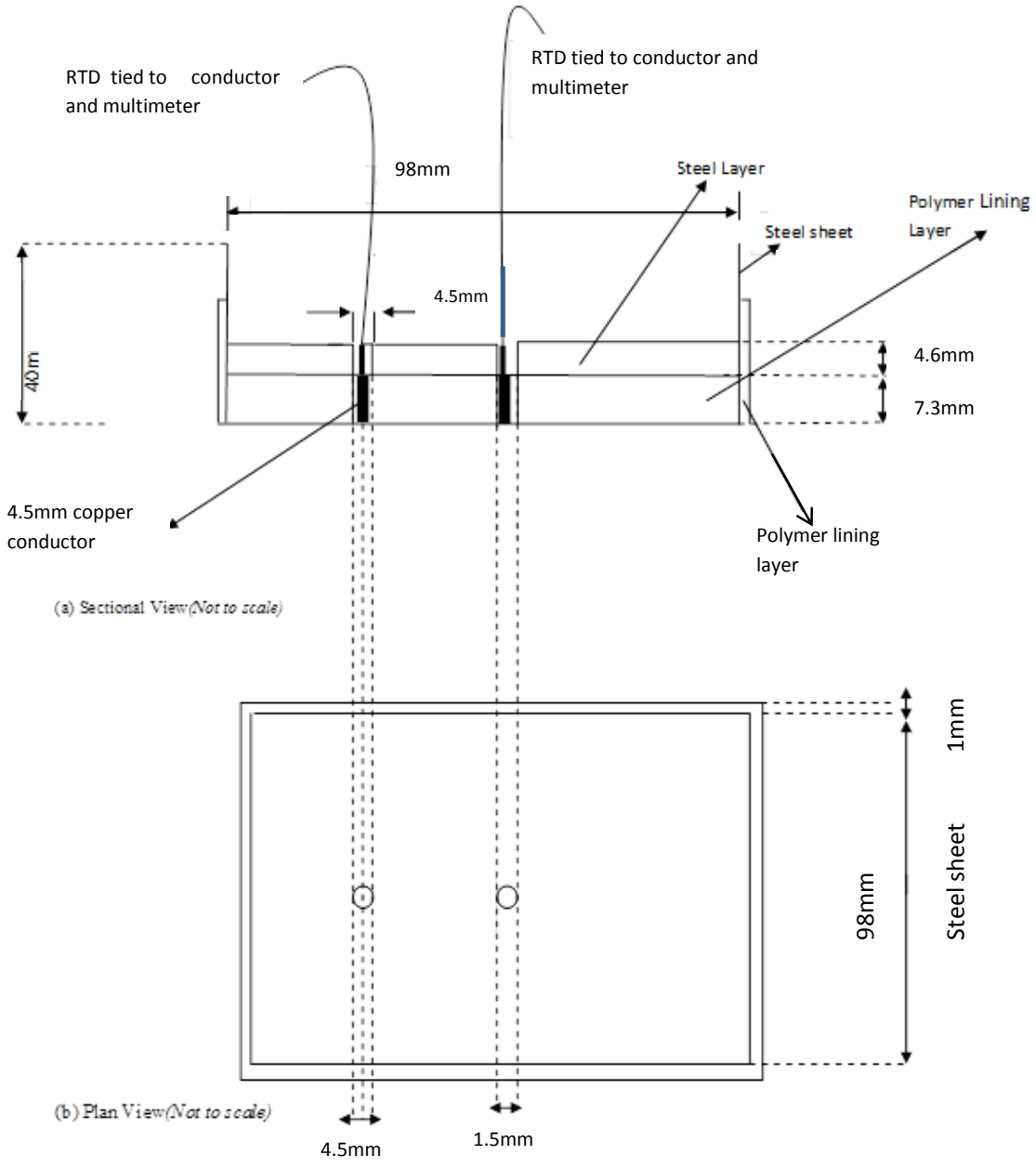

Fig 3.3.3: Schematic representation of the first trial laboratory run.

The test piece of figure 3.3.1 is shown schematically by figure 3.3.3 above which shows a clamped and suspended hollow cube, together with fly-lead RTD cables with the RTD tied to a thin copper conductor that is running through the hole from the stainless steel and polyurethane linings.

3.4 Laboratory Experimental Procedure

Before a commitment could be made to actually purchase a real time data acquisition system with multi-channel adapters to measure the temperatures , a multi-meter was used as it would measure the RTD resistance and the resistance would then be used to compute the temperature from the equation 3.2.1.

Temperature was then plotted against time when the above set-up was immersed in a warm water bath to the level of the polyurethane lining. The water bath was under constant stirring using a magnetic stirrer with low power supply to ensure that the water bath temperatures approximated constant levels. The material of construction of the water bath was low conductivity glass to minimise energy loses. The figure below illustrates the temperature-time relationship from the first laboratory test run.

Characterisation of the response of the probe:

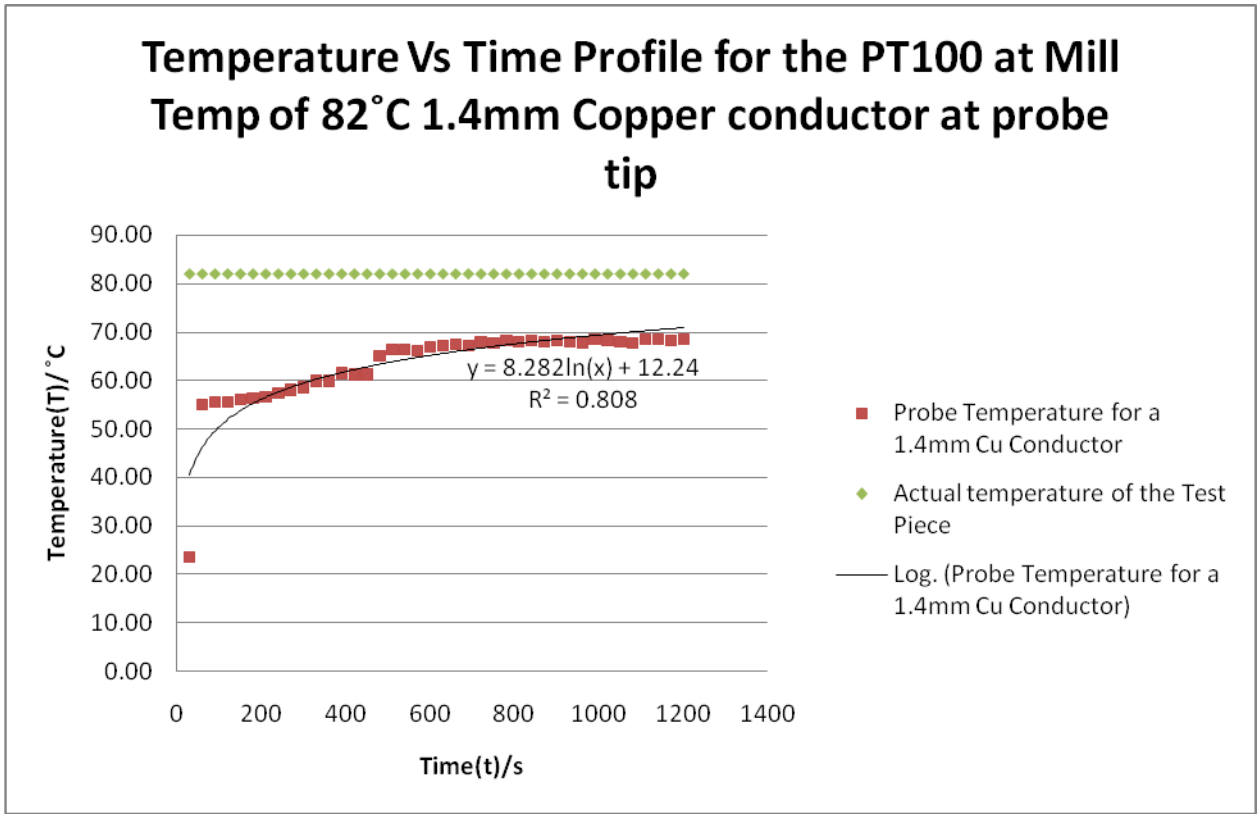

Fig 3.4.1: Temperature-time response with a 1.4mm copper conductor diameter at water bath temperature of 82^{o}C.

Using a 1.4mm copper conductor diameter and a water bath temperature of 82^{o}C, it took more than 20 minutes for the indirectly measured temperature to approximate the water bath temperature. This copper diameter was considered inadequate for the expected applications and the set-up had to be reviewed.

Modifications to the first experimental run:

Following the above observations, changes were made to the experimental set-up. These changes included:

(a)Reducing the water bath temperature so as to approximate the projected M4 IsaMill discharge temperature. This was done by reducing the bath temperature from 82˚C to 50.5˚C (Though the actual projected slurry discharge temperature of the M4 is in the region of 40˚C).

(b)Lining the test-piece steel walls with the liner material (polyurethane) and immersing a significant part of the test-piece into the water bath to improve the contact between the lining and the water bath.

(c)Increasing the number of test probes from one to two and also changing the copper conductor diameter from 1.4mm to 1.5mm and 4.5mm respectively in the two probes in the new experimental set-up. Two multi-meters had to be used for this modification as it was too early to commit to a multi-channel data logger. The effect of increasing the copper diameter was to be observed by measuring the temperature-time responses of the two different diameters simultaneously in one water bath.

The above changes are illustrated pictorially as below in figures 3.4.2 and 3.4.3

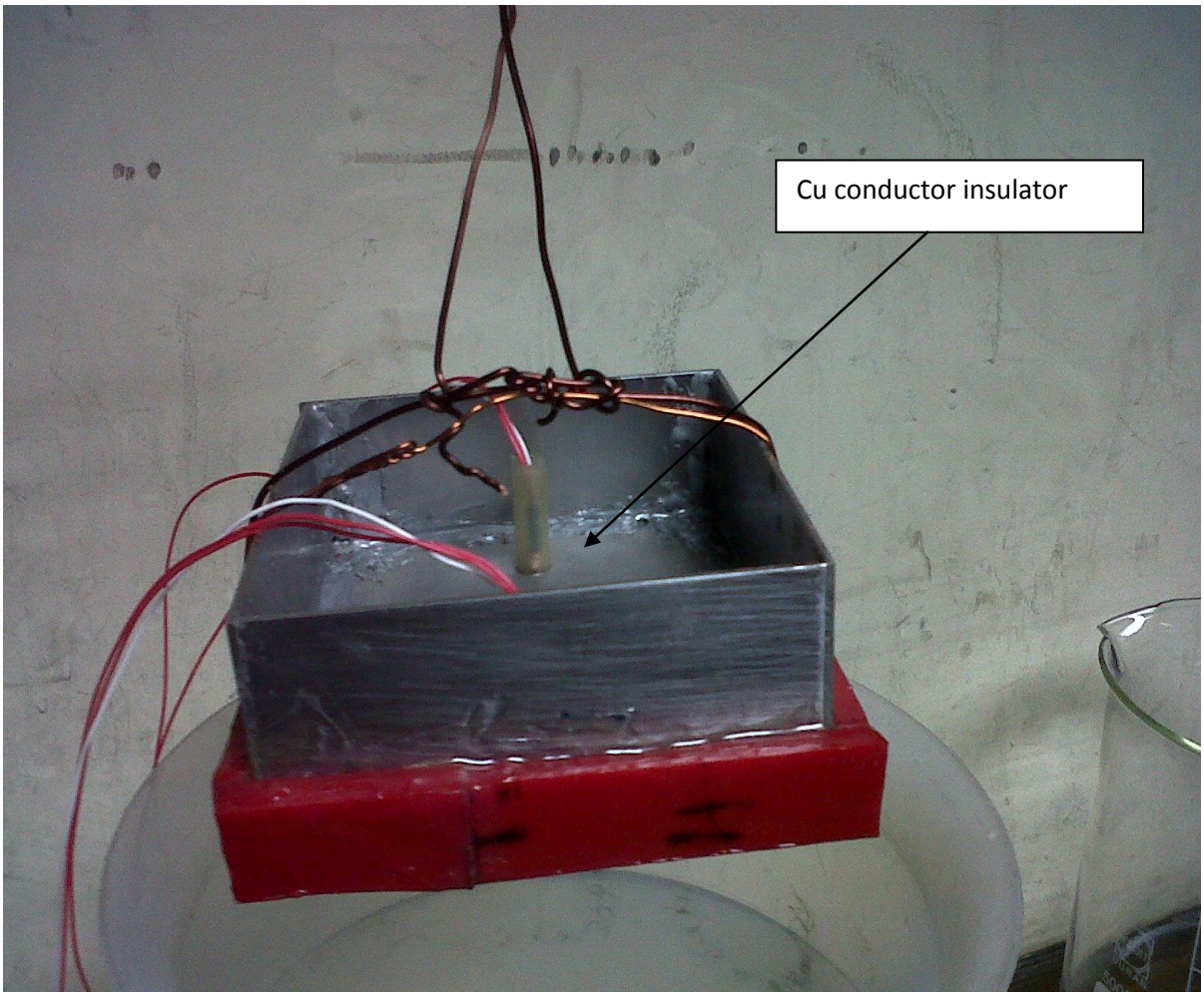

Fig 3.4.2: Modified test-piece with poly urethane lining on the sides.

Fig 3.4.2 above shows the test-piece with base fully lined with polyurethane and steel walls partially lined with the polymer. The number of probes has been increased to two, one with a 1.5mm copper conductor and the other with a 4.5mm copper conductor.

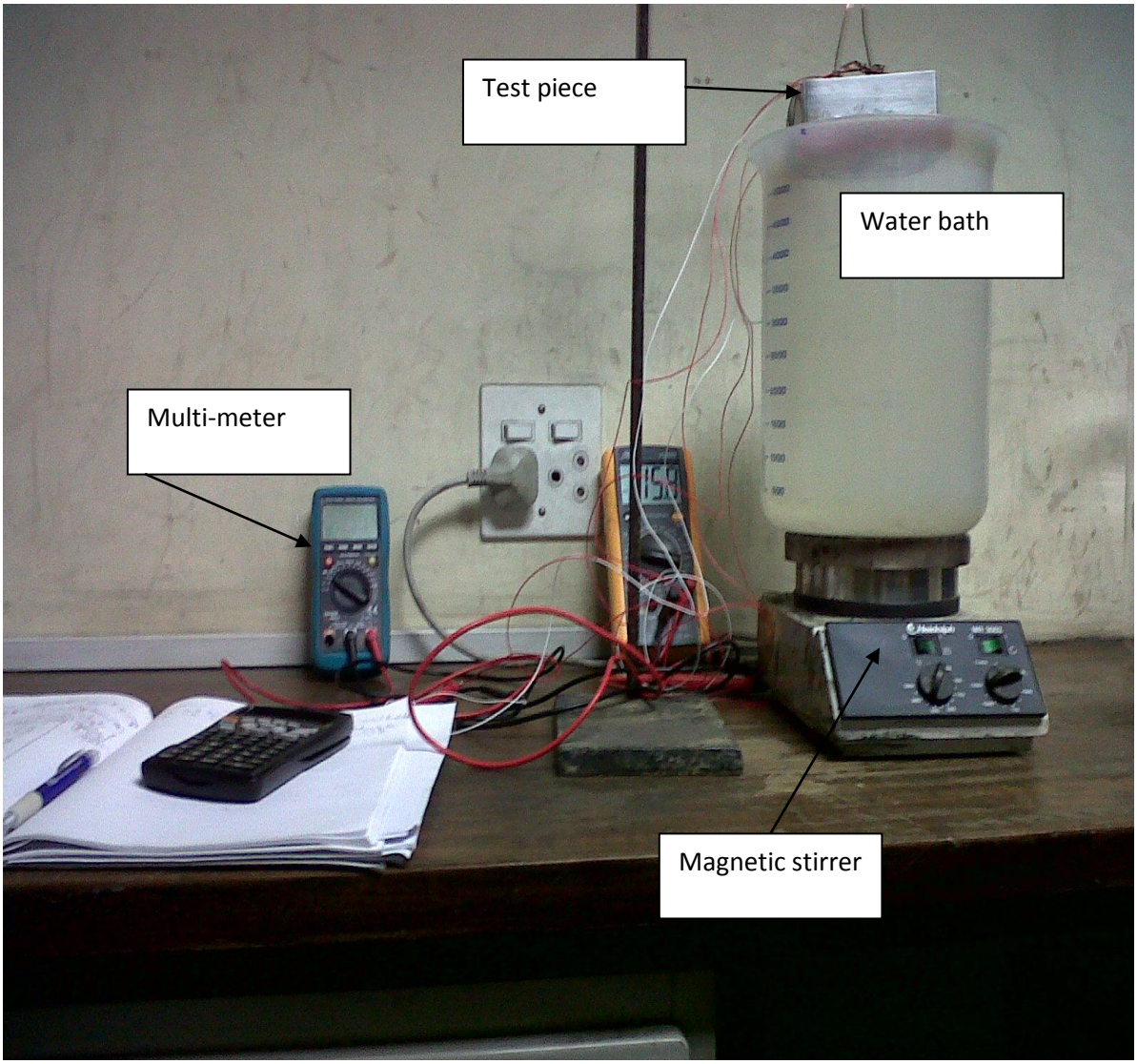

Fig 3.4.3: Illustration of the reviewed experimental set-up with two probes and two multi-meters to measure variation of temperature with time.

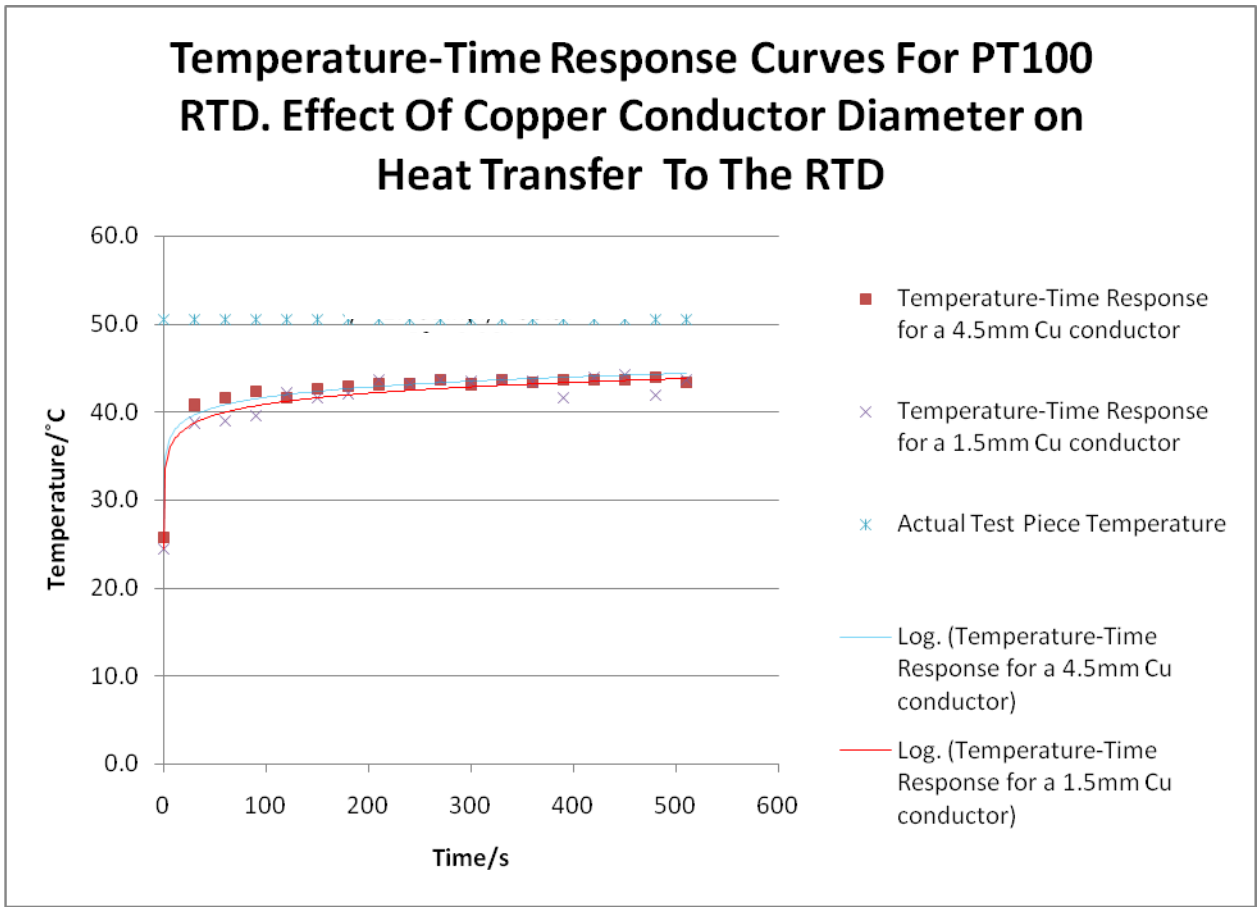

Fig 3.4.4: Temperature-time response for 1.5mm and 4.5mm conductor diameters at a water bath temperature of 50.5^{o}C.

The following observations were made:

Thermal conductivity increases with increase in copper conductor diameter. The maximum attainable temperature using the copper conductor to transfer heat to the probe was 43.9˚C using the 4.5mm copper conductor and 43.6˚C using the 1.5mm conductor. There was a general increase in maximum attainable temperature with increasing copper conductor diameter which is in line with the Fourier's heat transfer equation. The minimum temperature difference between the probe temperature and the actual water bath temperature is (50.5˚C-43.9˚C) = 6.6˚C.From the graph and from a practical point of view, it was necessary to use the maximum available and practically useable conductor diameter .

The figure below illustrates further tests that were done at different water bath temperatures and higher copper conductor diameters.

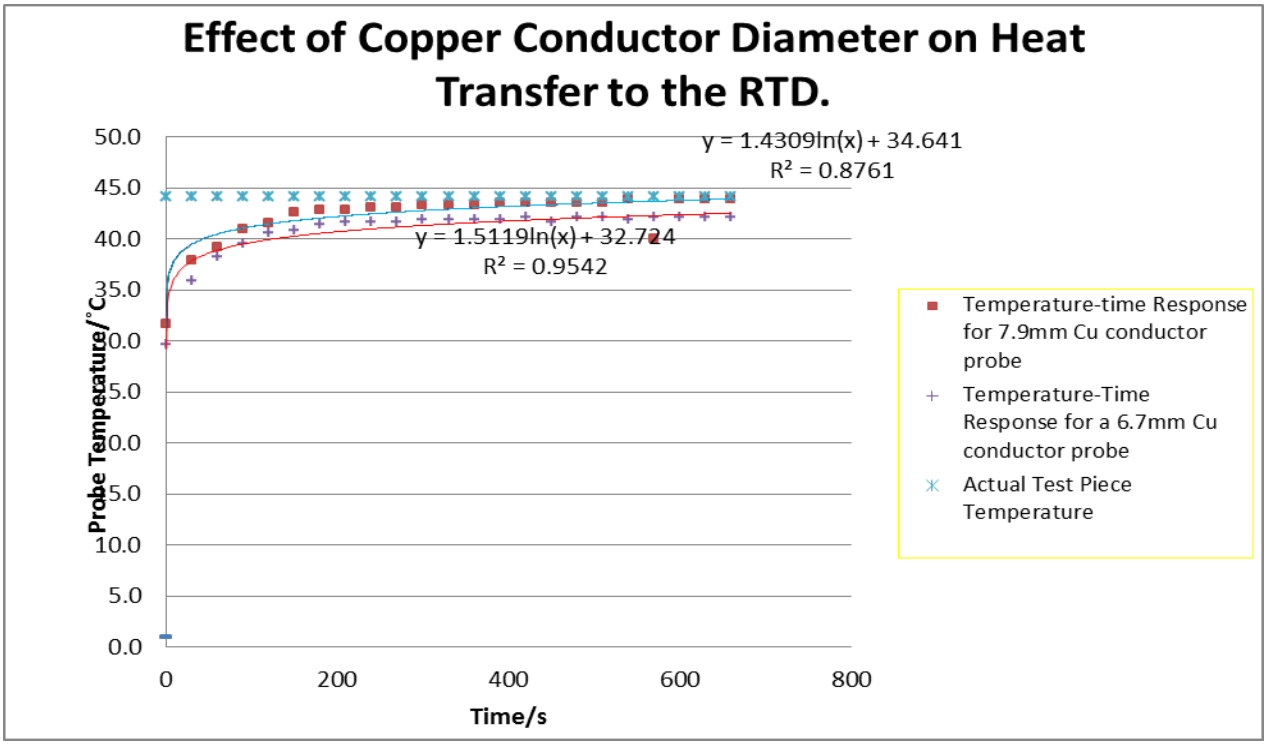

Fig 3.4.5: Temperature-time response curve for a 6.7mm and 7.9mm conductor at a 44^{o}C.

The copper conductor diameters used for the trials were 6.7mm and 7.9mm as shown above. These were then used to simulate the temperature-time response of the mill using a mill temperature of 44^{o}C. The water bath temperature was maintained constant throughout the experimental run.

The schematic diagram below, figure 3.4.6 illustrates how the 7.9mm copper conductor was integrated into the test piece to minimise energy loss during the heat transfer process.

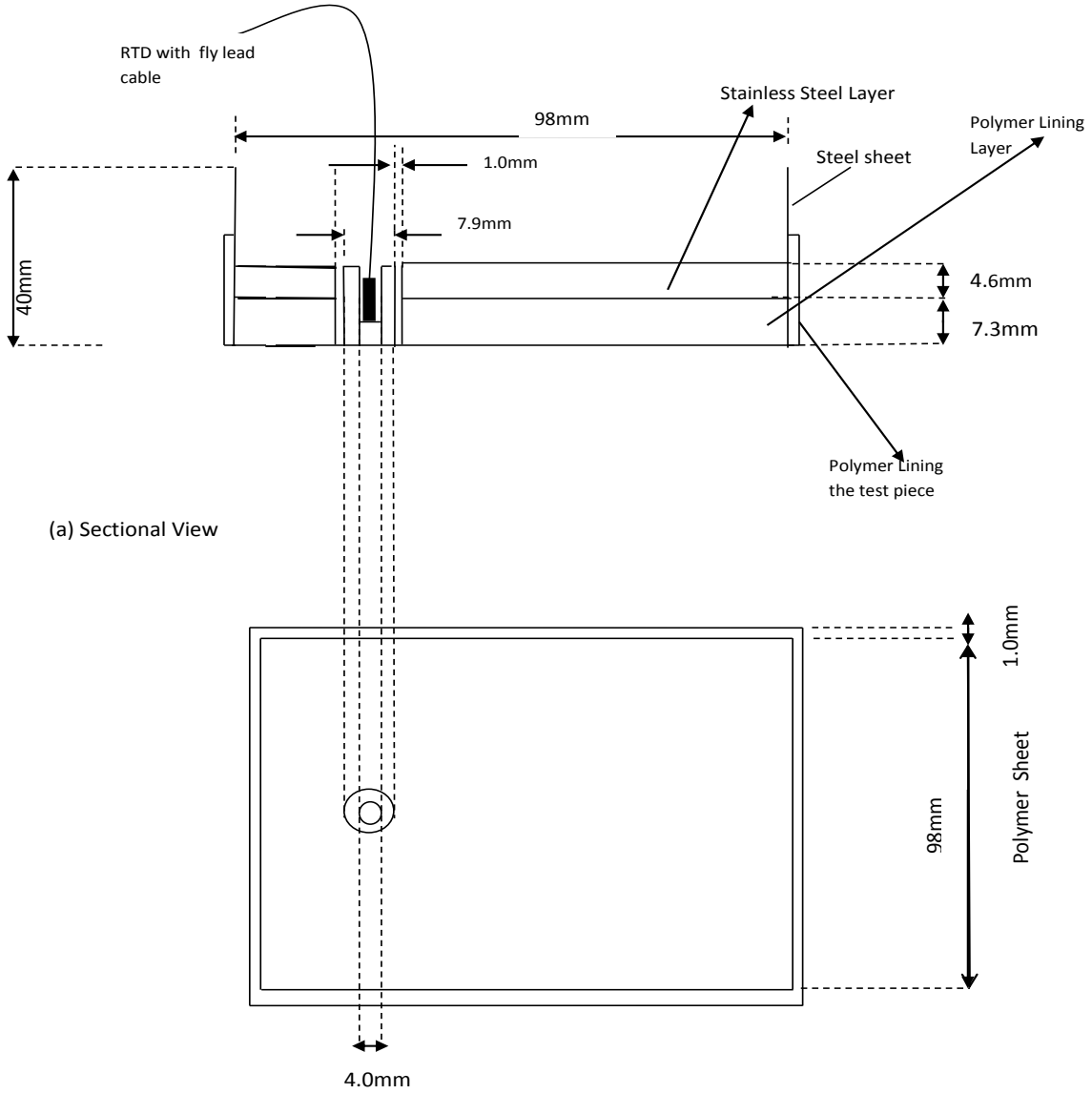

*All drawings not to scale.

Fig 3.4.6: Schematic representation of the temperature measuring equipment for the laboratory to pilot test work.

The table below is a summary of the design and specifications for the requirements of the experimental test works from lab to pilot scale adaptation.

Table 3.4.1: Test equipment list and specifications.

Equipment/ Item	**Specifications**
PT100 RTD	3mmX2mm bead with a 2m long, 2 wire fly lead cable.
Annealed copper conductor(99.99% cathode grade)	7.9mm diameter and 11.5mm height with a drilled hole in the middle. The hole is 4mm in diameter and 7.5mm in depth.
Conductive Silicone paste	This paste is thermally conductive and is inserted into the conductor hole so that when the RTD is inserted into the hole the paste will fill the air spaces to ensure maximum amount of heat is transferred from the copper to the RTD by eliminating air which is a poor conductor.
Flexible plastic tubing	This is approximately 7.9mm internal diameter and 1mm thick and 11.5mm in height. The copper conductor will be inserted into this tubing to minimise heat losses from the copper as plastic is a poor thermal conductor.
Multi-meter	To measure RTD resistance and thus subsequently temperature for the lab tests.
Micro Data acquisition data logger	Multi-channel data logger for pilot test works to measure temperatures of several RTDs simultaneously.
PC with visual display	For pilot test works. PC system also to have spreadsheet software and data storage capacity.

3.5 Summary

The resistance temperature measuring device (RTD) was found to be the appropriate temperature measuring device for the proposed work. The RTD's response was found to be good enough for steady state measurements.

CHAPTER 4

PILOT SCALE EXPERIMENTAL METHODS AND TEST EQUIPMENT SET-UP

4.1 Introduction

This chapter details the scale up process from laboratory tests to pilot facility level. It gives information on the mill commissioning and sensor calibration as well as precautions taken during the scale up process.

4.2 Experimental Procedure

The pilot plant test work was carried out at Anglo American Technical Solutions' Crown mines campus in Johannesburg. A 4 Litre (M4) Isamill was used for this research. A constant solids fraction slurry of 35% solids (w/w) was pumped to the IsaMill feed tank. This slurry was produced by a ball mill that produced 75% of -70μm in a wet milling operation. The PSD of the ball mill was maintained by taking samples every hour and monitoring to ensure that the ball mill discharge was within the above PSD range. Figure 4.1.1 below is a pictorial representation of the ball mill and the associated accessories. The pilot plant mill variables that were measured were as follows:

- The power of the mill,
- The temperatures of the feed and discharge slurries,
- The temperatures at the mill liner would be measured at the axial centre of each space between the impellors
- Ambient temperature.
- Feed rates,
- Media load.
- Feed and product particle size distribution and

Samples of feed and discharge slurry would be taken at each steady state.

The design of the temperature probes on the mill shell would minimise the effect of ambient temperature on the measurements. The speed of response of the probes on the mill shell would limit the ability of the method to sense rapid dynamic changes to a certain extent. However, this

would not be a challenge in the test works as steady state measurements would be taken. It was estimated that the temperature rise would be about 13^{o}C under typical conditions, so a temperature measurement accuracy of 0.01 ^{o}C was expected to provide accurate information.
The experimental work was done in stages with the details shown diagrammatically below.

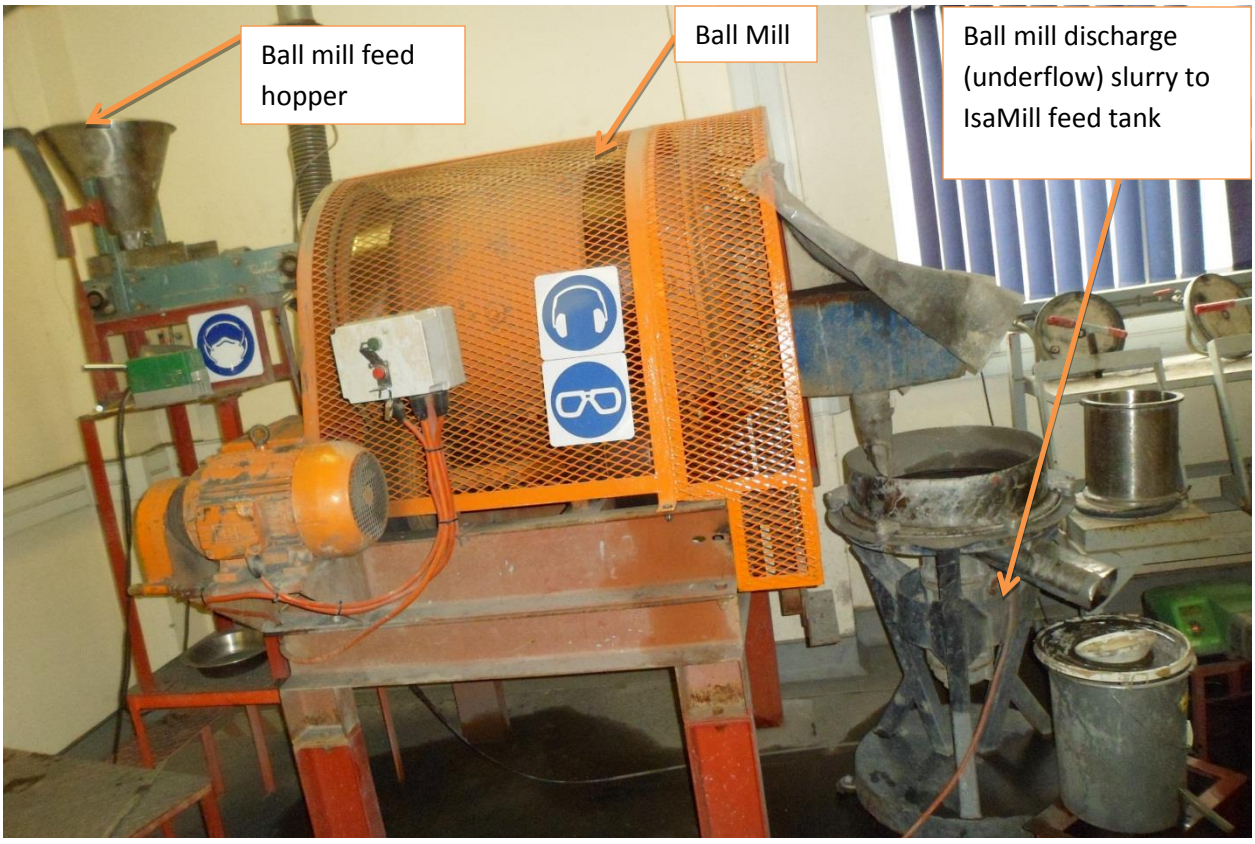

Fig 4.2.1: Ball mill supplying feed slurry to the IsaMill (Courtesy of Anglo American Technical Solutions).

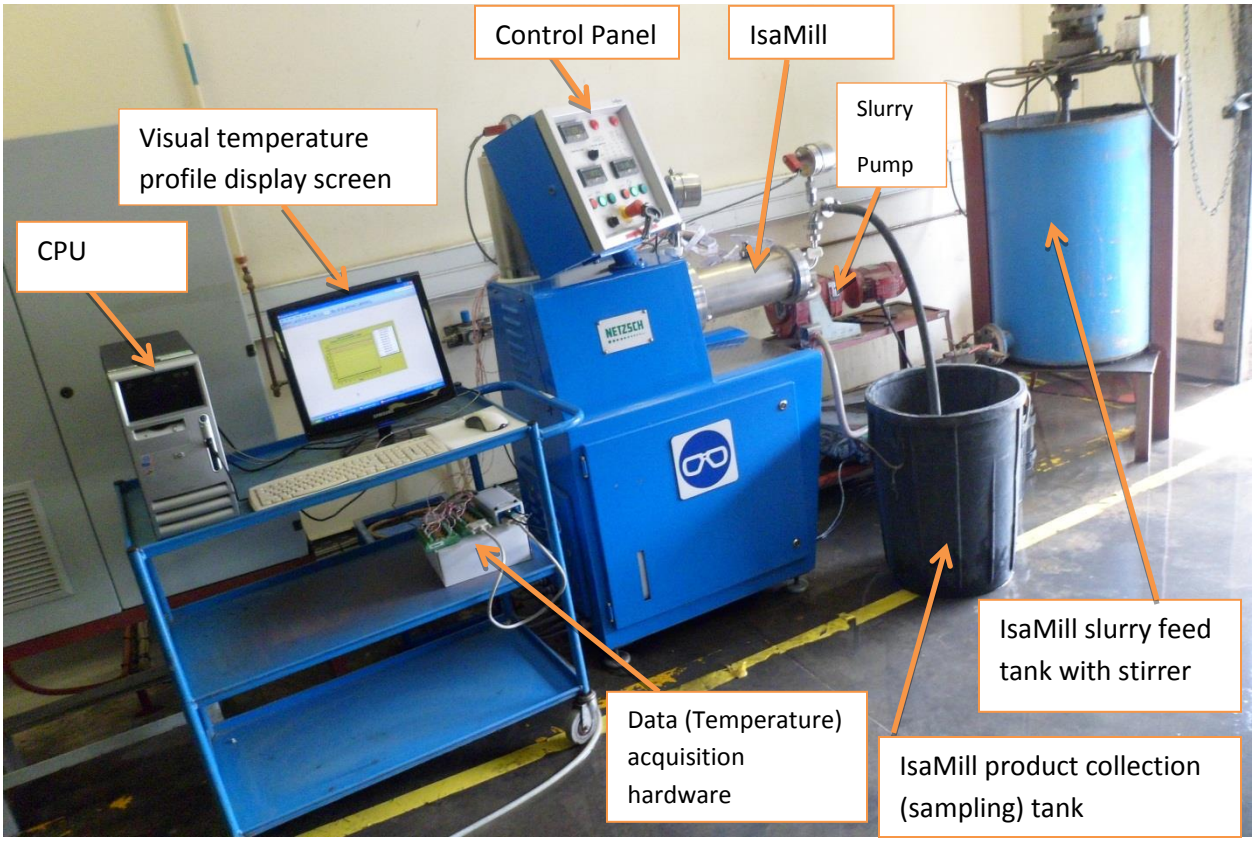

Fig 4.2.2: Pictorial representation of the experimental set-up of the M4 test work (Courtesy of Anglo American Technical Solutions).

The IsaMill slurry feed tank had two stirrers to keep it under constant agitation to ensure thorough mixing within the tank. Feed to the mill was supplied from the tank by use of a positive displacement pump (peristaltic pump) to prevent back flow of the slurry. The slurry pump had a variable speed drive to enable investigation of the effect of the variation of the impellor tip speed on mill axial temperature. During the experimental test work, the following temperatures were measured; room temperature, slurry feed temperature, slurry discharge temperature, temperatures along the sections of the mill length as illustrated by Figure 4.2.3 below.

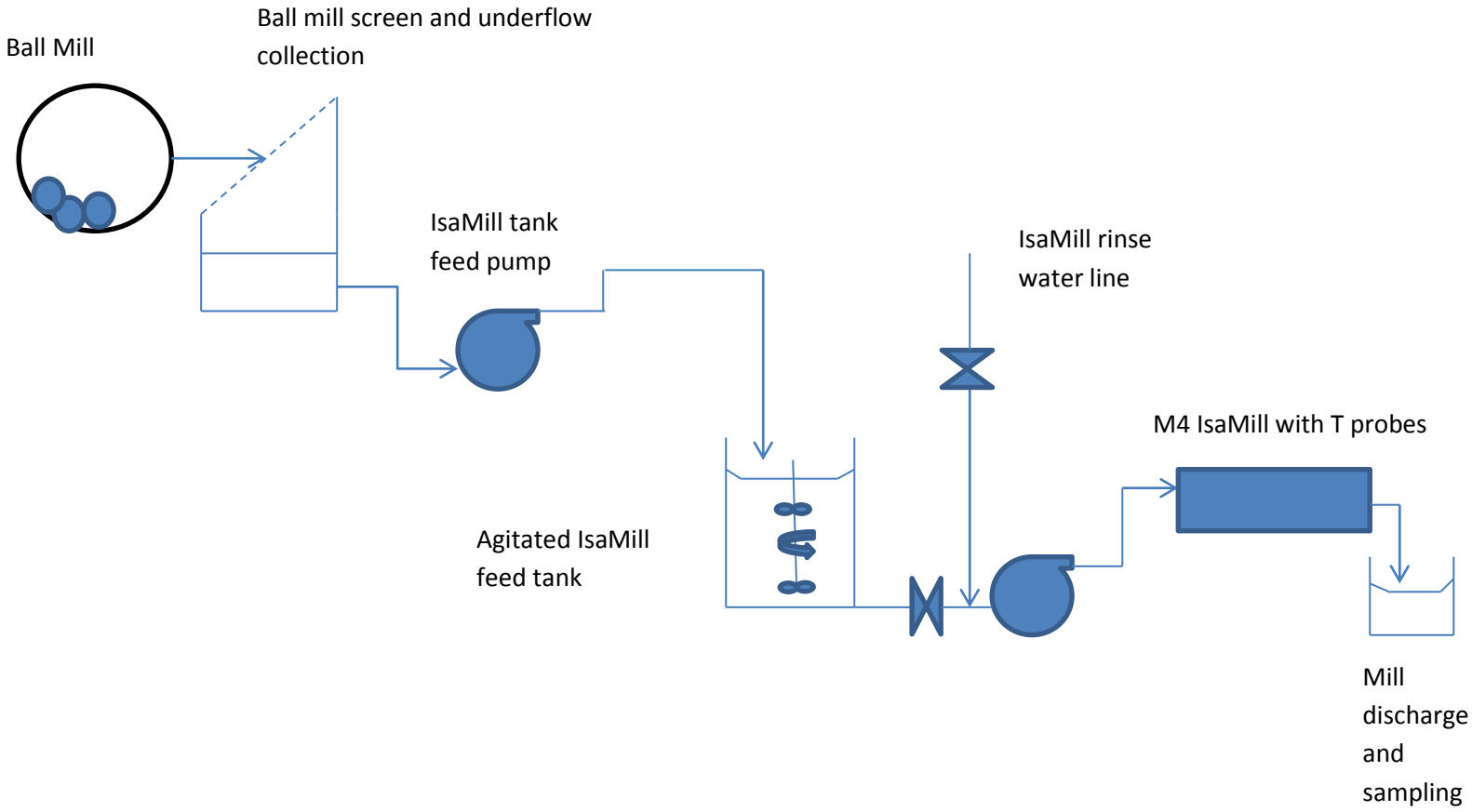

Fig 4.2.3. Process flow diagram of the test rig.

Figures 4.2.4 is a pictorial representations of the grinding chamber with the temperature probes inserted along the length of the mill.

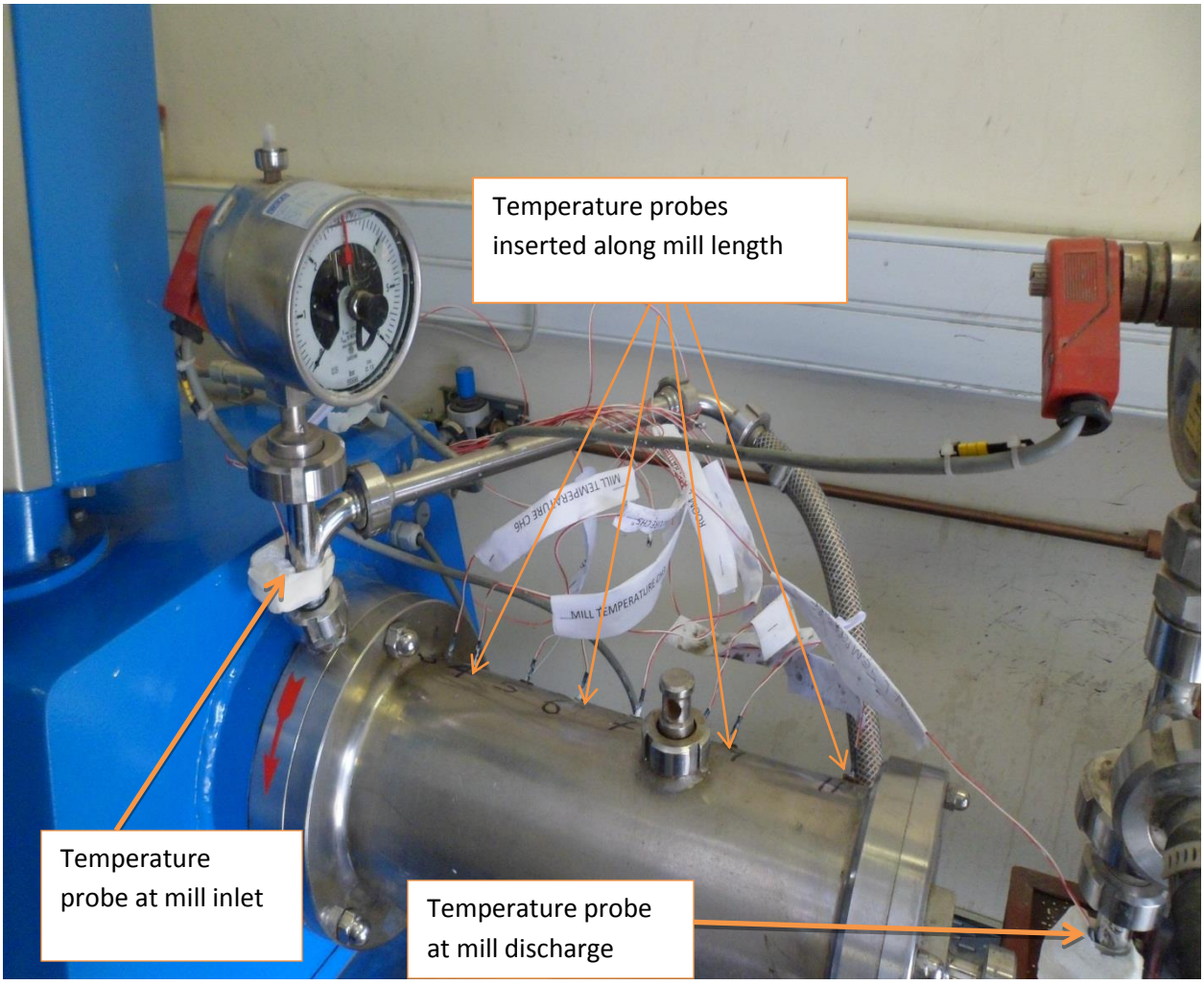

Figure 4.2.4.Temperature probes inserted along the length of the IsaMill, from the feed of the mill to the discharge of the mill.

In addition to the temperature along the mill length, the pressure inside the mill as well as the mill power draw were also measured to observe the effect of changing the mill variables on these.

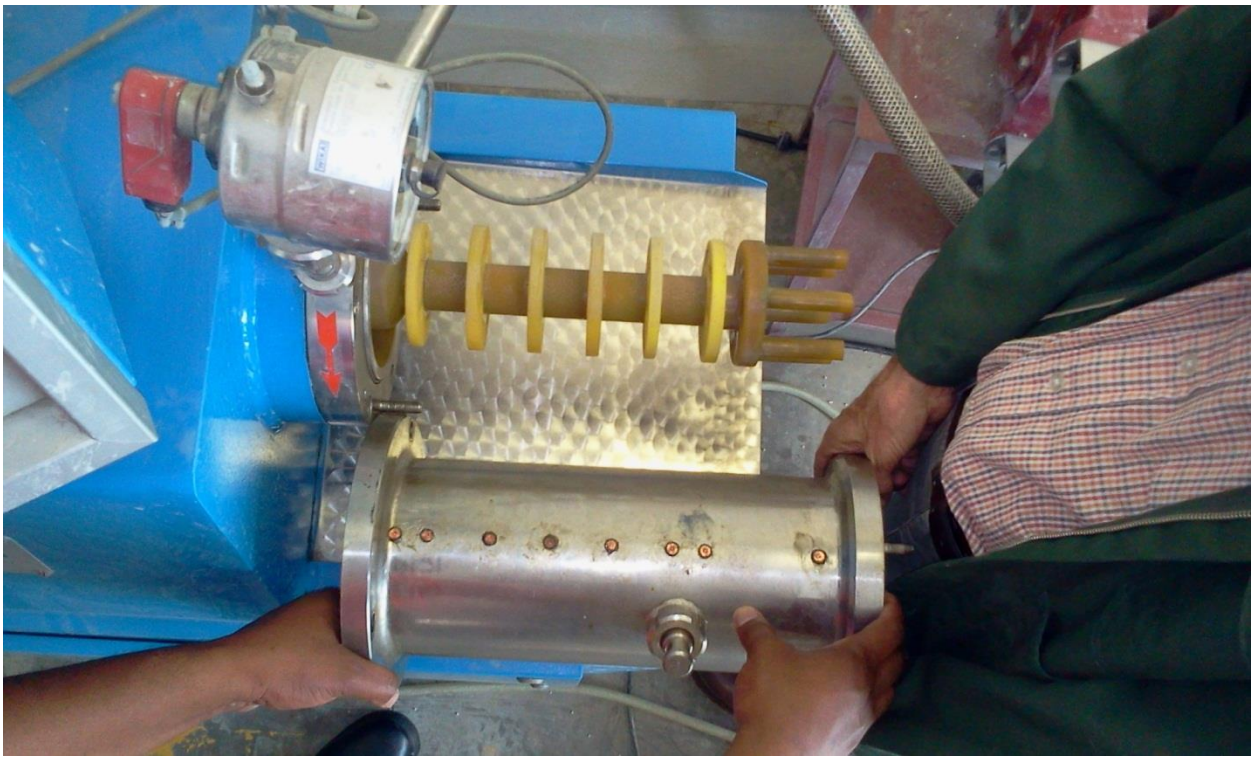

Fig 4.2.5: Photograph of the relative positions of the grinding discs and the temperature sensors from first disc (left) to product separator (right).

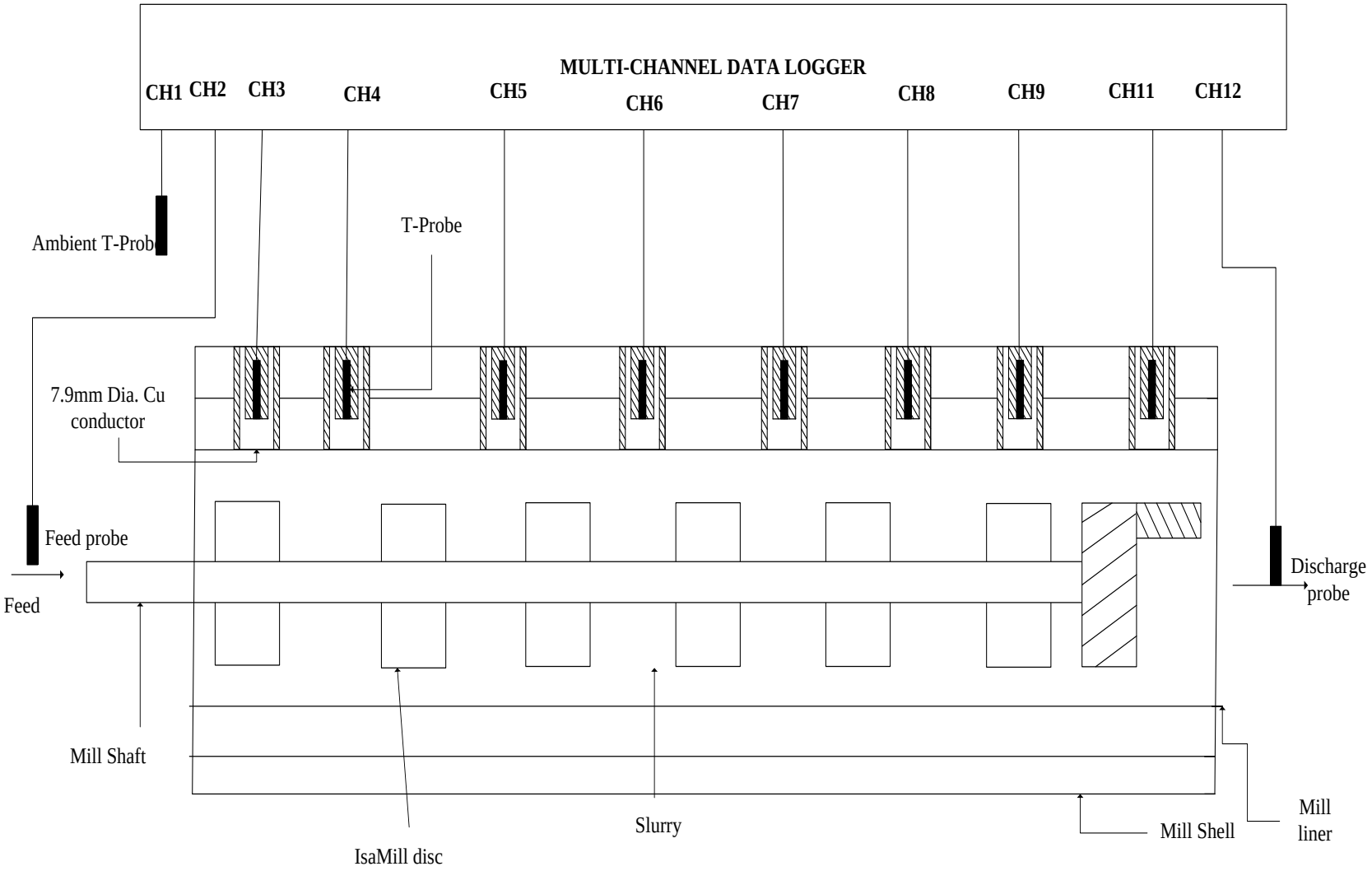

Figure 4.2.6: Schematic representation of the test equipment.

The specifications for the probe hole depth, copper conductor insulation thickness, copper conductor diameter and length, conductive silicone and the RTD diameter were arrived at during the laboratory trial and design stage in Chapter 3.

The following test matrix was used to investigate the axial temperature characteristics of the IsaMill.

Table 4.2.1: Project Test Matrix

Media Load (litres)	**1.5**			**2.0**			**2.5**		
Feed Flow Rate(ℓ/min)	2.0	2.5	3.0	2.0	2.5	3.0	2.0	2.5	3.0
Stirrer Tip Speed (rpm)	1500	1500	1500	1500	1500	1500	1500	1500	1500
	1750	1750	1750	1750	1750	1750	1750	1750	1750
		2000	2000		2000	2000		2000	2000

Three variables of importance to Anglo American operations were chosen as shown above being media load, feed flow rate and stirrer tip speed in order of priority to Anglo's operations. The tip speed of 2000rpm at a feed flow rate of 2(ℓ/min) was skipped for all media loads as previous runs showed that at these high tip speeds and low media load , media back-flowed and choked the feed line. The choice of the values of the variables above was based on Anglo American's experience with the IsaMill in actual operation.

The above test matrix was subdivided into three test sets for each media load as it would be operationally easier to simply add onto the lower media load to get the higher media load, thus test were done with the 1.5 litre media load and after all tests at 1.5 media load were completed, the tests at 2.0 litre media load were then carried out until the media load was topped to 2.5 litres.

The above table shows that a minimum of 24 experiments could be done. However, to ensure reproducibility and statistical accuracy , duplicates and triplicates of the above tests were done as shown in the three sub-matrices below as well as the measurements of the power draw and mill internal pressure obtained during the runs. The superscript represents the number given to an experiment that was carried out at the given conditions.

Table 4.2.2: Experiments carried out at 1.5 litres media load (37.5% v/v).

Media Load 1.5 (litres)			
Feed Flow Rate(ℓ/min)	2.0	2.5	3.0
Stirrer Tip Speed (rpm)	$1500^{1,4,7}$	$1500^{10,13,16}$	$1500^{19,22}$
	$1750^{2,5,8}$	$1750^{11,14,17}$	$1750^{20,23}$
		$2000^{12,15,18}$	$2000^{21,24}$

Thus, a total of 21 experiments were carried out under the above conditions at a media load of 1.5 litres (37.5 % media load v/v of the mill). The experiments were carried out in the order of their numbers , that is 1 , 2 , 4 , 5 , 7 , 8 , 10 ,…..21 , 22 , 23 , 24.

Table 4.2.3: Power draw and pressure inside the grinding chamber at different experimental conditions.

Experiment Number	Power Draw(KW)	Pressure Inside the IsaMill(bar)
1	1.6	0.30
4	1.7	-
7	1.7	0.50
2	2.1	-
5	2.2	0.60
8	2.2	0.65
10	1.6	0.50
13	1.6	0.50
16	1.6	0.50
11	2.1	0.65
14	2.1	0.65
17	2.1	0.65
12	2.8	0.85
15	2.8	0.90
18	2.8	0.90
19	1.4	0.35
22	1.6	0.50
20	2.0	0.65
23	2.0	0.65
21	2.7	0.85
24	2.6	0.80

The above digits have two significant figures as these were the direct digital readings that were coming from the measuring devices.

Table 4.2.4: Experiments carried out at 2.0 litres media load.

Media Load 2.0 (litres)			
Feed Flow Rate(ℓ/min)	2.0	2.5	3.0
Stirrer Tip Speed (rpm)	1500[28,31]	1500[37,40]	1500[46]
	1750[29,32]	1750[38,41]	1750[47]
		2000[39,42]	2000[48]

Thirteen experiments were carried out at a media load of 2.0 litres (50% v/v media load).

Table 4.2.5: Power draw and pressure inside the grinding chamber at different experimental conditions of 2.0 litres media load.

Experiment Number	Power Draw(KW)	Pressure Inside the IsaMill(bar)
28	1.6	0.4
31	1.6	0.50
29	2.2	0.65
32	2.0	0.70
37	1.7	0.50
40	1.6	0.50
38	2.2	0.60
41	2.0	0.60
39	2.8	0.90
42	2.7	0.90
46	1.6	0.50
47	2.1	0.65
48	2.8	0.85

Table 4.2.7: Experiments carried out at 2.5 litres media load (62.5% v/v).

Media Load 2.5 litres			
Feed Flow Rate(ℓ/min)	2.0	2.5	3.0
Stirrer Tip Speed (rpm)	1500[55]	1500[64,67]	1500[73]
	1750[56]	1750[65]	1750[74]
		2000[66,69]	2000[75]

Table 4.2.8: Power draw and pressure inside the grinding chamber at different experimental conditions of 2.5 litres media load.

Experiment Number	Power Draw(KW)	Pressure Inside the IsaMill(bar)
55	1.7	0.50
56	2.1	0.65
64	1.7	0.50
67	1.7	0.50
65	2.2	0.65
69(a)	2.9	0.85
69(b)	2.8	0.75
73	1.7	0.50
74	2.3	0.65
75	2.9	0.85

To check reproducibility of the results, the above test matrix was made such that each variable under investigation would be repeated three times, thus resulting in a total of seventy two experiments. However due to the reproducibility of the results , forty five experiments were actually conducted ensuring that the minimum of eighteen experiments were done and all of them were done at least twice each i.e of these eighteen planned experiments , nine were repeated three times.

4.3 Resistance Temperature Device (RTD) Calibration:

Before the RTDs could be used to measure the temperatures of the mill, they were calibrated using the method below:

The relationship between the actual temperature and the measured temperature is represented as;

$T = a + b\check{T}$ were T is the actual temperature (from the calibrated thermometer), $\check{T}$ is the measured temperature, a is the off-set, b is the gain (Eagle Technology RTD manual).

The RTDs were inserted into similar conditions (they were immersed into a thermos flask and shaken until the temperature read from the micro-data acquisition display showed steady state temperature readings with a calibrated liquid-in-glass thermometer to measure the actual temperature versus the RTD temperature for each RTD and plots were done to evaluate the values of the constants a and b. Below is a summary of the calibration results for RTD no.12. The same principle was used for the other RTDs.

A five point calibration was done for each of the RTDs used in the test work. The temperatures used for the five point calibration were, -0.9^{0}C , 19.9^{0}C , 33^{0}C , 43.6^{0}C and 51.9^{0}C as read on the standard thermometer.

Calibration Results:

The following steady state temperature-time curve was obtained for probe no.12 when immersed in ice crushed ice in water in which the standard temperature was -0.9^{0}C as the direct reading from the thermometer. The average observed RTD temperature was -0.922^{0}C.

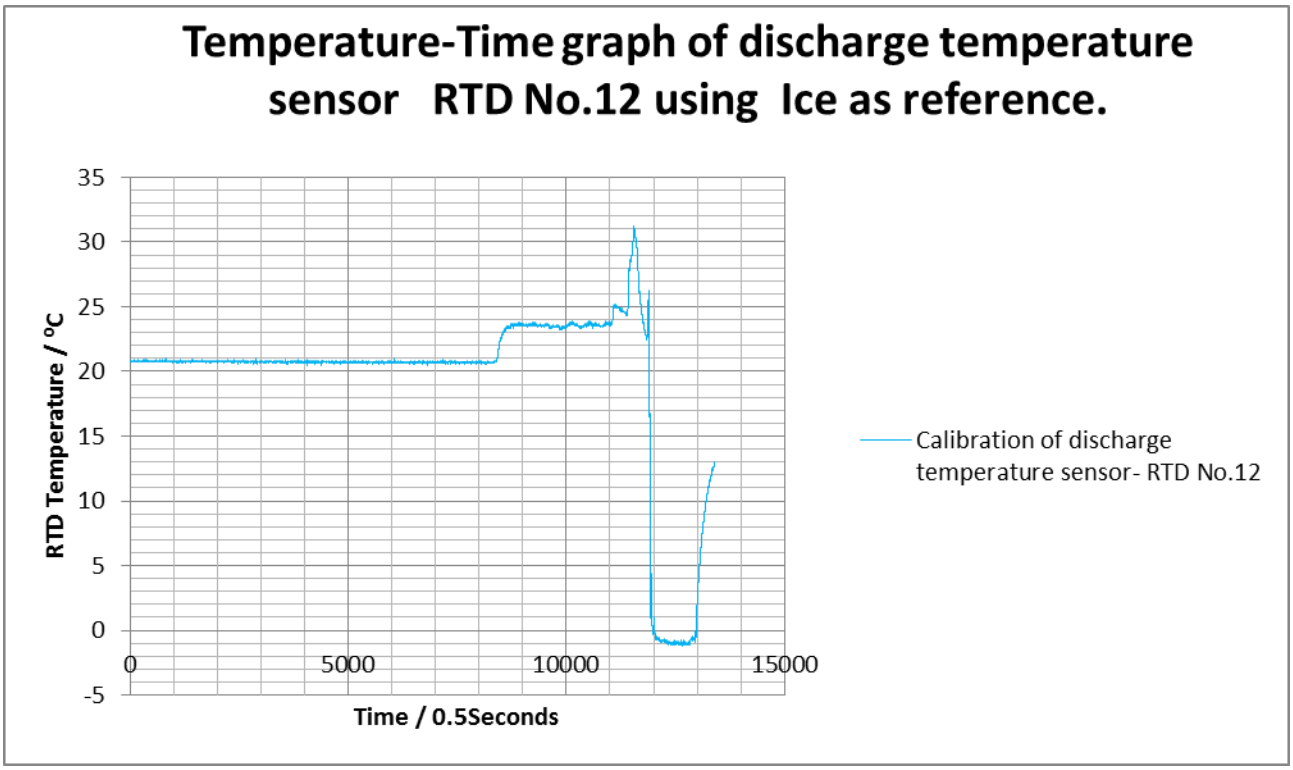

Fig4.3.1: Plot of temperature vs time for temperature probe no.12 at standard temperature of -0.9^{0}C.

Fig4.3.2. below is a temperature-time graph for probe no.12 at a standard temperature of 43.6^0C.

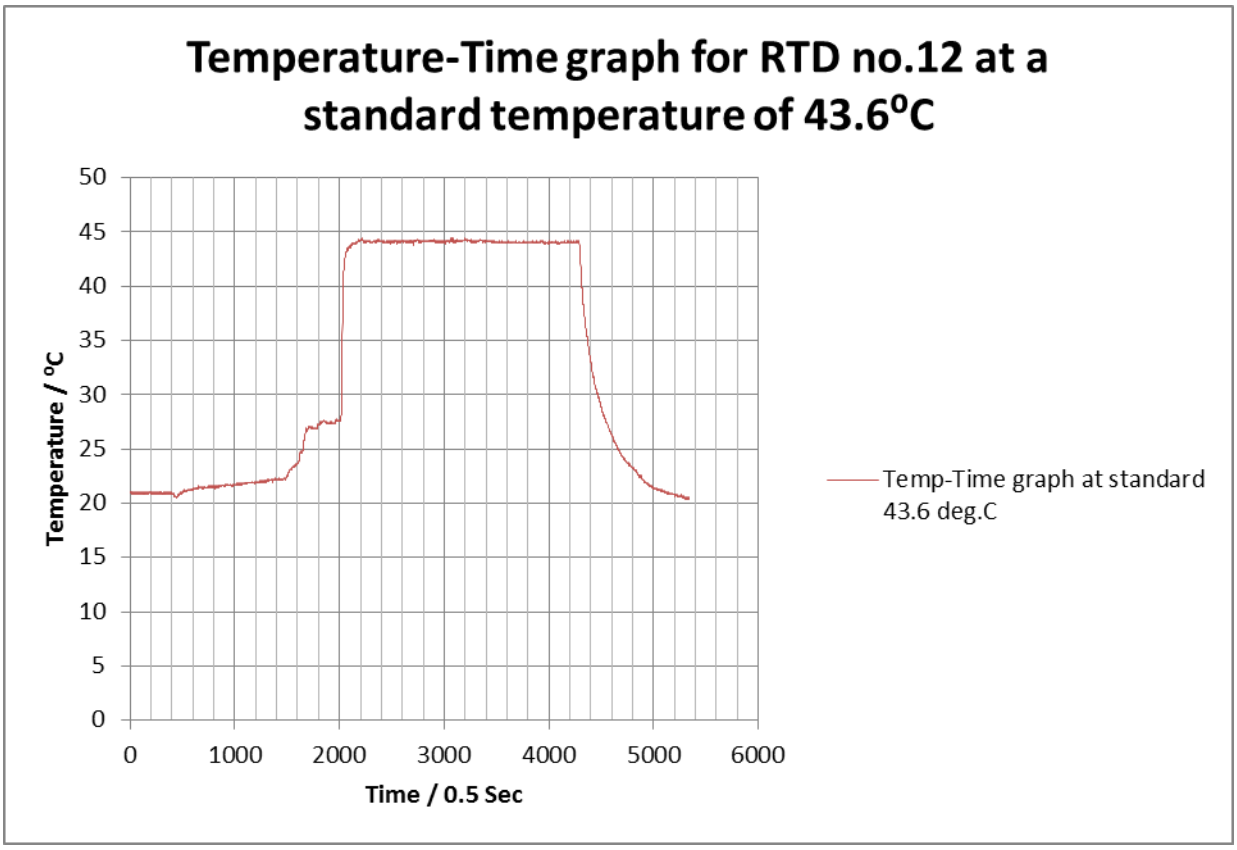

Fig 4.3.2: Plot of temperature vs time for temperature probe no.12 at standard temperature of 43.6^0C.

The RTD measured temperature is 44.139^0C.

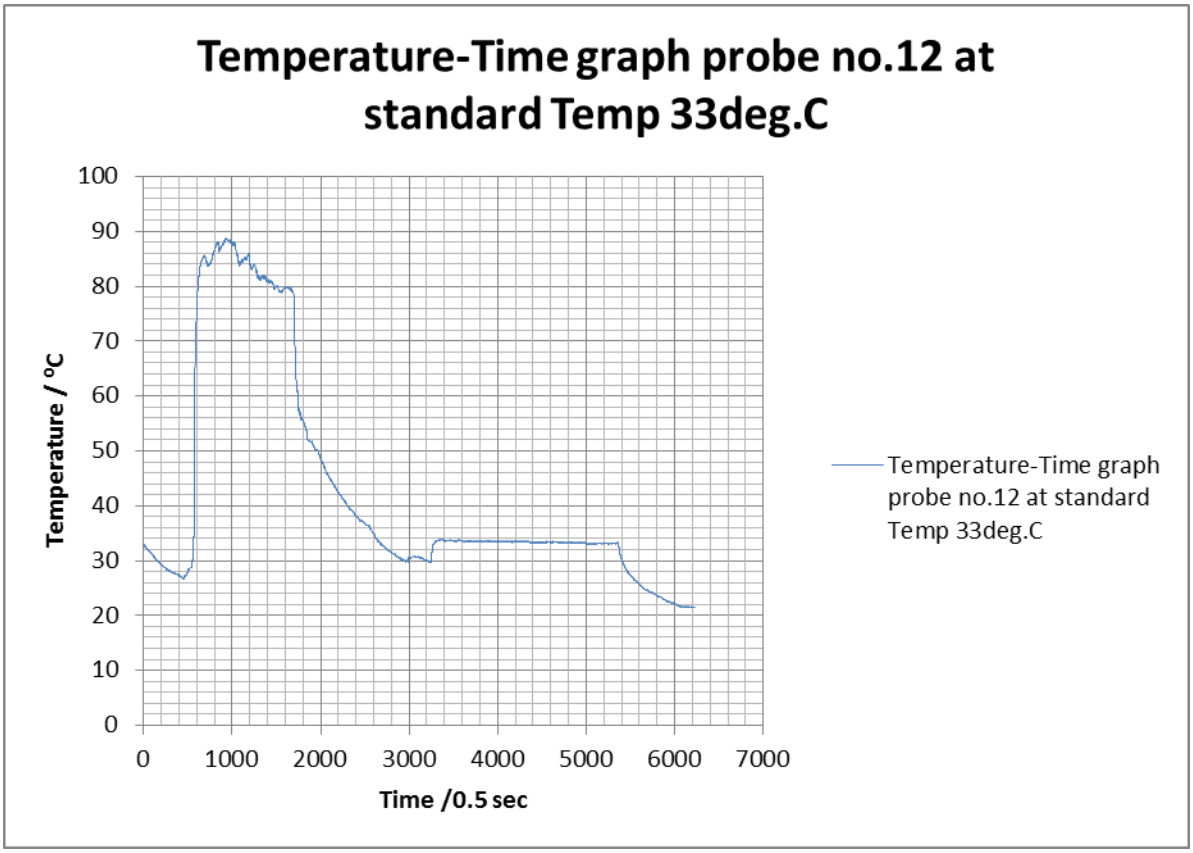

Fig 4.3.3: Plot of temperature vs time for temperature probe no.12 at standard temperature of 33^0C, i.e for the time interval 3400 – 5200 (0.5sec).

The measured probe temperature was 33.343^0C

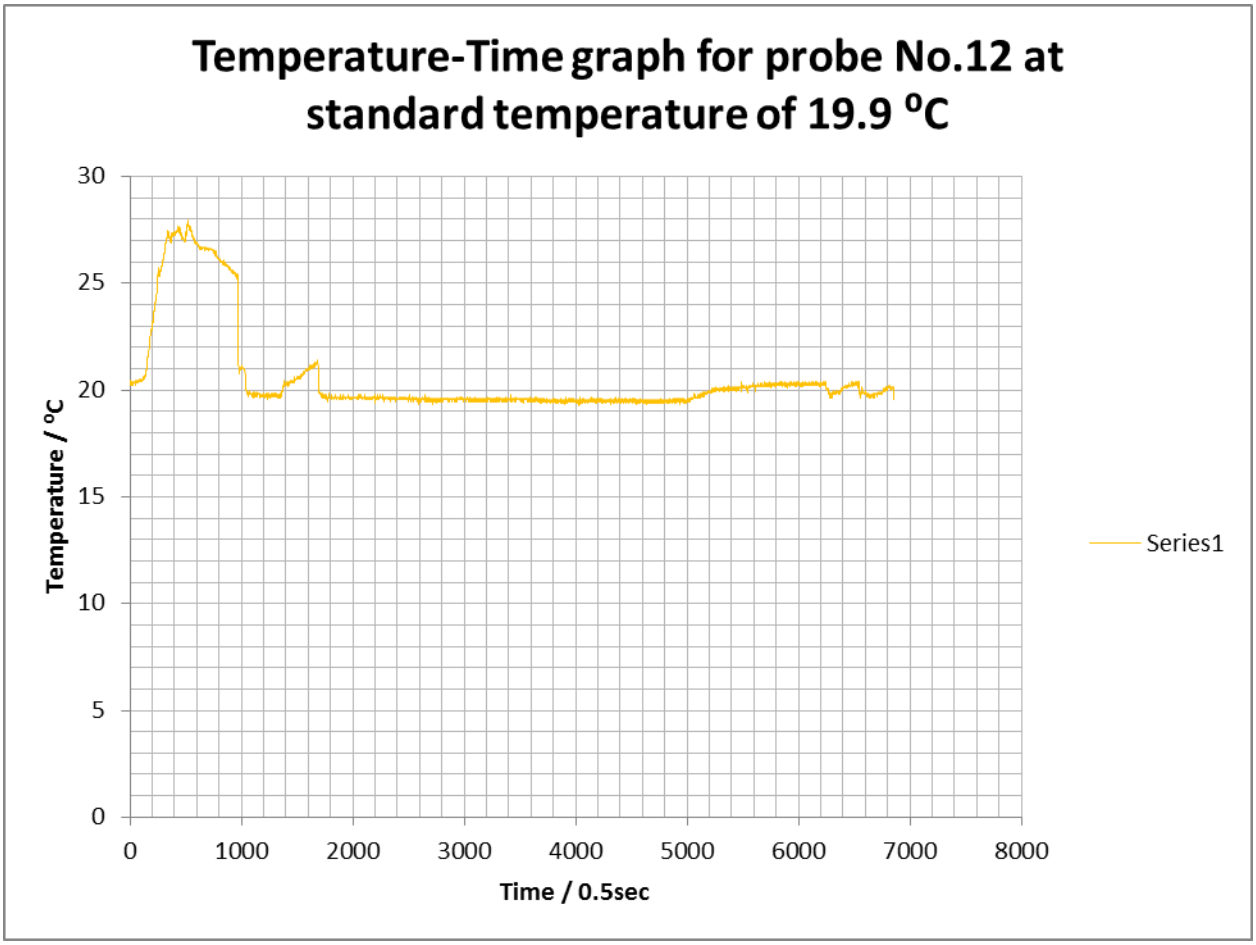

Fig 4.3.4: Plot of temperature vs time for temperature probe no.12 at standard temperature of 19.9^{0}C.

The measured probe temperature was 19.584^{0}C.

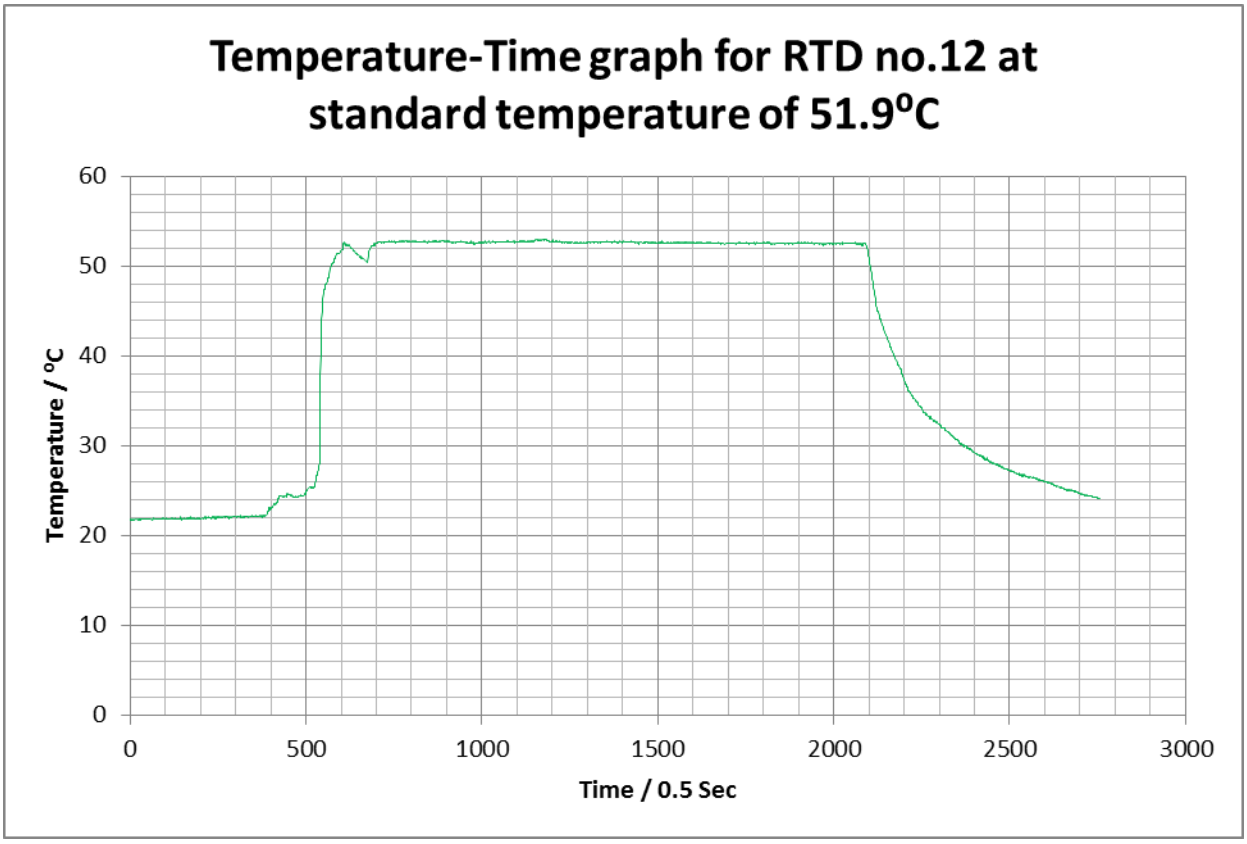

Fig 4.3.5: Plot of temperature vs time for temperature probe no.12 at standard temperature of 51.9^{0}C.

The measured probe temperature was 52.6722^{0}C.

Table 4.3.1 below is a summary of the relationships between standard and measured temperatures for the five calibration points for probe no.12.

Table 4.3.1 Measured Probe Temperature vs Standard Temperature.

Measured probe Temperature/ ^{0}C	Actual(standard) Temperature / ^{0}C
-0.922	-0.9
19.584	19.9
33.692	33
44.139	43.6
52.6722	51.9

The above results for temperature probe no.12 were plotted to give the calibration curve for the specific RTD as below.

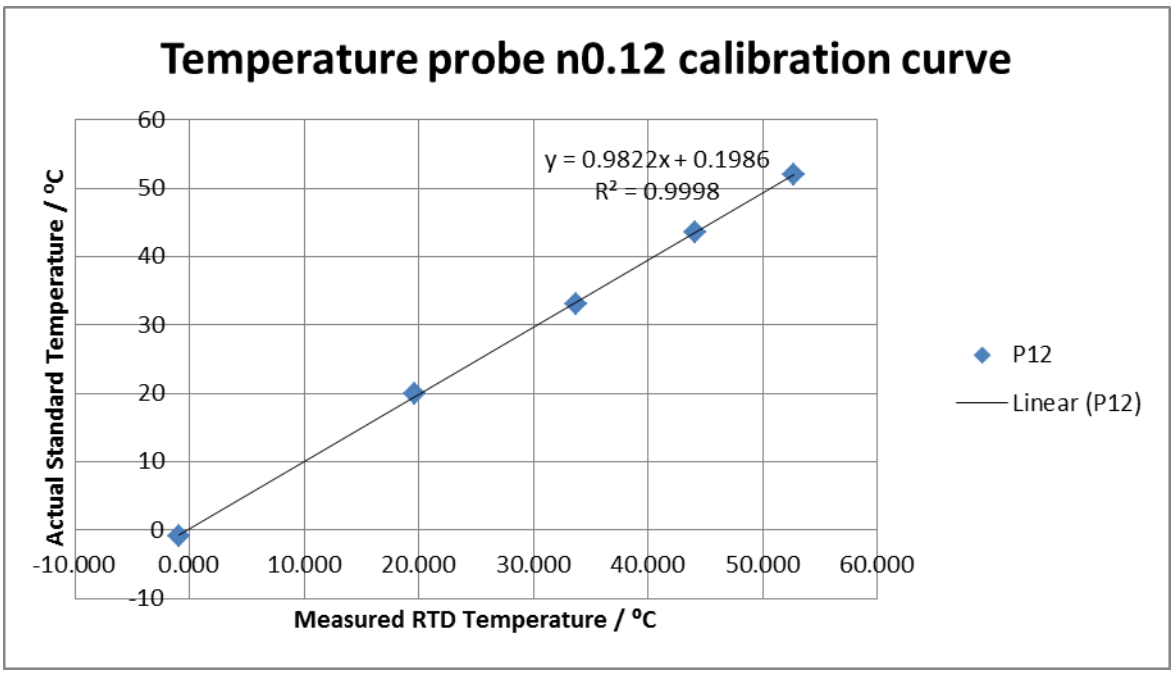

Fig 4.3.6: Calibration curve for RTD assigned the number 12.

From the fit of the calibration curve above, the constants a and b were obtained from the graph to give the gain and off-set of the RTD. Each of the values of the constants a and b for each RTD were input into the data acquisition application programme, Wave View and were saved into the programme as an executable file for all temperature measurement runs.

The same approach was used for the other 4 calibration points outlined above

Data Acquisition System:

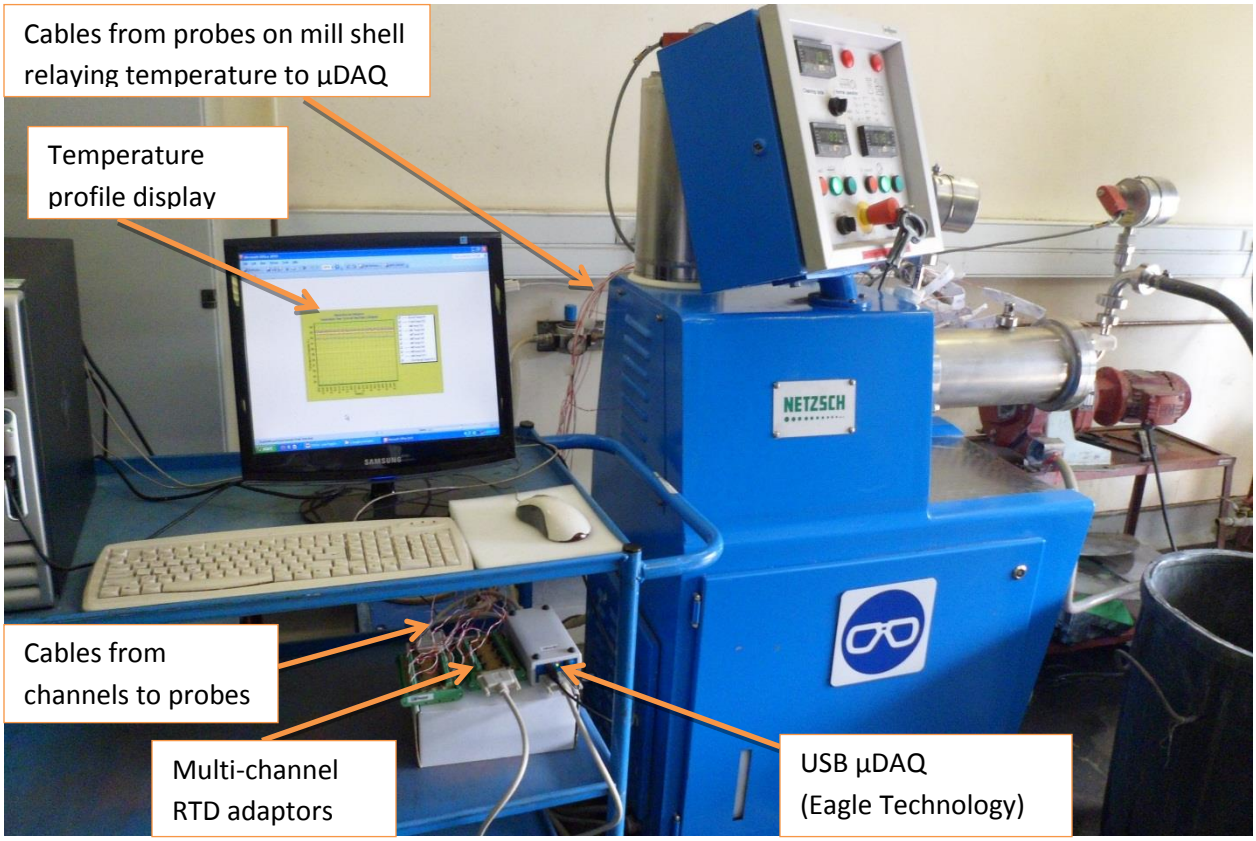

Fig 4.3.7: Illustration of the data acquisition system.

The fly lead cables will complete the circuit of the RTD. As temperature for each RTD probe varies, the resistance of the RTD also varies proportionately, increasing with increase in temperature. The data acquisition system operates on the principle of a potential divider circuit with a Wheatstone bridge.

4.4 Mill Start-up procedure:

The ball mill was started up first to generate a P80 of -77µm. The ball mill was operated in a wet-milling mode. Samples were taken to analyse the ball mill output in terms of the particle size distribution and the mill was controlled to ensure a steady flow of the slurry to the ball mill discharge tank.

The ball mill discharge slurry was pumped to the IsaMill feed tank. The pumping rate was maintained such that there was always a volume in the ball mill discharge tank that was above the pump suction point.

Feed in the IsaMill feed tank was maintained above the first stirrer of the feed tank to ensure perfect mixing within the stirrer. The IsaMill feed tank slurry S.G was monitored and maintained by ensuring to an average solids percentage of 35%. The IsaMill feed pump was initially fed with water and simultaneously the mill was started up. The IsaMill was flushed with the rinsing water from the feed pump to ensure smooth start-up of the mill and also to ensure that all safety features were functioning properly and to check if the mill was running steadily without any unfamiliar sounds and fluid leakages from the seals and also from the drillings through which the temperature probes had been inserted. The temperature and pressure gauges were also monitored during these blank runs to check functionality. The response from the data acquisition system was also observed to see how the resistance temperature devices were performing.

The slurry was slowly introduced into the mill while shutting the water supply. The response from the mill control gauges was also observed and also the response from the RTDs was observed as more and more slurry was introduced into the system. The mill runs were done firstly with the lowest level of media load per the test matrices(Tables 2, 4 and 6 respectively) as it would be simpler to then simply top up the media volume for the higher media volume test runs without actually having to strip the mill as pointed out earlier.

For values of the media load, the required volume would simply be measured in a measuring cylinder and then poured in through the media feed point. Tip speed would be set by adjusting the variable speed drive of the mill shaft on the control panel and three levels of tip speed were used as per the test matrices (Table 1). The appropriate slurry flow rate to the mill was measured by: changing the speed of the feed pump, (a positive displacement peristaltic pump) and waiting for the mill to attain steady state and then measuring the slurry discharge rate under timed conditions. Mill steady state conditions were observed by monitoring the RTD temperature response curves as they flatten out over time. This would then indicate that the temperature at each point along the length of the mill was constant. Under these steady state conditions, a measuring cylinder would then be used to measure the time that would be required to fill the cylinder to a specified volume. This information would then be used to determine the slurry volumetric flow rate.

The above specifications of the levels of tests and mill variables' operating ranges were based on Anglo American Technical Solutions' experience with the M4 test mill in terms of the operable feed rates, typical tip speeds and typical load volumes for the media.

To change from one process condition to the next, the required change would just be effected while the mill would be running in continuous mode and the temperature profiles would be monitored until steady temperature was observed. The only process change that would require stopping of the mill was the addition of media to the mill.

The various combinations of the mill variables as prescribed on the test matrices were used and steady state data was collected and saved per each of the test conditions. The process was said to be at steady state when the temperature-time curve for each RTD remained constant.

The Figure below is a typical steady state temperature- time curve for experiment 16 on temperature sensor no.12 under the conditions shown on the test matrix.

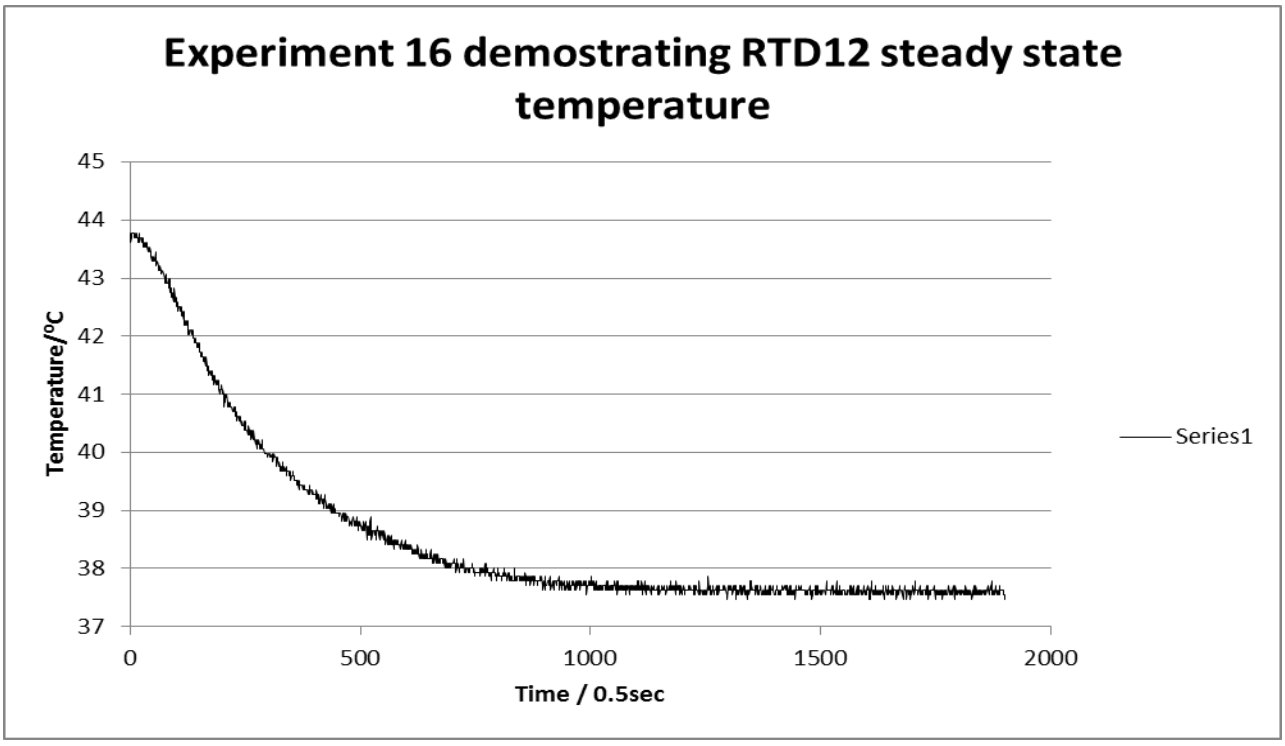

Fig 4.4.1: Temperature time curve demonstrating experiment 16.

Temperature is dropping as conditions change from high temperature process conditions to conditions resulting in a low temperature steady state.

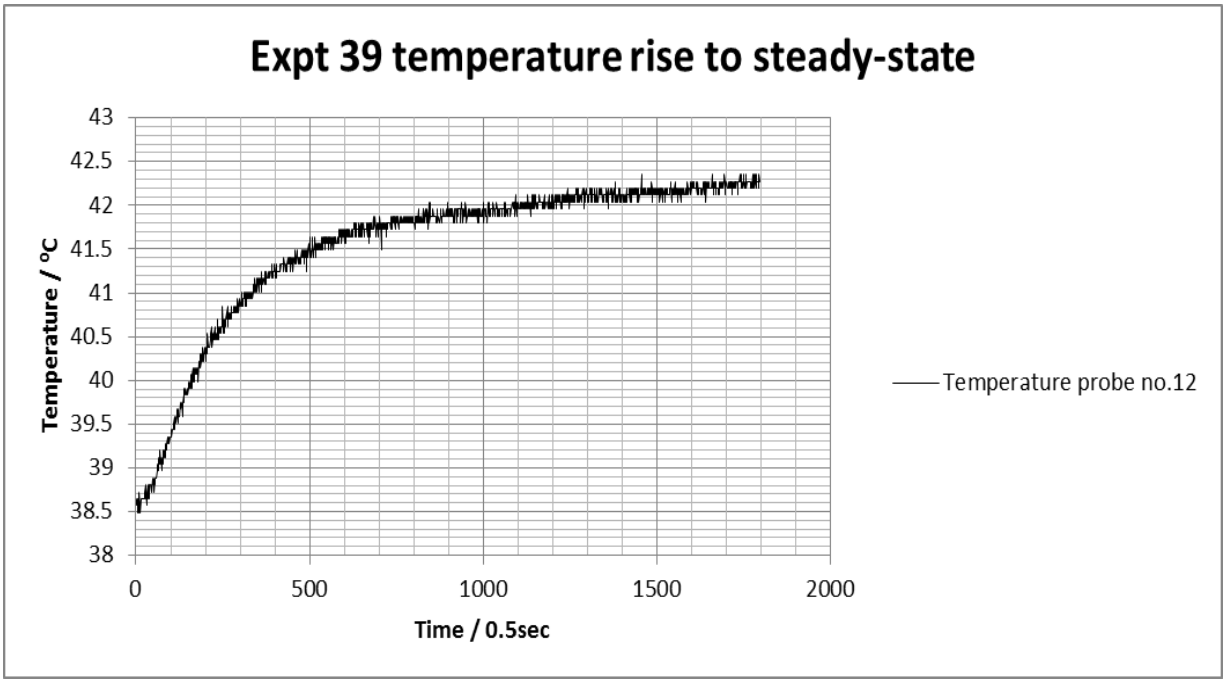

Fig 4.4.2: Temperature rise to a high temperature steady state conditions.

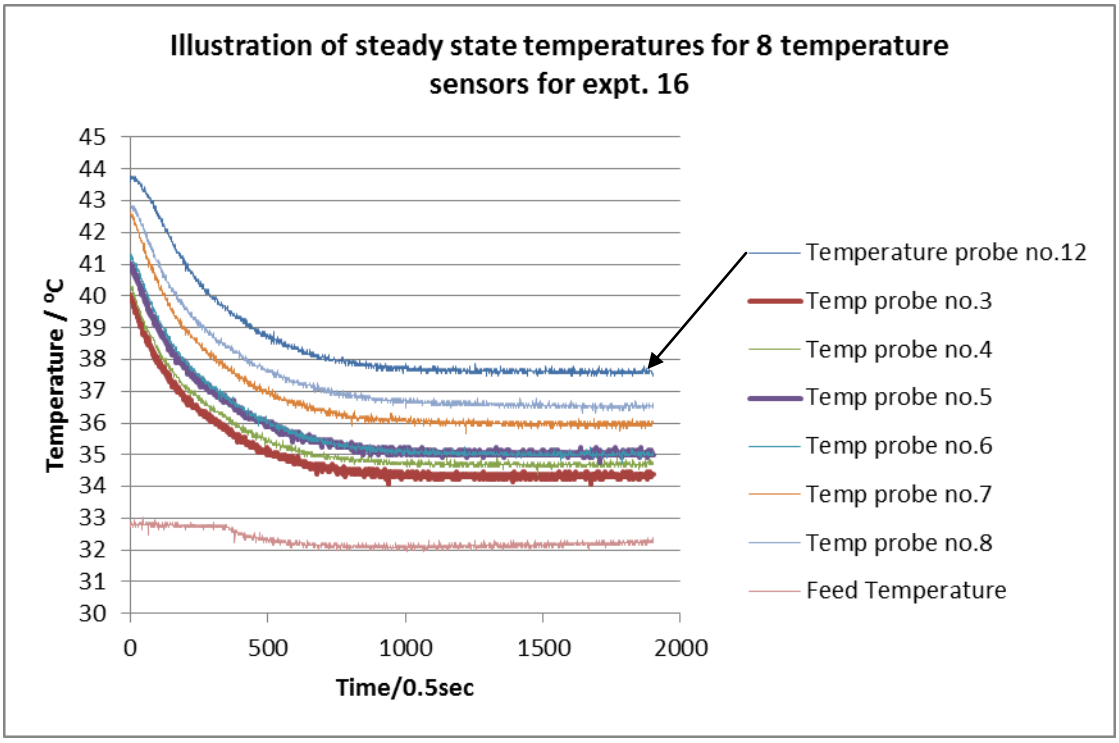

Fig 4.4.4: Temperature-Time response curves showing steady state attainment for experiment 16 for eight RTDs along the mill length.

The feed temperature would change depending on the operations of the ball mill supplying the feed to the buffer tank. Tamb is the temperature of the surrounding environment. The particular test run would be terminated when all the RTD readings displayed steady state temperature as illustrated above.

4.5 Mill Shutdown Procedure:

After completion of the runs or to stop the mill, the slurry feed pipe would be disconnected from the slurry tank and connected to a water supply, thus water would replace the slurry. The mill flushing process would continue until the mill discharge started coming out as milky white with no evidence of solids. At that time the data acquisition system would have been switched off after saving the last steady state data. The mill would be switched off simultaneously as the feed pump was switched off.

4.6 Summary

The mill was successfully commissioned and test-work was conducted as per the experimental methods prescribed resulting in a set of data that are presented in the results analysis chapter, chapter 5.

CHAPTER 5

RESULTS AND ANALYSIS OF RESULTS

5.1 Introduction

This chapter presents extracts of results that were obtained from experimental test work. It shows qualitative statistical checks that were done to check data reproducibility in repeat tests and data integrity. General trends and profiles qualitatively obtained from the experimental work are shown. Also qualitative relationships between mill operating variables and temperature profiles are shown. An overall results summary sheet containing all details of Test No., feed rate, media load, mill tip speed, temperatures along the mill length, average mill temperature differences for the different conditions from feed to discharge, the power draw, feed and product size distribution are presented in appendix A.

Below are mill steady state temperatures for selected experiments during the experimental runs.

5.2 Checking data integrity and reproducibility:

Experiments 12, 15 and 18 were used to check data reproducibility and integrity. These experiments are triplicate runs under the same process conditions. Descriptive statistics was used to check reproducibility. The main measures of central tendency that were used to ascertain reproducibility of the data collected from the mill were the standard deviation as a percentage of the mean per each temperature probe as well as the standard deviation as a percentage of the temperature range from the feed to the discharge of the mill.

Table 5.1 below shows the results for the three experiments above.

Table 5.1: Temperature measurements for experiments 12, 15 and 18 along mill length.

Expts		Averages of Slurry Temperatures from feed to discharge								
	FeedTempCH2	MillTempCH3	Mill TempCH4	MillTempCH5	MillTempCH6	MillTempCH7	MillTempCH8	MillTempCH9	MillTempCH11	Dis TempCH12
12	31.00	38.34	38.78	39.60	39.65	41.29	41.36	41.06	40.50	41.76
15	32.89	40.02	40.36	41.00	41.27	42.59	42.79	42.59	41.92	43.76
18	29.12	36.26	36.84	37.28	37.39	38.61	38.91	38.58	37.95	39.80

To compare the above data on an equal basis, the data was normalised by using the lowest temperature as the reference temperature. Thus, experiment 18 was used as the reference experiment and the feed temperature of experiment 18 was used as the starting temperature for all the three experiments. Thus, for experiment 15, the corresponding feed temperature was obtained by subtracting 3.77^{o}C from the measured temperature of 32.89^{o}C to obtain an equivalent starting temperature of 29.12^{0}C similar to that of experiment 18. The same figure of 3.77^{o}C was subtracted in all the measured temperatures of experiment 15 to obtain the corresponding normalised temperatures. A similar approach was used to normalize the measured temperatures of experiment 12.

Table 5.2 below is a summary of the normalised temperatures as well as the descriptive statistical inferences that were made to the data to investigate the degree of repeatability of the data as well as its significance with reference to the actual temperature range which resulted under the operational conditions.

Normalised Data										
Expts	**Feed Temp**		**Averages of Slurry Temperatures from feed to discharge**					**Discharge Temp**		
	FeedTempCH2 /deg.Celcius	MillTempCH3	Mill TempCH4	MillTempCH5	MillTempCH6	MillTempCH7	MillTempCH8	MillTempCH9	MillTempCH11	Discharge T.CH12
12	29.12	36.46	36.90	37.73	37.77	39.41	39.48	39.19	38.62	39.88
15	29.12	36.24	36.58	37.23	37.49	38.82	39.02	38.81	38.15	39.99
18	29.12	36.26	36.84	37.28	37.39	38.61	38.91	38.58	37.95	39.80
STD Dev	0.00	0.12	0.17	0.27	0.20	0.41	0.30	0.31	0.35	0.09
Mean	29.12	36.32	36.78	37.41	37.55	38.95	39.14	38.86	38.24	39.89
STD Dev as % Mean	**6.42E-05**	**3.28E-01**	**4.62E-01**	**7.28E-01**	**5.23E-01**	**1.06E+00**	**7.73E-01**	**7.87E-01**	**9.06E-01**	**2.37E-01**
STD Dev as % Range	**Expt12**	1.11	1.58	2.53	1.83	3.85	2.81	2.84	3.22	0.88
from Feed to Discha	**Expt15**	1.10	1.56	2.51	1.81	3.81	2.78	2.81	3.19	0.87
	Expt18	1.12	1.59	2.55	1.84	3.88	2.83	2.86	3.25	0.89
	Average STI	**1.11**	**1.58**	**2.53**	**1.83**	**3.85**	**2.81**	**2.84**	**3.22**	**0.88**
	% of Range									
	Average STI	**2.29 %**								
	% of Range for all									

Except for temperature probe CH7, the standard deviations as percentage of the mean were less than 1.0% .The average standard deviation as a percentage of the mean was 0.64 %. The maximum value for the standard deviation as a percentage of the operating temperature range was 3.84% and the average standard deviation as a percentage of the operating temperature range was 2.29%. A similar approach to that above was used for experiments 11, 14 and 17 and below is a summary of the results.

Table 5.5 :Normalised data and analysis of normalised data

	FeedT.CH2	MillTempCH3	Mill TempCH4	MillTempCH5	MillTempCH6	MillTempCH7	MillTempCH8	MillTempCH9	MillTempCH11	DischargeT.CH12
Expt 11	28.13	32.23	32.87	33.52	33.42	34.80	35.08	34.67	34.11	35.64
Expt 14	28.13	32.05	32.39	32.90	33.01	34.11	34.45	34.20	33.55	35.61
Expt 17	28.13	32.50	32.99	33.38	33.36	34.44	34.82	34.52	33.85	35.96
Standard Dev.		0.19	0.26	0.27	0.18	0.28	0.26	0.19	0.23	0.16
Mean		32.26	32.75	33.27	33.26	34.45	34.78	34.46	33.83	35.74
Std Dev as % of mean in %		**0.58**	**0.79**	**0.81**	**0.55**	**0.83**	**0.75**	**0.57**	**0.68**	**0.45**
Avg Std Dev as % of mean		**0.67**	**%**							
Std Dev as %	Expt11	2.488	3.443	3.569	2.450	3.790	3.479	2.598	3.056	2.144
of Range %	Expt14	2.498	3.457	3.583	2.460	3.805	3.493	2.608	3.068	2.152
	Expt17	2.384	3.300	3.421	2.348	3.632	3.334	2.490	2.929	2.054
Average STD		**2.456**	**3.400**	**3.524**	**2.419**	**3.742**	**3.435**	**2.565**	**3.018**	**2.117**
Dev as % of										
Range										
Average STD		**2.96 %**								
as % of range										
for all Temp probes										

The average standard deviation as a percentage of the mean is 0.67%. The average standard deviation as a percentage of the temperature range is 2.96%.

The above values were considered to be within reasonable limits for practical operations, giving confidence in the measuring devices and providing the motivation to proceed with the proposed test method.

5.3 Graphical representation of test results to show the typical temperature profiles

The figures below are results showing the general temperature profiles obtained for different experimental conditions under steady state conditions. The graphs show the temperature as a function of displacement from feed to discharge of the mill. As the data was shown to be reproducible by statistical analysis above, individual experimental runs are shown for different conditions just to show the characteristic temperature profiles along the mill length.

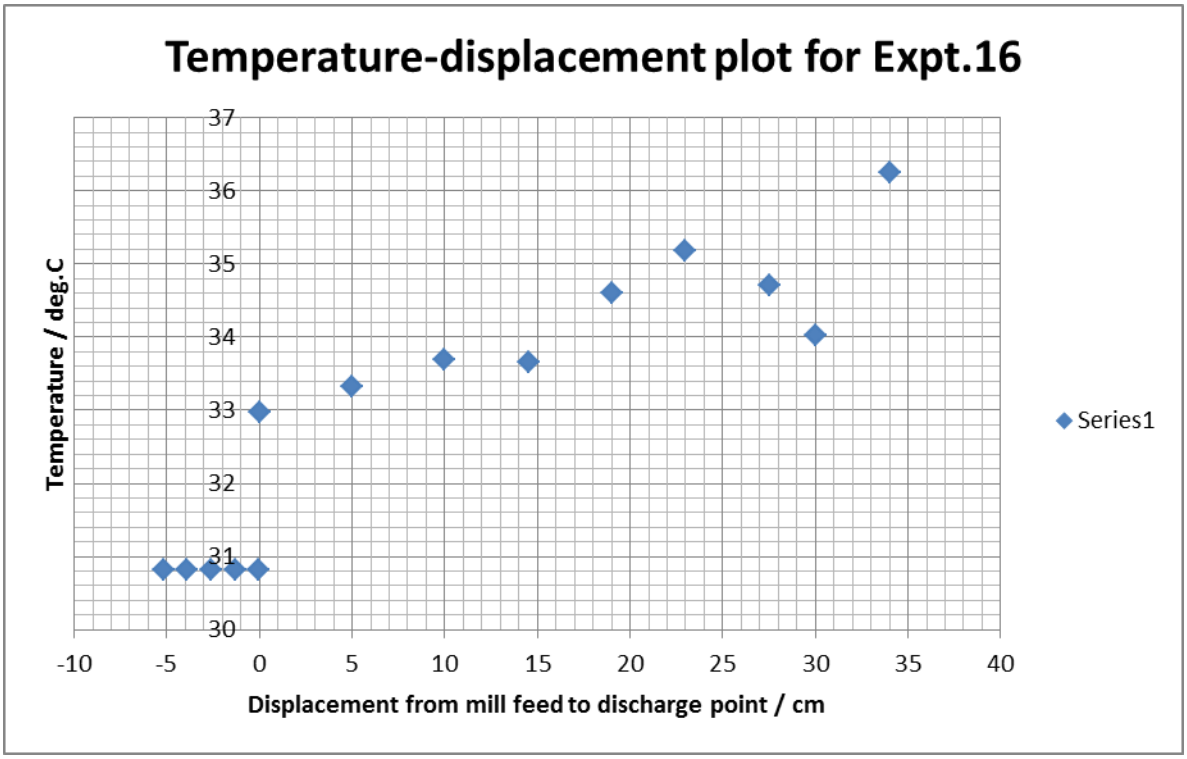

Fig 5.1: Temperature-Displacement graph.

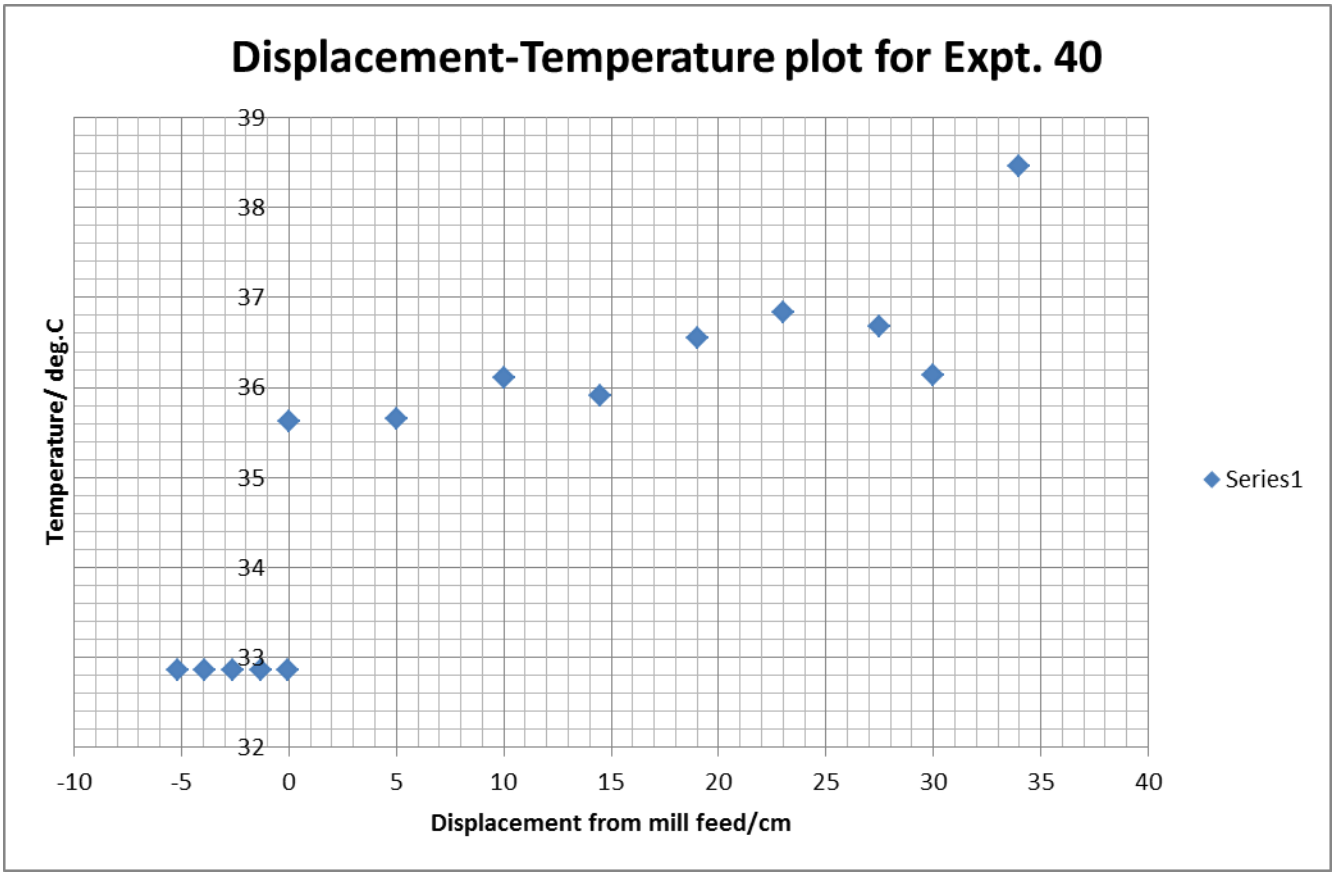

Fig 5.2: Temperature-Displacement graph. The test conditions are as per the previously presented test matrices.

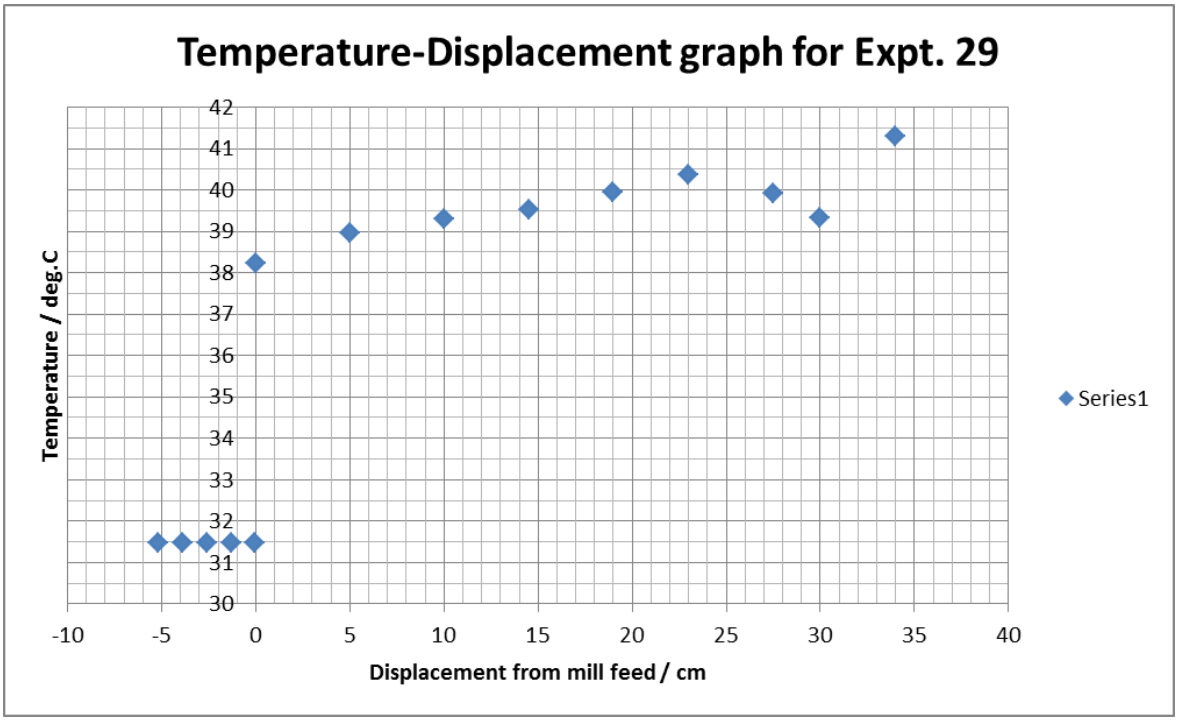

Fig 5.3: Temperature-Displacement graph.

In all the three plots above, there was a consistently recurring drop in the temperature of the two probes towards the end of the mill. On closer examination of the mill structure and geometry, a possible explanation to this drop in temperature was the absence of milling in the last section of the mill coupled with separation of media. This would then cause an artificial drop in the recorded temperature which is not dependent on the mill internal dynamics.

For the purposes of investigating the actual load behaviour inside the mill, these two temperatures were ignored. The figures below show the temperature-displacement relationships when the two probe temperatures were discarded. Thus only eight probe temperatures inclusive of the feed probe temperature were used for the results analysis.

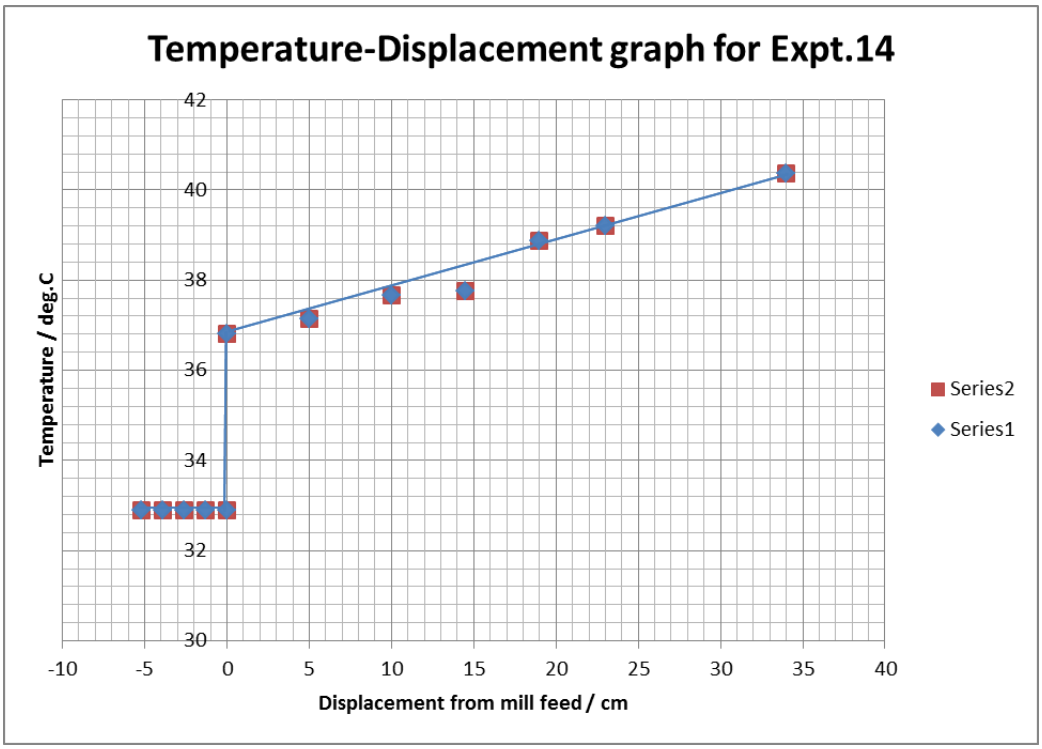

Fig 5.4 Temperature-Displacement graph

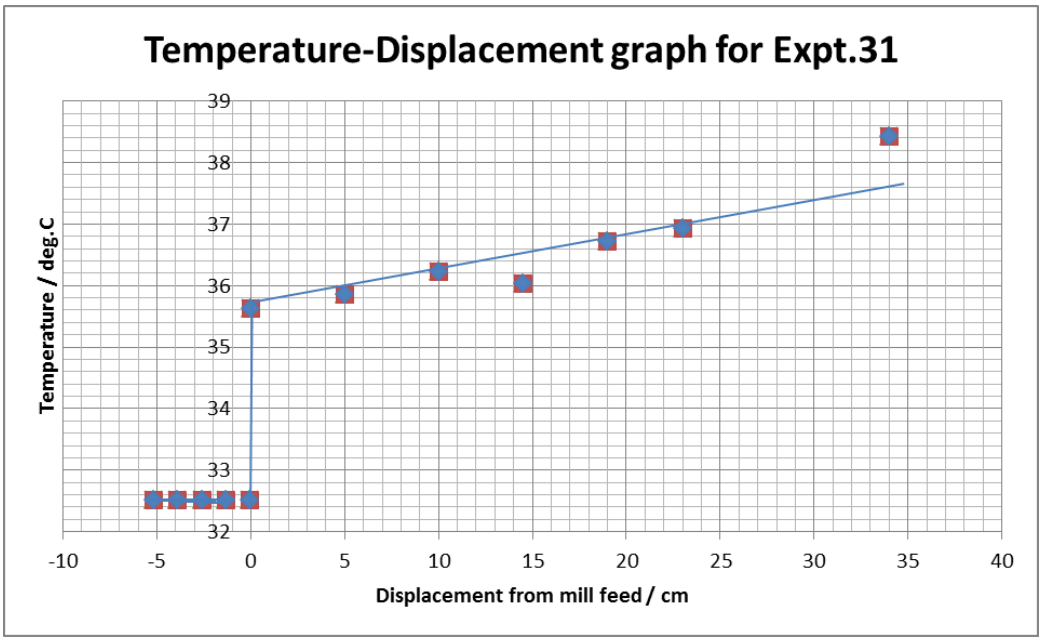

Fig 5.5: Temperature-Displacement graph

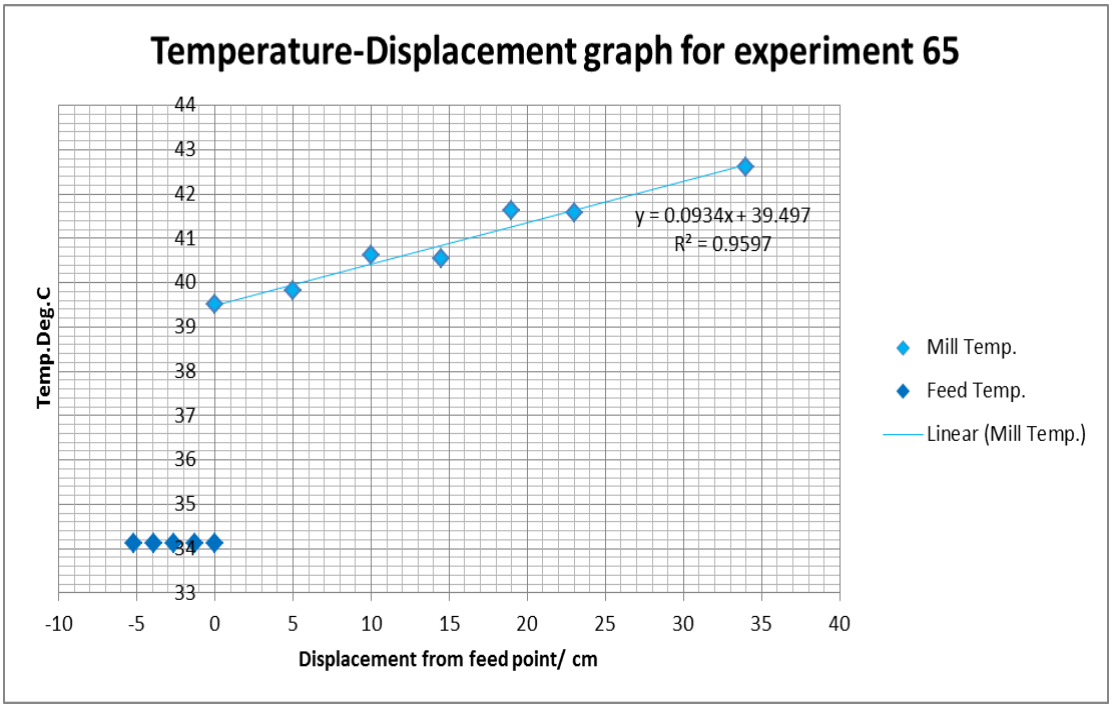

Figure 5.6 : Temperature-Displacement graph for experiment 65.

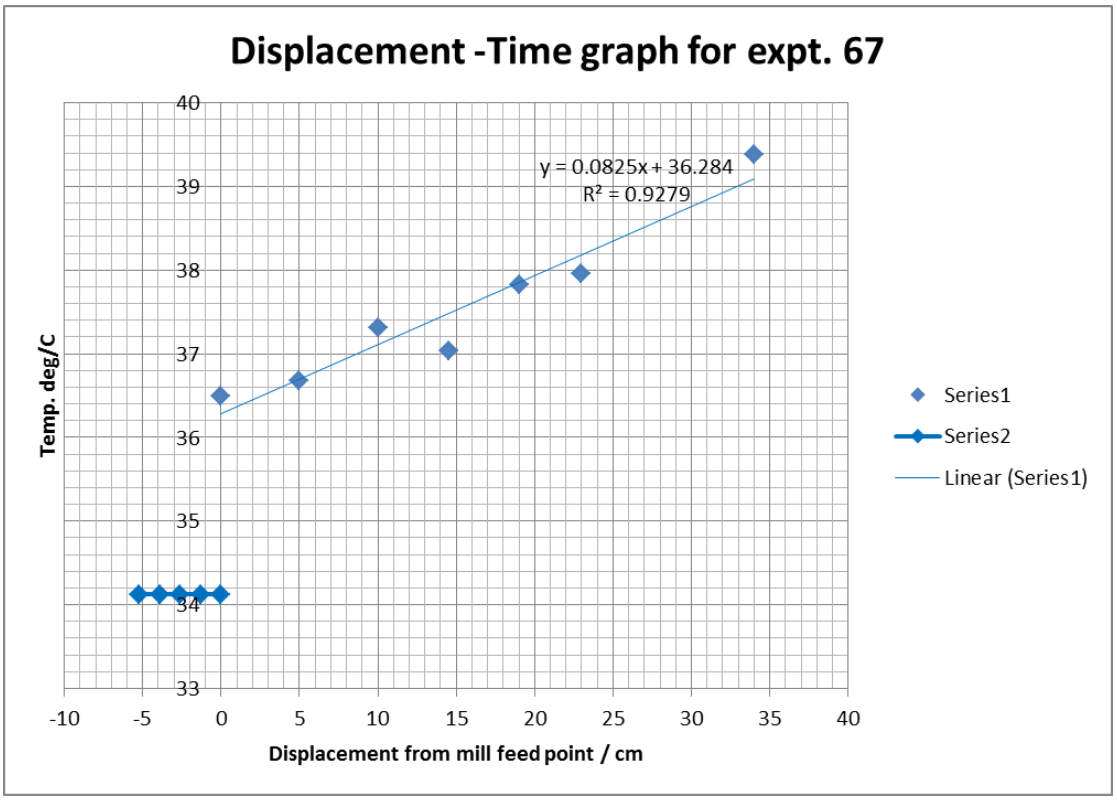

Figure 5.7: Temperature-Displacement graph for experiment 67.

Further analysis of the temperature-displacement relationships, expt.65 taken as an example:

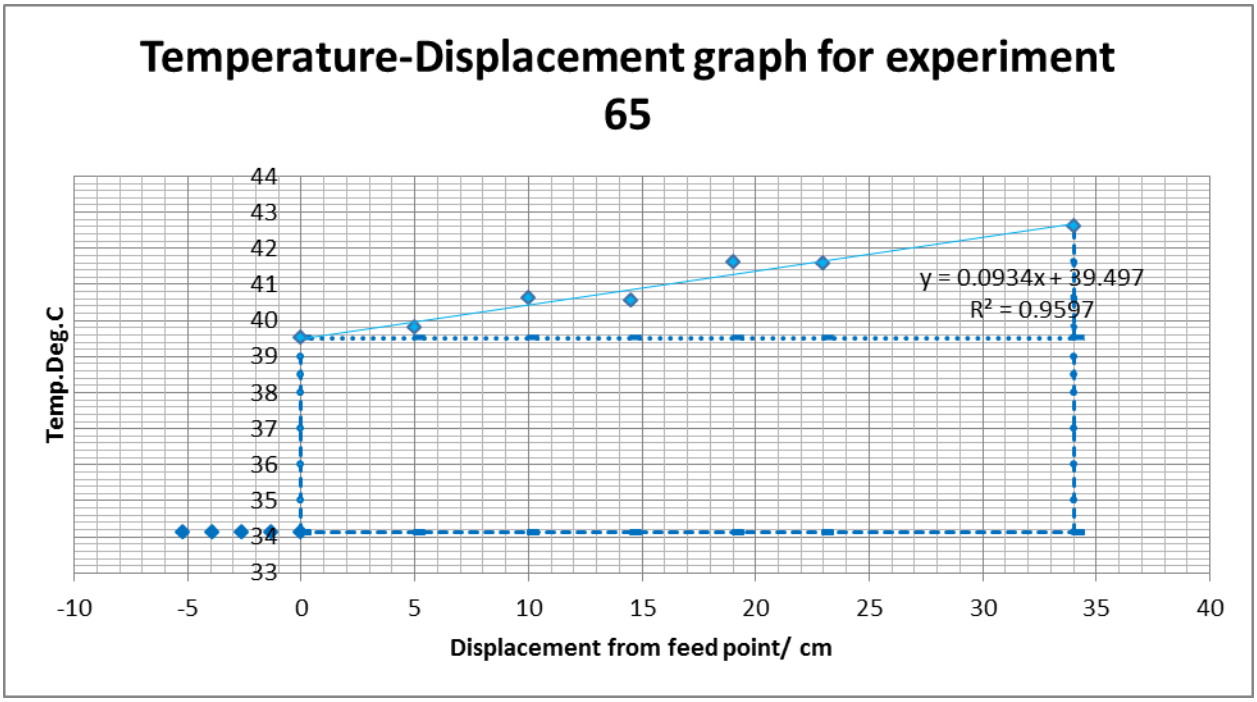

Fig 5.8 : Temperature-Displacement graph.

Closer examination of the above temperature-displacement relationship shows that as the feed enters the mill, there is a step rise in the slurry temperature and the slurry temperature then progressively rises linearly from the feed point to the discharge point. The step rise in the temperature can be attributed to the continuous recirculation of slurry, media and oversize particles which takes place within the mill due to internal media and oversize particle classification. Thus, the mill has a certain constant minimum temperature due to axial mixing

The rise in temperature along the mill length shows a progressive generation of energy due to milling along the length of the mill.

5.4 Effects of mill variables on the temperature profiles and PSD

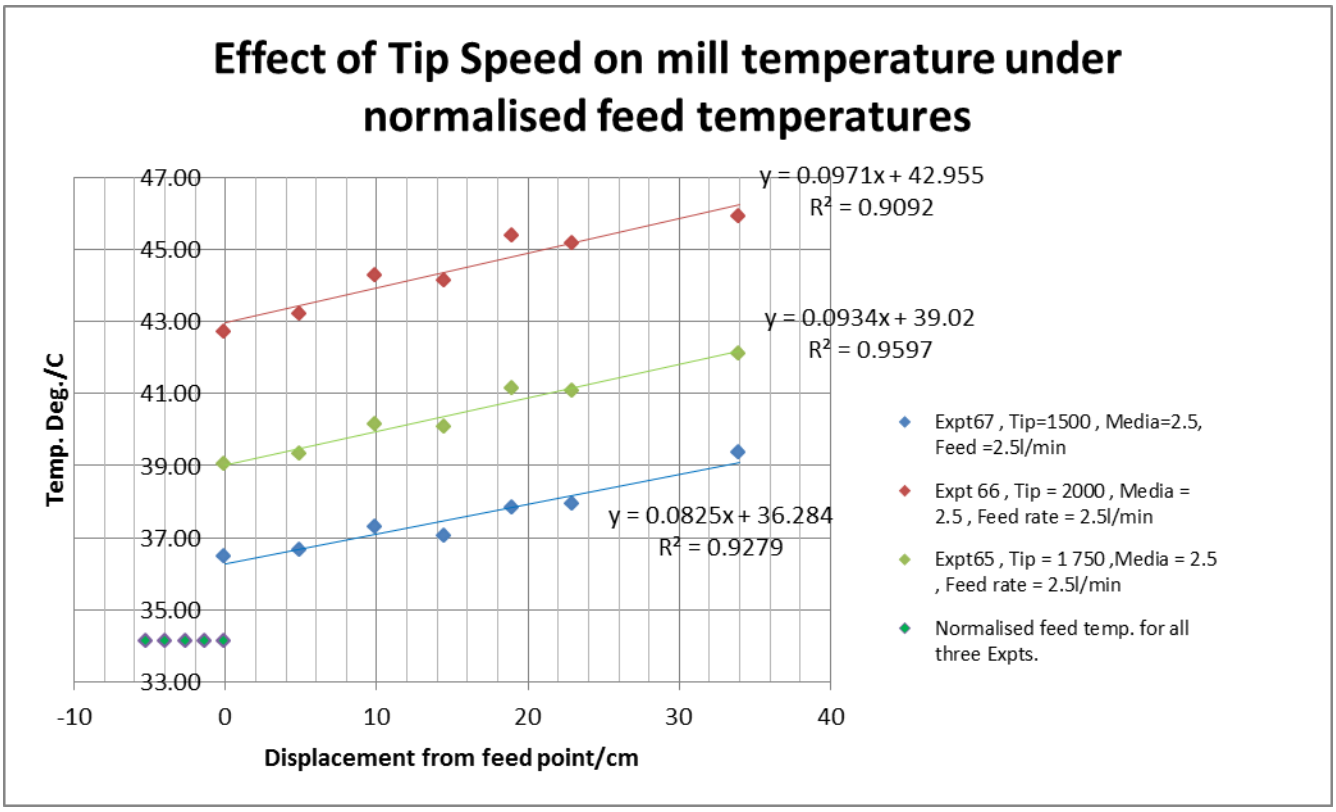

Fig 5.9: Temperature-Displacement graph: Effect of Tip speed on temperature profiles.

As the tip speed increases, more energy is generated in the mill. This is due to increase in attrition between the ore particles and the media.

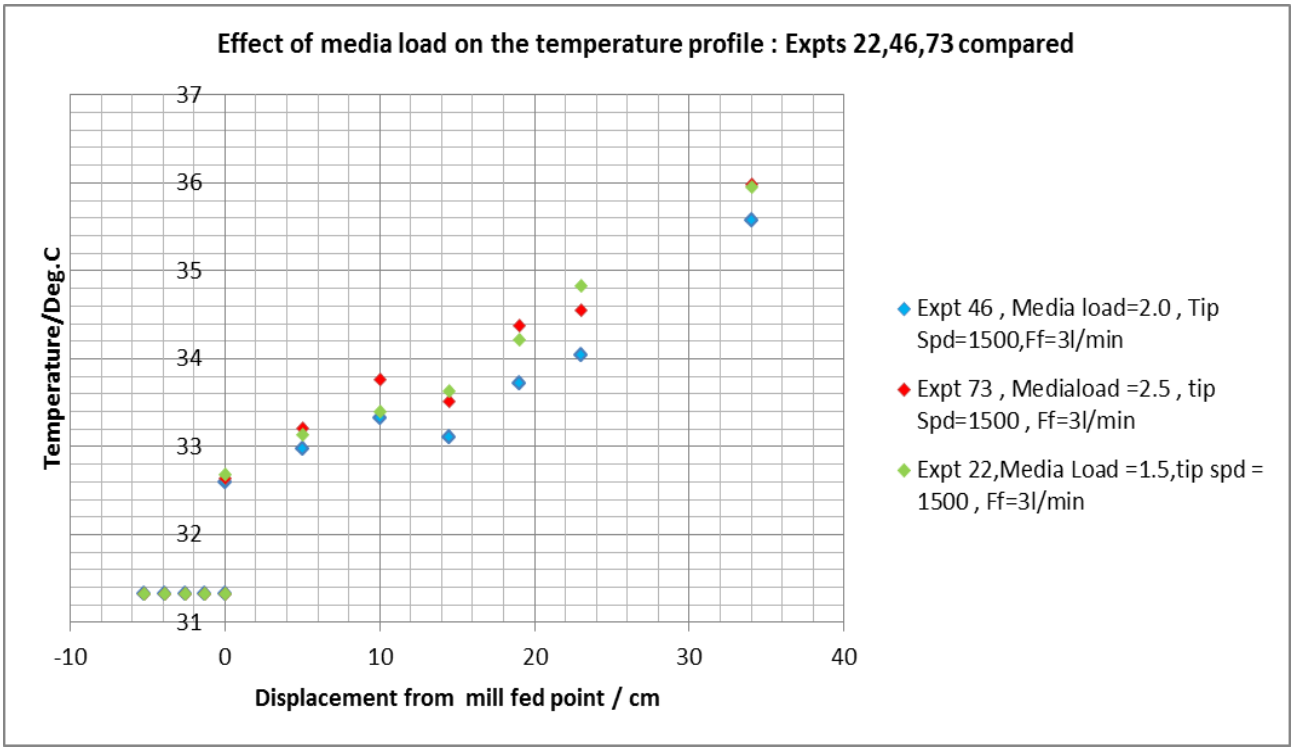

Fig 5.10: Temperature-Displacement graph: Effect of media load on the temperature profile.

The lowest temperature profile is when the media load is 2.0 litres (50%) of mill volume. However at media loads of 1.5 and 2.5 the effect of media load is not very clear cut as the temperatures at these loads are almost similar though they are higher than those at 2.0 litre media load.

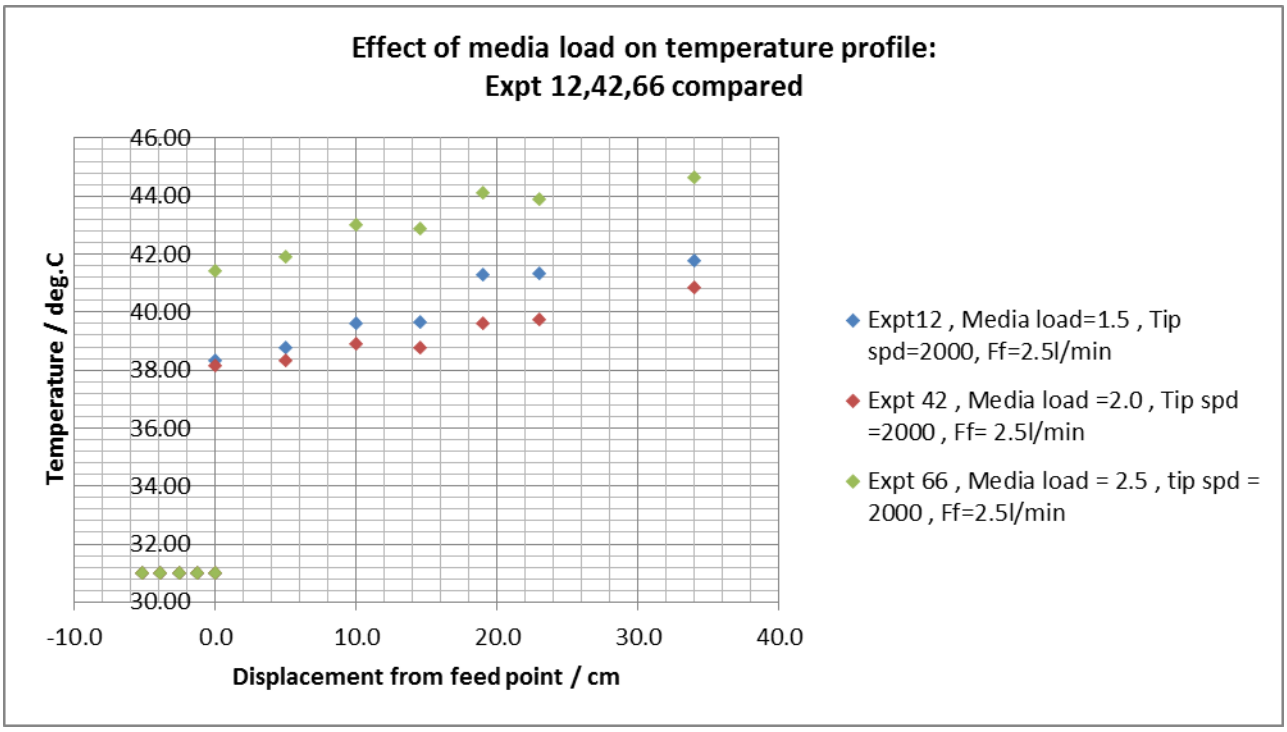

Fig 5.11: Temperature-displacement graph: Effect of media load on temperature profiles.

A second extract after Fig 5.10 was taken to further investigate the effect of media load on the profile and Fig 5.11 above shows that the 50% media load of 2.0 still has the lowest temperature profile. The highest temperature profile is obtained when the media load of 2.5 (62.5%) is used.

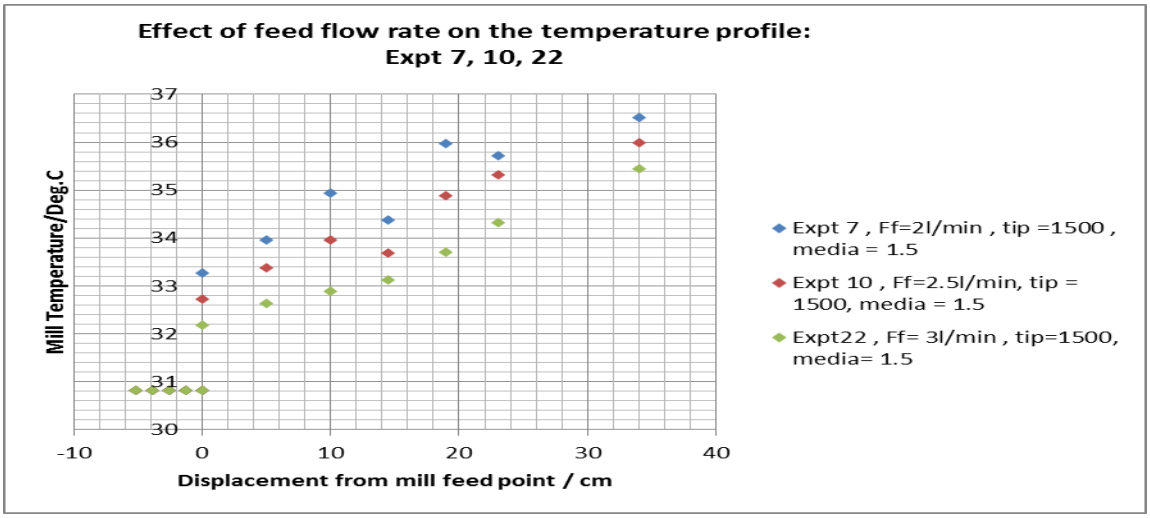

Fig 5.12: Effect of flow rate on the temperature

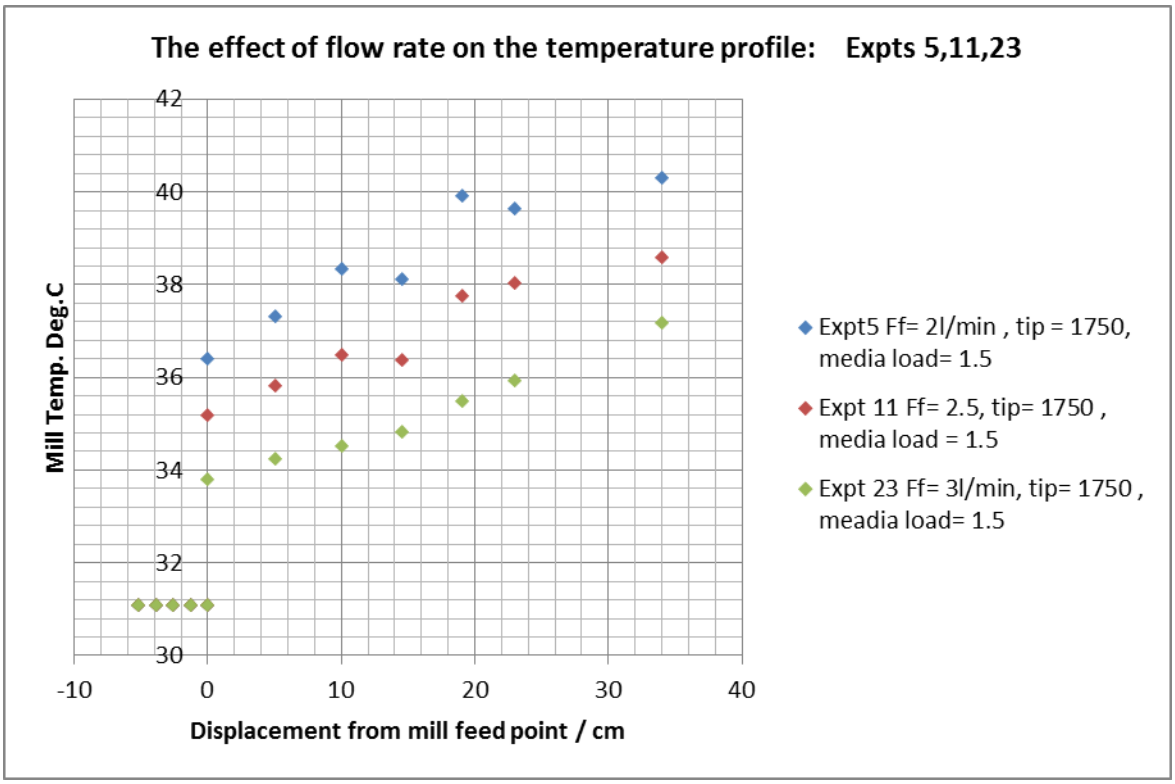

Fig 5.13: Effect of flow rate on the temperature profile.

As the flow rate increases, the temperature profile decreases. This is attributed to the little residence time that results due to high flow rate. This could be due to the heat generated being distributed over more slurry for the same quantity of heat generated, so temperature decreases.

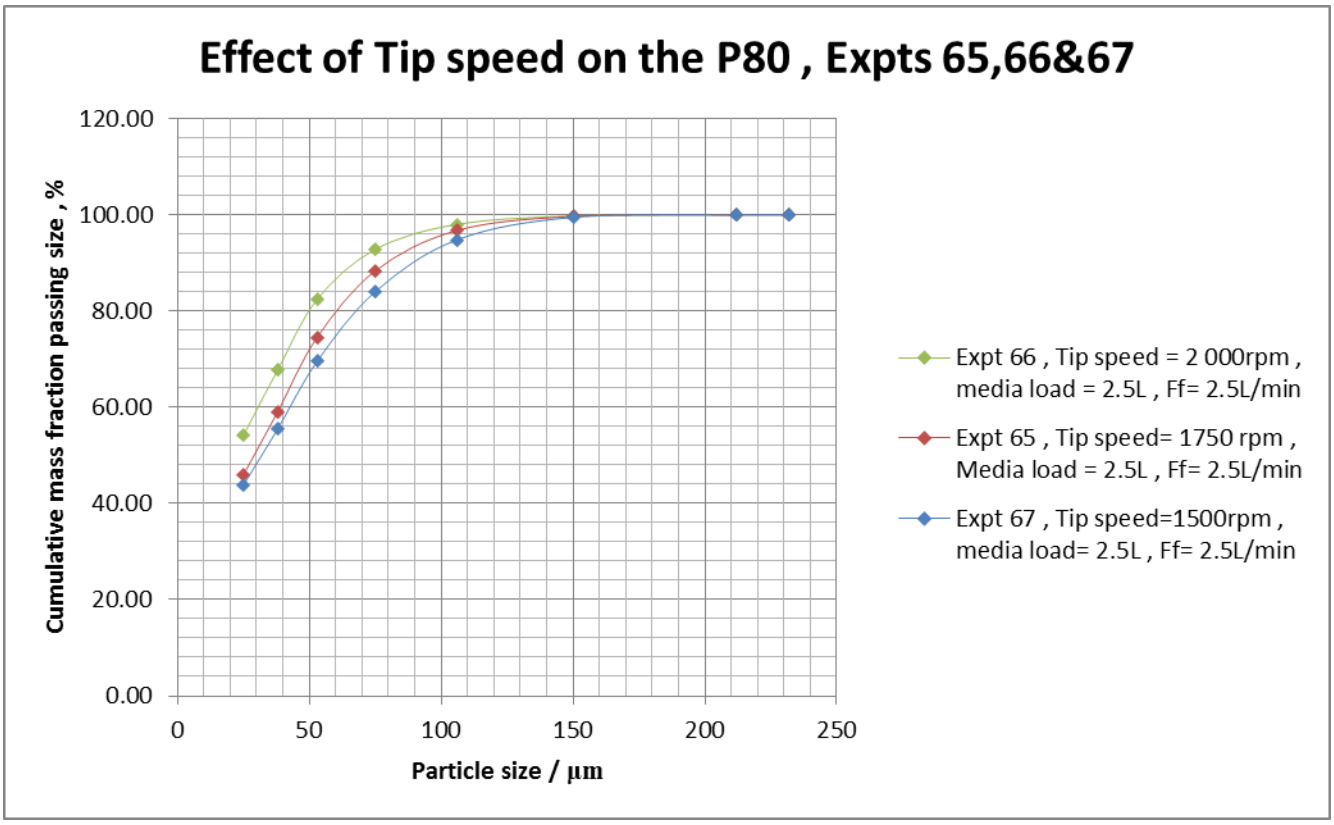

Fig 5.14: Effect of tip speed on PSD.

The higher the tip speed, the sharper the particle size distribution is. At higher tip speeds, there are greater chances that more particles will be subjected to the same amount of attrition forces, thus increasing the chances of them breaking to the same extent.

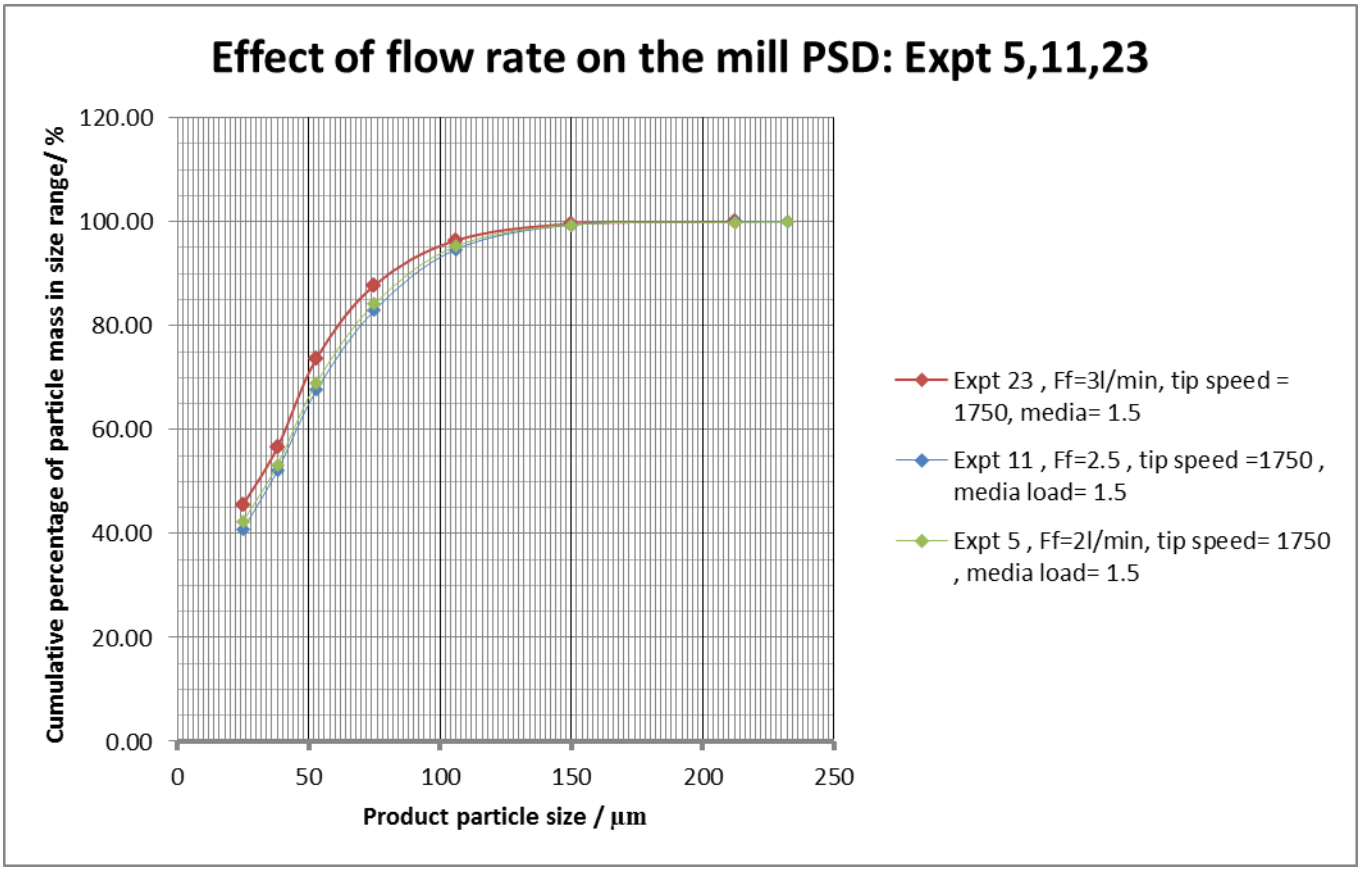

Fig 5.15: Effect of flow rate on the PSD.

For the tests that were done, the relationships between PSD and flow rate is not very clear-cut.

The effect of media load on product PSD.

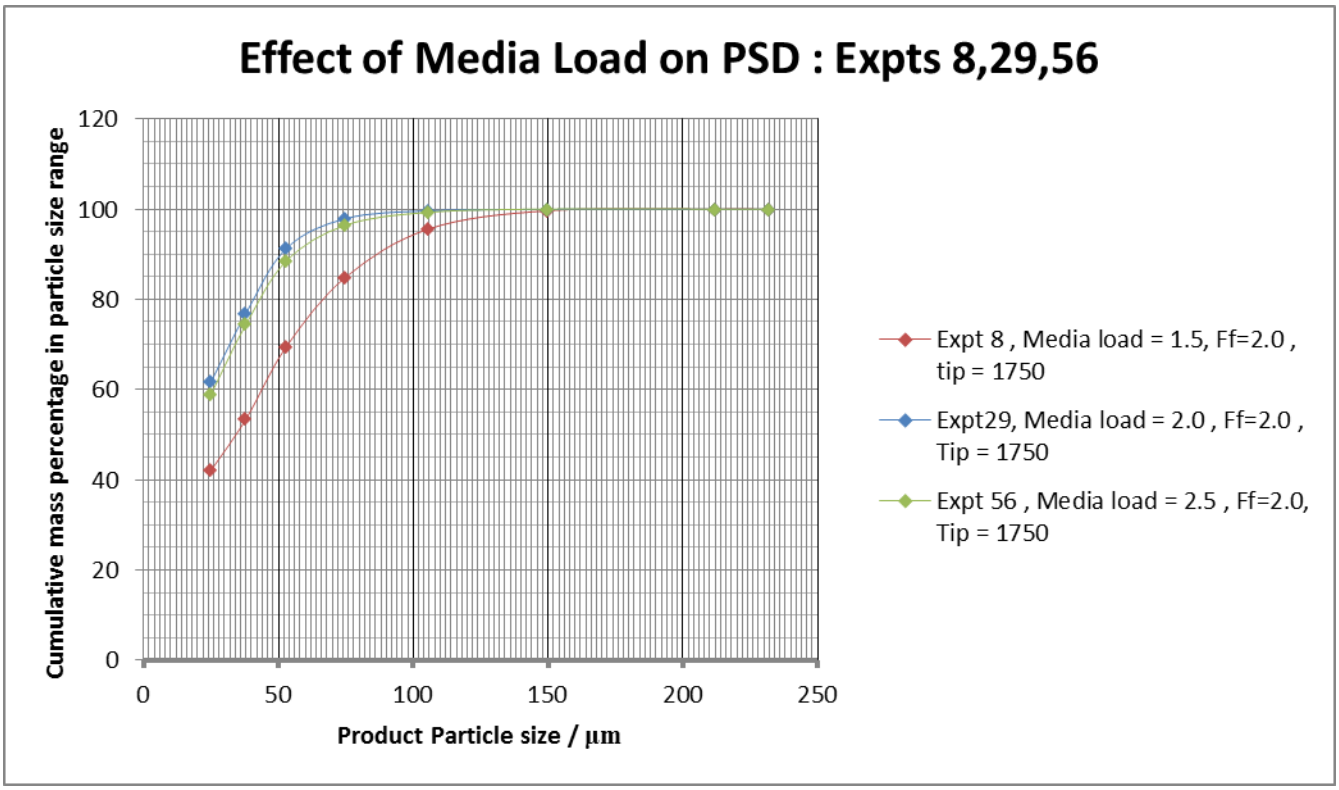

Fig 5.16: Effect of media load on PSD.

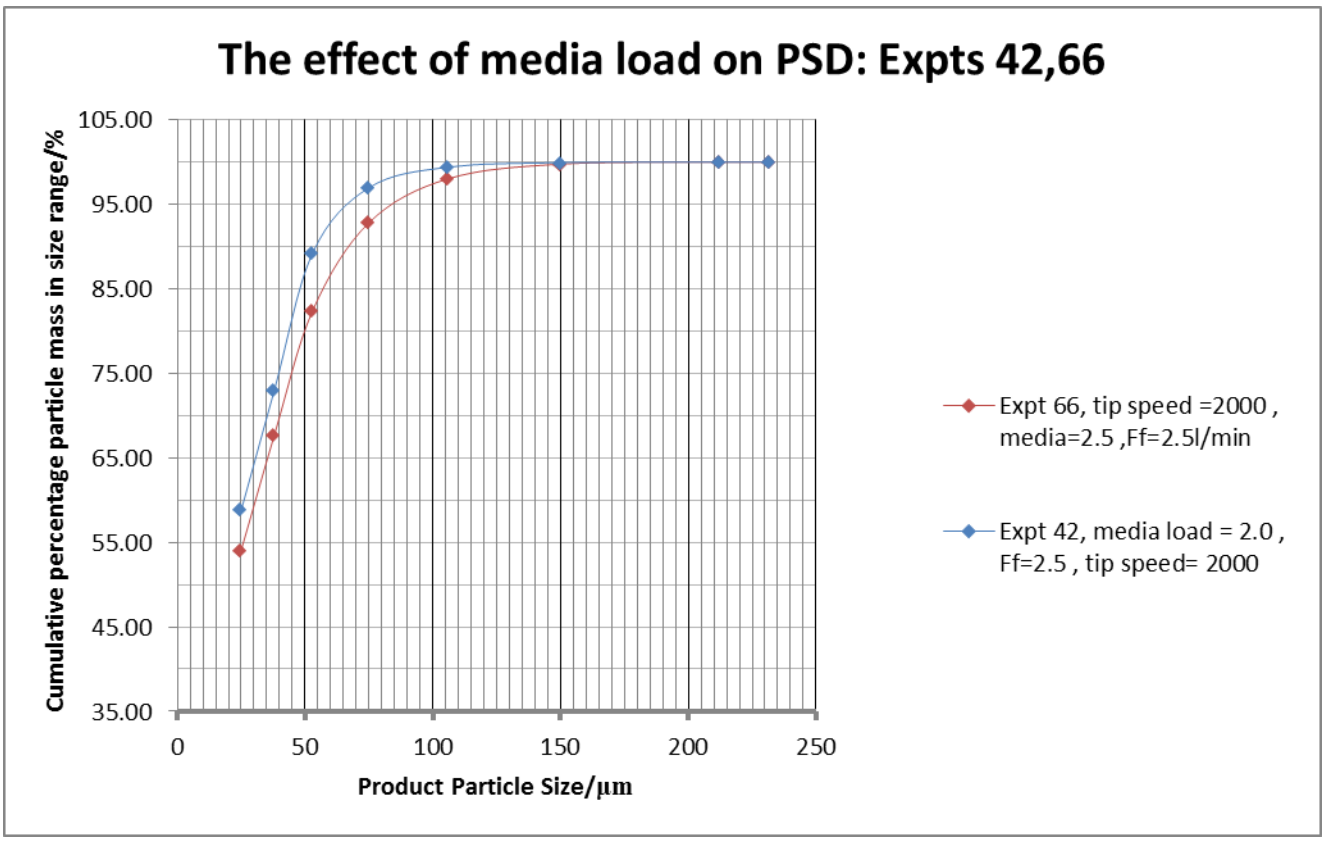

Fig 5.17: Effect of media load on PSD.

The PSD is finer at 2.0 media load than at 2.5 media load.

The table 5.6 below is a qualitative summary of the interrelationships between the mill variables and the resulting temperature profiles and product particle size distributions. A mathematical model was needed to show the quantitative relationship. This is described in Chapter 6.

Table 5.6: The effect of process variables on the temperature profile and particle size distribution (PSD).

Process variable	**Effect on temperature profile**	**Effect on particle size distribution**
Tip speed	Mill temperature rises with increase in tip speed.	PSD becomes finer with increase in tip speed.
Flow Rate	Mill temperature drops with increase in feed flow rate.	PSD becomes finer with increase in flow rate.
Media load	Temperature increases with increase in media load.	The PSD is narrowest at media load of 2.0 narrower at media load of 2.5 and narrow at a media load of 1.5

5.5 Conclusion

In summary, the mill temperature rises with increase in tip speed and media load. The temperature decreases with increase in feed flow rate. PSD becomes finer with increase in tip speed and flow rate. At higher media loads, the PSD is finer than it is at lower media loads.

Following the above qualitative analysis of the different variables affecting the process performance of the IsaMill, a mathematical model was proposed to have a quantitative description of the interaction between these mill variables.

The next chapter, Chapter 6, describes the procedure used in developing the predictive model as well as the comparison of the model results with experimental test results.

CHAPTER 6

MODEL DEVELOPMENT AND TESTING

6.1 Introduction

In order to quantitatively analyse load behaviour in the IsaMill, a predictive model which was based on a steady state mass and energy balance was developed. This Chapter uses the experimental results from Chapter 5 above to develop a semi-empirical mathematical model that describes the milling process. Through a back-calculation process, the model parameters were determined. These model parameters were then used to develop a mathematical model that could be used to predict the degree of mixing in the IsaMill.

6.2 Model Basis and Structure

The following assumptions were used in developing the model:

(1) The specific heat capacity of the slurry is constant.
(2) Slurry density is maintained in the feed to the mill.
(3) The heat transfer coefficient is uniform along the length of the mill (also at steady state , the feed specific heat capacity is the same as the in-mill and discharge specific heat capacities, Cp was calculated from available mineralogical data from Anglo labs).
(4) A uniform backflow within the mill.
(5) Power draw from the mill is distributed uniformly between the seven sections into which the mill is divided
(6) Energy used in size reduction was taken to be negligible (Metzger 2011).
(7) Energy losses due to noise were considered negligible.
(8) Ambient temperature was assumed constant during each mill steady state.
(9) Energy absorbed by media was considered negligible.

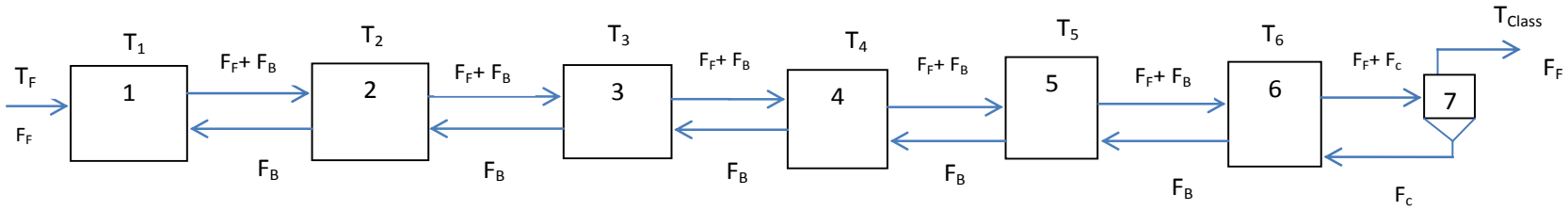

Fig. 6.1 : Model flow diagram.

Fig 6.1 above is a diagrammatic illustration of the model process flow diagram. The IsaMill was divided into seven perfectly mixed cells as illustrated above, each cell with a back mixing component represented by F_B.

Let β = $\frac{F_B}{F_B + F_F}$ ----------6.1

========> $F_B = \frac{\beta}{1-\beta} F_F$ ----------6.2

thus $F_B = \alpha F_F$ where $\alpha = \frac{\beta}{1-\beta}$ ----------6.3

Let the recirculation ratio be $C = \frac{F_C}{F_F + F_C}$ ----------6.4

=====> $F_C = \frac{CF_F}{1-C}$ ----------6.5

Let $\theta = \frac{C}{1-C}$ ----------6.6

The following mill variables were used in the model development process:

1. Power draw, P (KW)

2. Feed flow rate, F_F (Kg/s)

3. Slurry specific heat capacity, C_p (KJ/Kg.K)

4. Measured mill temperatures, T_i (^oC)

5. Slurry feed temperature T_F (^oC)

6. Heat transfer coefficien, h ($KJ/m^2.K$)

7. Ambient temperature, T_{Amb} (^oC)

8. Separator recirculation ratio, C (ratio)

9. Separator backflow F_c (Kg/s)

10. Backmixing flow rate, F_B (Kg/s)

11. Mill back mixing coefficient, α or β (interchangeable as per equations 6.2 and 6.3). β is always a positive number less than one. The closer it is to one, the more back mixing there is. A lower back mixing coefficient will mean process approaching more plug flow and the reverse will mean process approaching more perfect mixing.

12. Cell heat transfer areas, $A_1 – A_7$ (m^2)

These mill operating variables and parameters were integrated into the material and energy balance as below:

The following was the basis for the overall energy balance:

Energy of the slurry feed to the mill + Energy input by the mill =

Energy in exit slurry at elevated temperature + Energy Loss to the environment through the mill shell + Energy used in size reduction.----------6.7

Energy used in size reduction was considered negligible.

Thus, considering the full section of the mill, below is an illustration of the overall mill mass and energy balance.

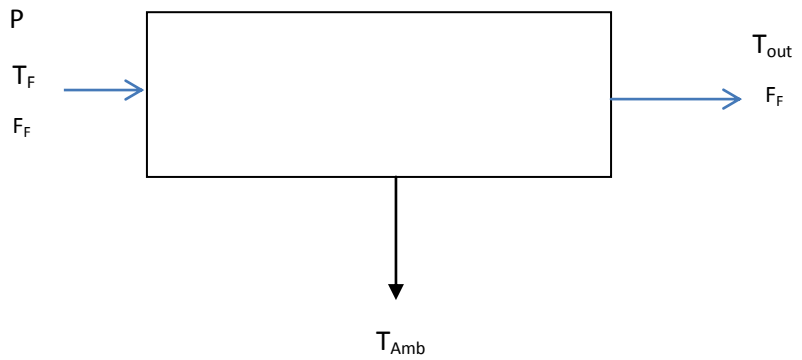

Fig 6.2: Illustration of the mill mass and energy balance.

The above mass balance equation then translates to:

$$F_F C_p T_F + P = F_F C_p T_{out} + hA(T_{out} - T_{Amb}) \quad \text{----------6.8}$$

The above energy conservation principle was used to calculate the temperatures within individual cells along the length of the mill. An approach similar to the tanks-in-series model of Makokha and Moys, 2011 was adopted. Below is an illustration of how the approach was used in the first section of the mill, denoted as cell no.1. The mill was divided into seven cells, in six of which the actual grinding action took place. The last cell involved separation of media and oversize particles from the slurry at discharge. The power draw of the mill, P was divided by seven to indicate energy supplied to each of the seven cells.

6.3 Model Development

Material and energy balance on cell1.

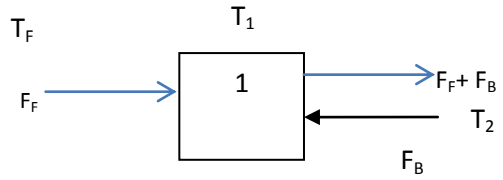

Fig. 6.3: Material and energy balance on cell 1.

$$F_F C_P T_F + \frac{P}{7} + F_B C_P T_2 = (F_B + F_F) C_P T_1 + hA_1 (T_1 - T_{Amb}) \text{ ---------- } 6.9$$

Substituting $\alpha = \frac{\beta}{1-\beta}$

And replacing F_B with αF_F,

The equation 6.9, above when re-arranged reduces to:

$$-[(1+\alpha) F_F C_P + hA_1] T_1 + \alpha F_F C_P T_2 = -\frac{P}{7} - F_F C_P T_F - hA_1 T_{Amb} \text{ ---------- } 6.10$$

Material and energy balance on cell2.

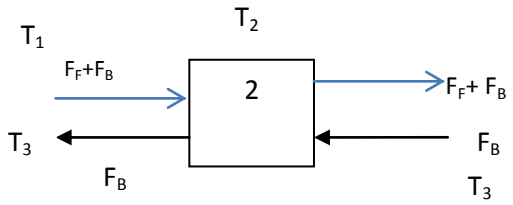

Fig 6.4 : Material and energy balance on cell 2.

$(F_F + F_B)C_P T_1 + \frac{P}{7} + F_B C_P T_3 = (F_B + F_F)C_P T_2 + F_B CpT_2 + hA_2(T_2 - T_{Amb})$ Substituting $\alpha = \frac{\beta}{1-\beta}$

, the above equation reduces to

$$F_F(1+\alpha)C_P T_1 + \alpha F_F C_P T_3 - [(1+\alpha)F_F + \alpha F_F + hA_2]T_2 = -\frac{p}{7} - hA_2 T_{Amb}$$

Rearranging gives;

$$F_F(1+\alpha)C_P T_1 - [(1+\alpha)F_F + \alpha F_F + hA_2]T_2 + \alpha F_F C_P T_3 = -\frac{p}{7} - hA_2 T_{Amb} \text{ ----------6.11}$$

Using the same technique, carrying out a combined mass and energy balance and rearranging the equations by putting constants on the right hand side of the equation for the subsequent cells gives:

Balancing on cell 3,

$$(F_F + F_B)C_P T_2 + F_B C_P T_4 + \frac{P}{7} = (F_F + F_B)C_P T_3 + F_B C_P T_3 + hA_3 T_3 - hA_3 T_{Amb}$$

$$==> (F_F + \alpha F_F)C_P T_2 + \alpha F_F C_P T_4 + \frac{P}{7} = (F_F + \alpha F_F)C_P T_3 + \alpha F_F C_P T_3 + hA_3 T_3 - hA_3 T_{Amb}$$

$$= [F_F(1+\alpha)C_p + \alpha F_F C_P + hA_3]T_3 - hA_3 T_{Amb}$$

$$F_F(1+\alpha)C_P T_2 - [F_F(1+\alpha)C_P + \alpha F_F C_P + hA_3]T_3 + \alpha F_F C_P T_4 = -\frac{P}{7} - hA_3 T_{Amb} \text{ ------6.12}$$

Balancing on Cell 4,

$$(F_F + F_B)C_P T_3 + F_B C_P T_5 + \frac{P}{7} = (F_F + F_B)C_P T_4 + F_B C_P T_4 + hA_4 T_4 - hA_4 T_{Amb}$$

$$===> (F_F + \alpha F_F)C_P T_3 + \alpha F_F C_P T_5 + \frac{P}{7} = (F_F + \alpha F_F)C_P T_4 + \alpha F_F C_P T_4 + hA_4 T_4 - hA_4 T_{Amb}$$

$$===> F_F(1+\alpha)C_P T_3 - [F_F(1+\alpha)C_P + \alpha F_F C_P + hA_4]T_4 + \alpha F_F C_P T_5 = -hA_4 T_{Amb} - \frac{P}{7}$$

$$F_F(1+\alpha)C_P T_3 - [F_F(1+2\alpha)C_P + hA_4]T_4 + \alpha F_F C_P T_5 = -\frac{P}{7} - hA_4 T_{Amb} \text{ ----------} 6.13$$

Balancing on Cell 5,

$$(F_F + F_B)C_P T_4 + \frac{P}{7} + F_B C_P T_6 = (F_F + F_B)C_P T_5 + F_B C_P T_5 + hA_5 T_5 - hA_5 T_{Amb}$$

$$(F_F + \alpha F_F)C_P T_4 + \frac{P}{7} + \alpha F_F C_P T_6 = (F_F + \alpha F_F)C_P T_5 + \alpha F_F C_P T_5 + hA_5 T_5 - hA_5 T_{Amb}$$

$$===> (1+\alpha)F_F C_P T_4 - [(1+\alpha)F_F C_P + \alpha F_F C_P + hA_5]T_5 + \alpha F_F C_P T_6 = -hA_5 T_{Amb} - \frac{P}{7}$$

$$F_F(1+\alpha)C_P T_4 - [F_F(1+2\alpha)C_P + hA_5]T_5 + \alpha F_F C_P T_6 = -\frac{P}{7} - hA_5 T_{Amb} \text{ ----------} 6.14$$

Balancing on Cell 6,

$$(F_F + F_B)C_P T_5 + F_C C_P T_7 = (F_F + F_C)C_P T_6 + F_B C_P T_6 - \frac{P}{7} + hA_6 T_6 - hA_6 T_{Amb}$$

$$==> (F_F + \alpha F_F)C_P T_5 + F_C C_P T_7 = (F_F + \theta F_F)C_P T_6 + \alpha F_F C_P T_6 - \frac{P}{7} + hA_6 T_6 - hA_6 T_{amb}$$

$$===> F_F(1+\alpha)C_P T_5 - [F_F(1+\theta)C_P + \alpha F_F C_P + hA_6]T_6 + F_C C_P T_7 = -\frac{P}{7} - hA_6 T_{Amb}$$

$$F_F(1+\alpha)C_P T_5 - [F_F(1+\theta+\alpha)C_P + hA_6]T_6 + \theta F_F C_P T_7 = -\frac{P}{7} - hA_6 T_{Amb} \text{ ----------} 6.15$$

Balancing on Cell 7,

$$(F_F + F_C)C_P T_6 + \frac{P}{7} = F_F C_P T_7 + F_C C_P T_7 + hA_7 T_7 - hA_7 T_{Amb}$$

$$===> (F_F + \theta F_F)C_P T_6 = F_F C_P T_7 + \theta F_F C_P T_7 + hA_7 T_7 - hA_7 T_{Amb} - \frac{P}{7}$$

$$===> (1+\theta)F_F C_P T_6 = F_F C_P T_7 + \theta F_F C_P T_7 + hA_7 T_7 - hA_7 T_{Amb} - \frac{P}{7}$$

$$(1+\theta)F_F C_p T_6 - [(1+\theta)F_F C_P + hA_7].T_7 = -hA_7 T_{Amb} - \frac{P}{7} \text{ ---------- } 6.16$$

The above mass and energy balances result in seven equations (for cells 1 to 7) , seven variables (T1 to T7) and two mill parameters(β and C). Thus , there will be need for an optimisation technique to help in coming up with a solution to the matrix of equations by assigning initial estimates to the two parameters and running the programme iteratively until convergence.

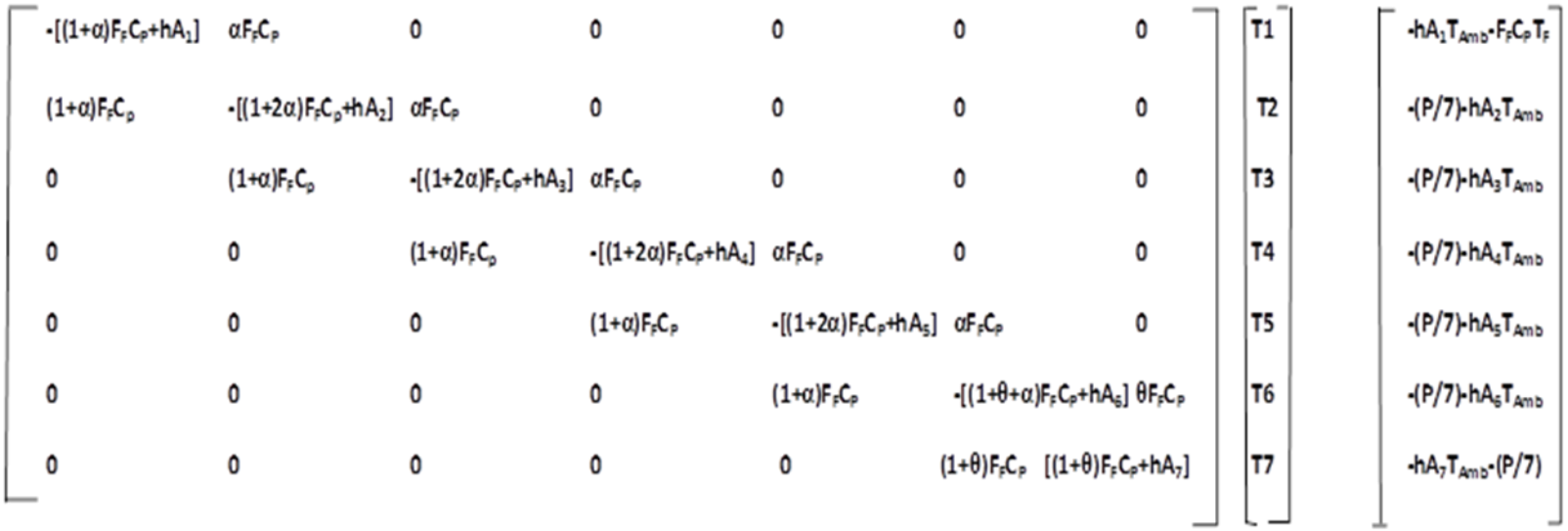

Figure 6.5: Matrix representation of the material and energy balance equations.

The above matrix can be represented by the below matrix multiplication equation:

[A][T]=[C]----------6.17

Where matrix A represents the coefficients of temperature, T represents the temperature column matrix and the C matrix represents the constants.

Thus, to find [T], both sides of the above equation are multiplied by the inverse of matrix A (Holman, J.P, Heat Transfer, 10th Edition, McGraw Hill International Edition). ===>$[T]=[A]^{-1}[C]$----------6.18

An Excel Matrix Inversion technique was used to solve the above system of equations with initial estimates of the mill internal parameters β and C. An Excel add-in , Solver was then used to compute the optimum values of β and C , with the objective function being to minimise the sum of square of errors between model and measured values subject to the constraints that β and C are non-negative and less than or equal to one. Running this programme would then produce the predicted model temperatures.

The values of β and C were then computed for each process condition to have an indication of the nature of load behaviour in the IsaMill under various process conditions and also to relate these parameter values to the different mill variables by varying one variable while keeping the other mill operating variables constant.

This analysis was achieved by plotting the variation between the mill parameters β and C and each particular process condition to have an indication of the optimum mill operating conditions that would help achieve the most desired process outputs for particular operational needs, that is whether the operational need is output tonnage or a particular particle size distribution.

The model predictions were then compared with the actual measured temperatures and below are graphical extracts showing the relationship between the measured temperatures and the model temperatures as functions of the displacement of the temperature sensors from feed point to discharge point. The displacement of the feed temperatures were conveniently assigned negative values for illustrative purposes to graphically show how the feed temperature changes as the slurry enters the mill. The section below describes how the Fig. 6.5 matrix model constants were arrived at. These constants were input into the excel model spreadsheet to compute the optimum values for the mill parameters β and C.

Calculation of the model constants

Slurry composition

The average in-mill slurry composition is 35% solids (m/m). The S.G of the UG2 ore is 3.8 (Anglo laboratory reports) and the S.G of water is 1.0.

From the 35% (m/m) slurry composition above, let one litre of slurry be *X kg*.

Therefore, one litre slurry contains 0.35*X* kg of ore and 0.65*X* kg of water.

Now, to calculate the specific gravity of the slurry, considering one litre of slurry, since density of water = 1kg/l, therefore, 0.65*X* litres of water will be present.

Since density of the ore is 3.8kg/litre, therefore, the volume of the solids 0.35*X*/3.8

Therefore, total volume of slurry = 1 litre = 0.65*X*+0.35*X*/3.8

=➔ X = 1.348 kg,

From the above mass balancing, the average slurry S.G = 1.348 = 1.348 kg per litre of slurry

= 1 348 kgm^{-3} of slurry.

=➔ 35% solids kg ore = 0.35*1.348 kg = 0.4718 kg of solids per litre of slurry.

65% mass kg water = 0.65*1.348kg = 0.8762 kg of water per litre of slurry.

Now, considering a steady state mill operation, since $\rho = m/v$

⇨ $m = \rho v = 1\ 348 * V_{Slurry}$ (kg/s)

Using the above mass balance notation ➔ $m = \rho F_F = 1\ 348 F_F$ where F_F is the slurry feed flow rate (m^3/s) and F_F not being the same as Ff used in chapter 3.

Converting Slurry flow rate from, Litres per minute to M^3 per second;

- The recorded flow rate will be multiplied by (1/60 000), thus F_F = (L/60 000) m^3/s where L is the flow rate in litres per minute.

- Thus , a flow rate of 2.5litres per minute will translate to a mass flow rate of
- 1 348*2.5/60 000 kg/s = 0.0562 kg/s.

Calculation of the slurry specific heat capacity

(i) The specific heat capacity of water is 4 180 J/kg.K

(ii) The specific heat capacity of the UG2 ore; this is calculated basing on the average ore composition and the average specific heat capacities of the ore constituents.

The tables below show the average composition of the UG2 ore:

Table 6.1: Bulk mineralogical composition (Anglo American Laboratory data sheets, www.cmmp-france.com/chromitegb.html:18/03/2013, Haselton, et al , 1984)

Mineral	**Proportion %**	**Density(S.G)**	**Cp**
Pyroxene	38.4	3.2-3.46	621 J/kg.K
Chromite	36.8	4.5-5.09	900 J/kg.K
Feldspar	17.5	2.62	Calculated by correlation.
Olivine	0.6		
Alteration Silicates	3.9		
Other Silicates	1.7		
Base metal sulphides	0.3		
Other	0.8		
Total	100		

The minerals Pyroxene, Chromite and Feldspar are the main constituents of the UG2 ore and their physical property data was used to estimate the ore specific heat capacity, Cp ore. The table below gives the relative abundance of the Base Metal Sulphides in the feed, which mainly consists of pyrite, pyrrhotite, pentlandite and chalcopyrite.

Table 6.2: Base Metal Sulphides: relative abundance (Anglo laboratories data sheets)

Sulphide Group	**Proportion %**
Fe-Sulphides	26.9
Ni-Sulphides	49.3
Cu-Sulphides	23.8
Total	100.0
Mass %	0.26

The specific heat capacity of Feldspar (Albite) was calculated from the following correlation (Haselton, et al, 1984).

$Cp = 583.9 – 0.09285T+2.272X10^{-2}T^{2} – 642T^{-0.5} + 1.678T^{-2}$ J/mol.K, T = 28^{o}C = 301K.

= 539.53J/kg.K

Chemical formula for Albite; $NaAlSi_3O_8$ $M_r = 263.02$

Chemical formula for Pyroxene, $CaAl_2SiO_6$, $M_r = 218.1$, Cp = 135.3 J/mol.K

The average specific heat capacity of the ore was calculated from the individual proportions of the ore and the individual specific heat capacities of each constituent for the three major constituents of the UG2 ore.

Thus, the average specific heat capacity of the ore was calculated as:

$Cp_{Ore} = 0.384x621+0.368x900+0.175x539.53$

= 238.464+331.2+94.42

=664.08 J/kg.K

Cp_{H2O} =4 180 J/kg.K

Therefore, average slurry specific heat capacity is (0.35x664.08 +0.65x4 180) J/kg.K

= (232.43+2717)J/kg.K

=2 949.43 J/kg.K

=**2.949KJ/kg.K**

Calculation of the overall heat transfer coefficient, h

The concept of resistance to heat transfer through multiple barriers was used(www.spiraxsarco.com/resources/steam engineering:05/07/2013).

. The barriers to heat transfer through the mill include rubber lining, stainless steel shell and the film of air to the external environment.

Thus, $h = \frac{1}{R_1 + R_2 + R_3}$ ----------6.19

Where R_1, R_2,R_3 are the individual resistances to heat transfer from rubber lining , stainless steel shell and the thin film of air on the steel shell.(www.spiraxsarco.com/resources/steam engineering:05/07/2013).

$===> h = \frac{1}{\frac{x_1}{k_1} + \frac{x_2}{k_2} + \frac{x_3}{k_3}}$ ----------6.20

Where, x_1 is thickness of rubber lining, x_2 is the thickness of the steel shell and x_3 is the thickness of the thin air film surrounding the mill shell. k_1 is the thermal conductivity of the rubber lining , k_2 is the thermal conductivity of the steel shell and k_3 is the thermal conductivity of air.

Table 6.3: Mill Data (www.electronicscooling.com:2001,www.spiraxsarco.com/resources/steam-engineering:05/07/2013)

Material	**Thickness (mm)**	**Thermal Conductivity (W/m.K)**
Stainless Steel	7.5	28.56
Rubber	5.0	0.29
Air	2.14	0.025

Using the data table above and equation 6.20 above, below is an estimate of the overall heat transfer coefficient across the M4 mill.

$$h = \frac{1}{\frac{0.0075}{28.56} + \frac{0.005}{0.29} + \frac{0.00214}{0.025}} = 9.6989 W/m^2 k = 0.009699 KW/m^2.K$$

Calculation of heat transfer area:

Mill external diameter,D = 160mm = 0.16m.

Mill heat transfer area = πxDxL, where L is the length of the section of the mill where heat transfer will be taking place.

Thus, heat transfer area = 0.5029xL

Table 6.4 below is a summary of the relative positions of the temperature sensors from the feed point to the mill discharge point as well as the heat transfer areas associated with each section of the mill.

Probe/Sensor position	Displacement from feed point (cm)	Width of heat transfer section , L , (mm)	Heat transfer area,m^2(0.50265x10 $^{-3}$L) A_1---A_7
1	0	40	0.020
2	5	40	0.020
3	10	40	0.020
4	14.5	45	0.023
5	19	45	0.023
6	23	45	0.023
7	34	105	0.053

The above data were used in computing the model constants and they were input into the model matrix to calculate the optimum β and C values(under the given mill operating conditions) that would give the best fit between the observed experimental data and the model data.

The six figures below illustrate some of the observed relations between measured and model data. The balance of the steady state observations are illustrated in Appendix B.

6.4 Model Validation and Results

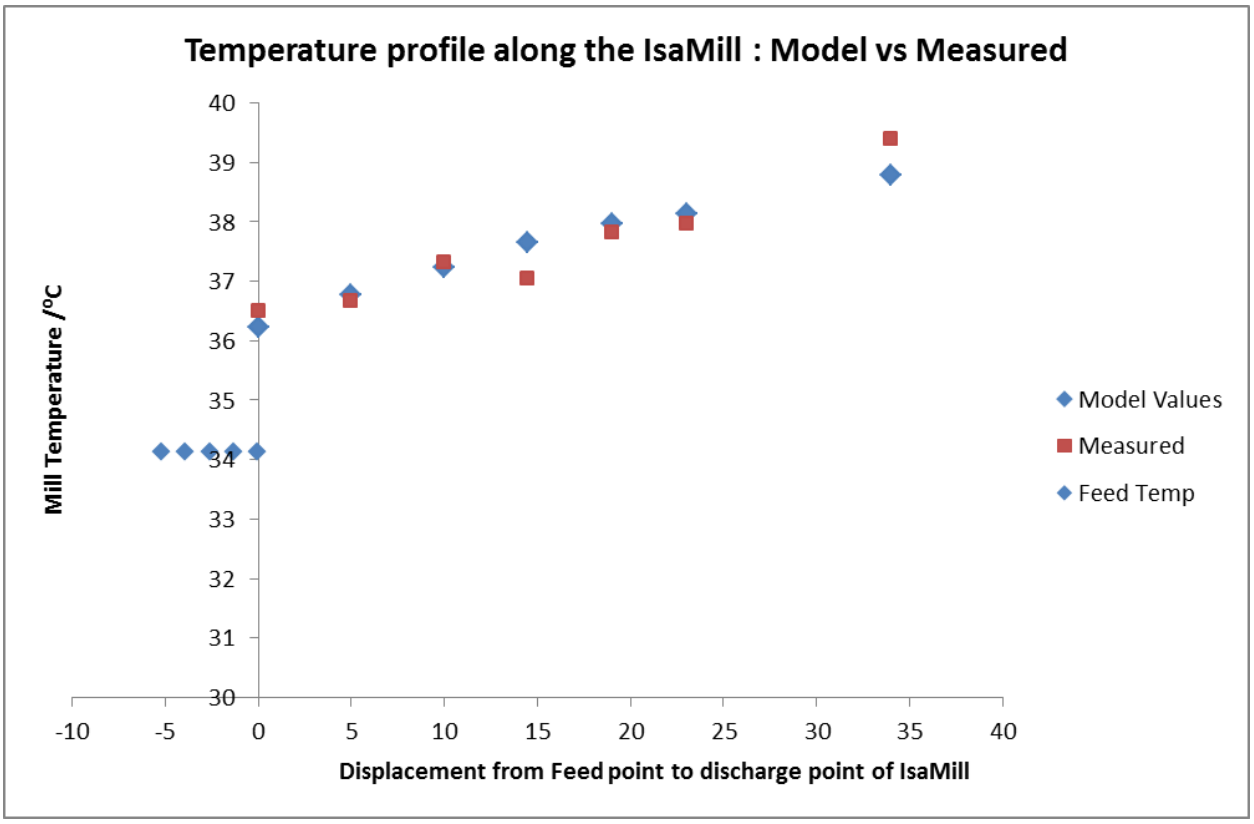

Fig 6.6: Expt. 67 Model Vs Experimental results.

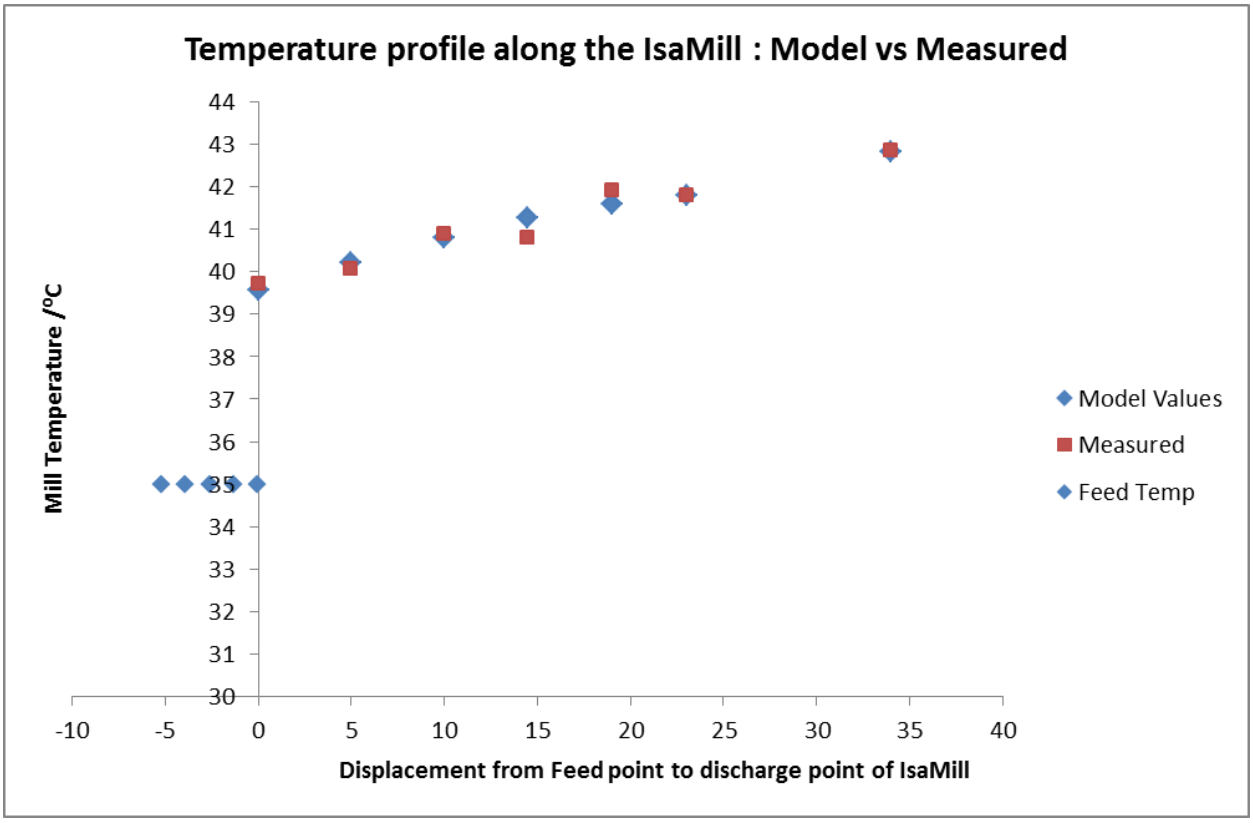

Fig 6.7: Expt. 69. Model Vs measured results.

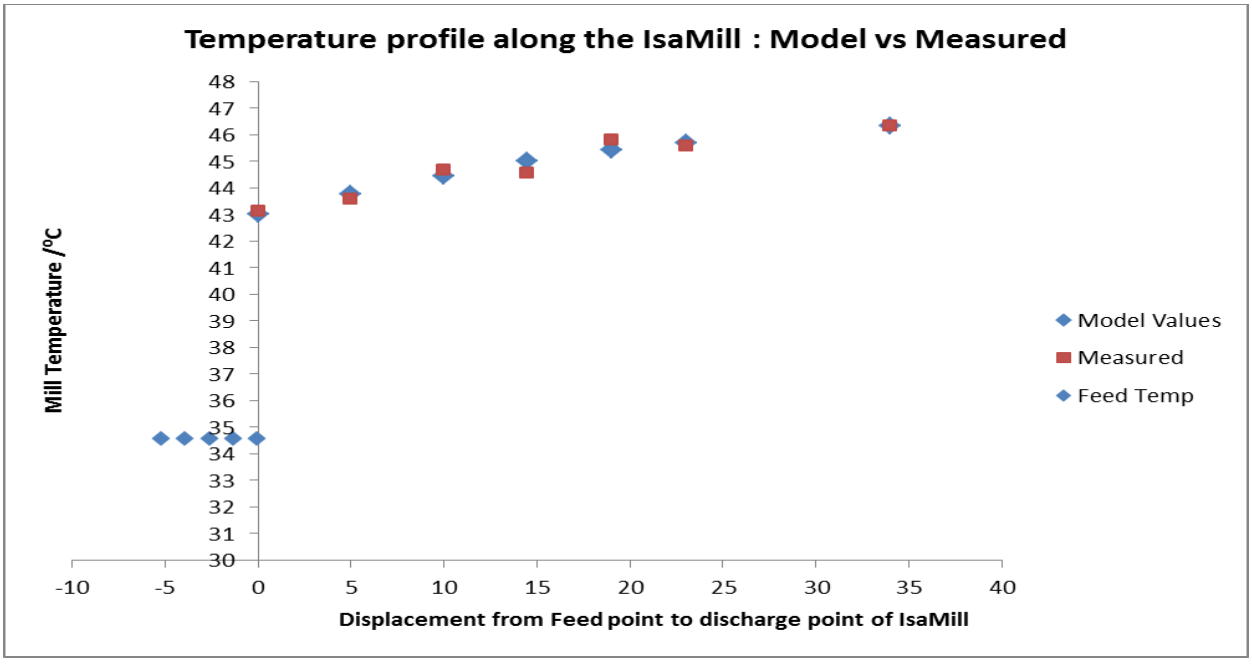

Fig 6.8: Expt. 66 Model vs measured results.

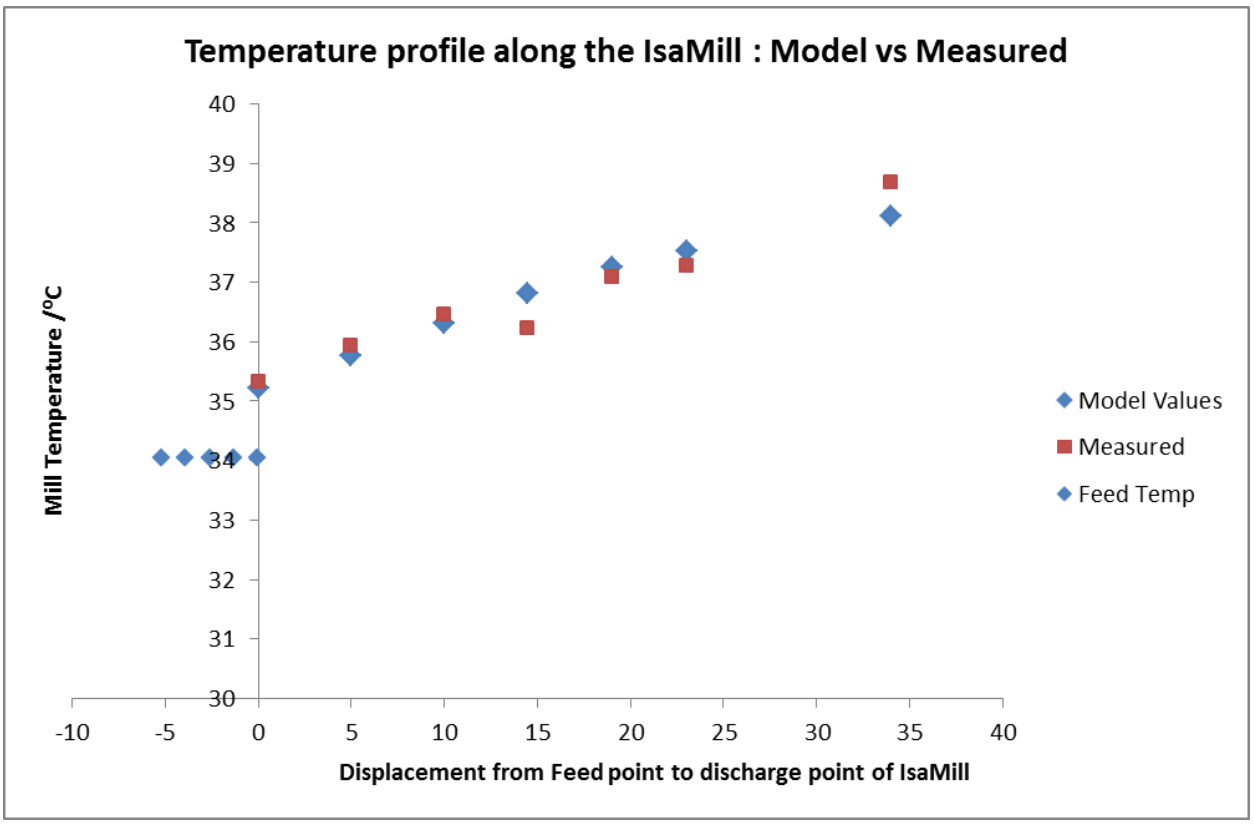

Fig 6.9: Expt. 73. Model vs measured results.

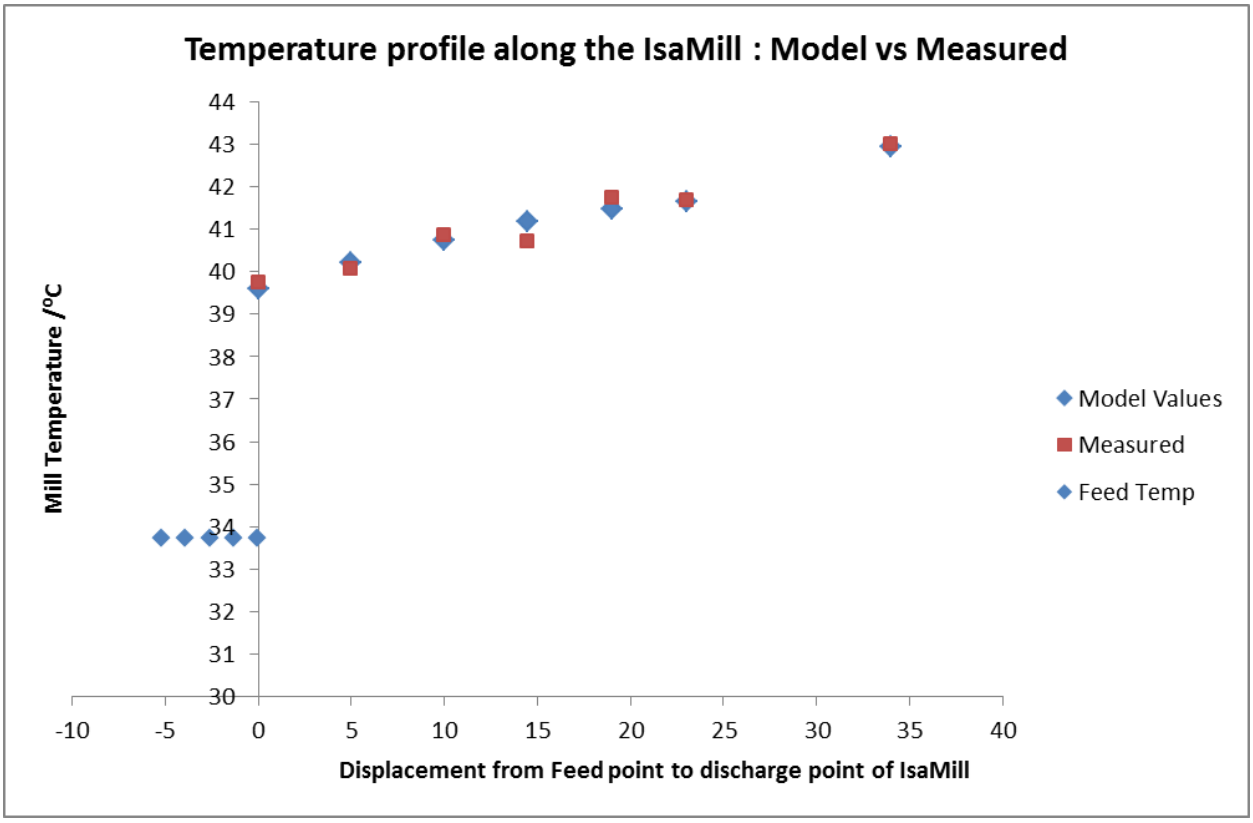

Fig 6.10: Expt. 75. Model vs measured results.

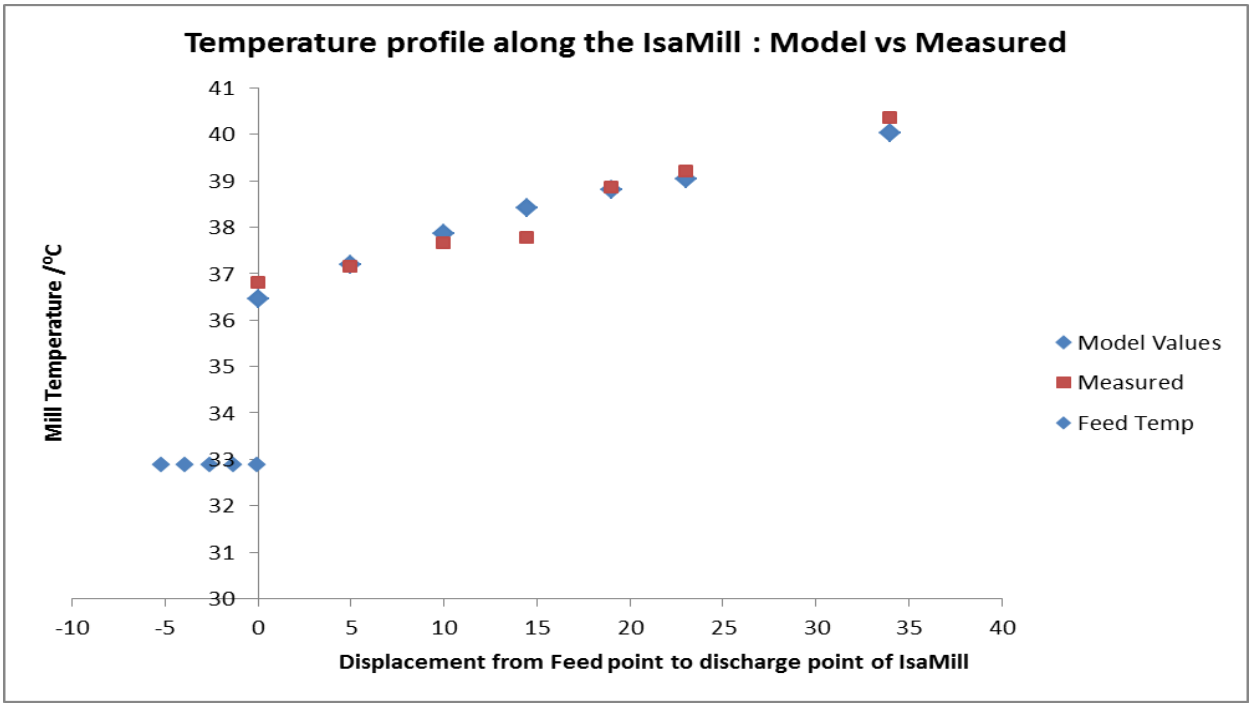

Fig 6.11: Expt. 14. Measured vs model results.

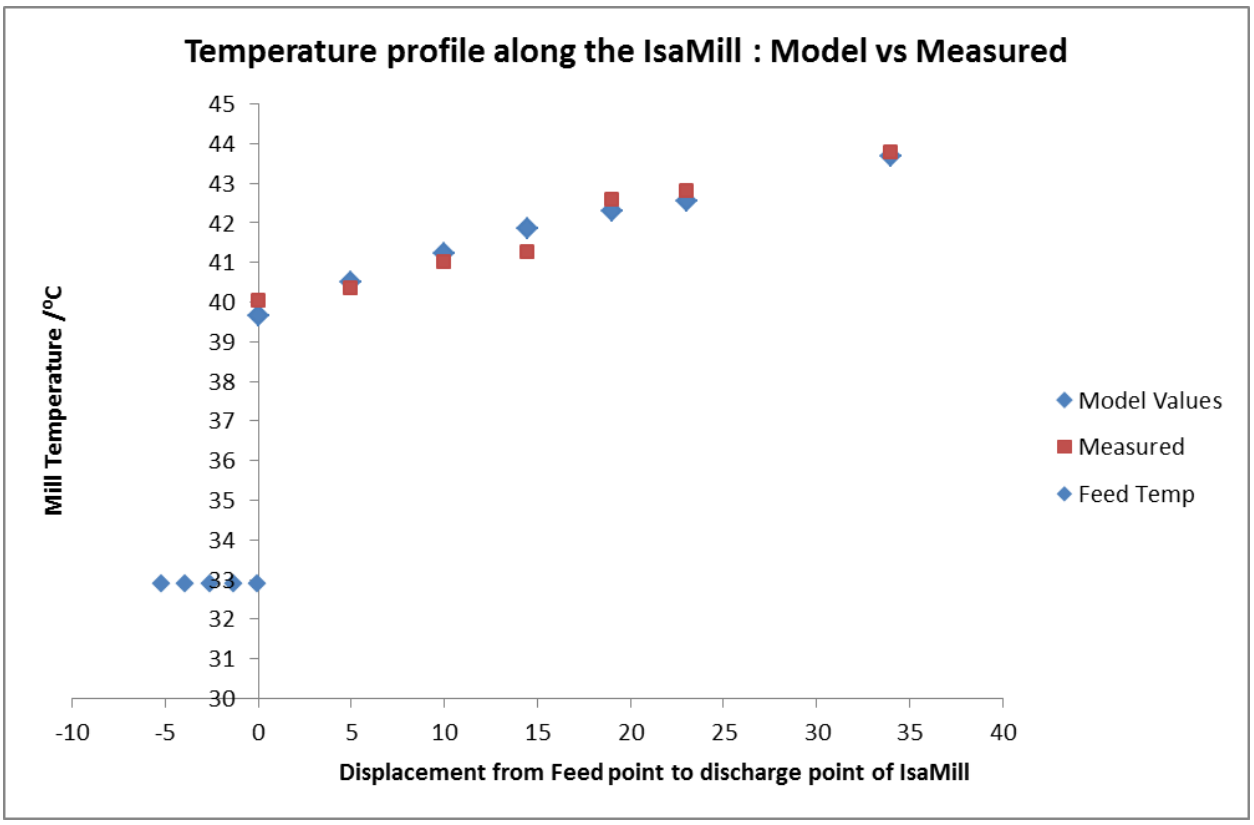

Fig 6.12: Expt. 15. Measured vs model results.

Analysis of the semi empirical model and development of the pure mathematical model

The previous section of this chapter described how the semi empirical model was developed and how the semi-empirical values of the back-mixing coefficient β, were determined for different process conditions. These optimised values of β obtained from optimisation with the solver programme were then plotted against the different mill conditions to see the relationships between them and the mill conditions. The figures below show the relationship between β and the various mill conditions as derived from the semi-empirical model.

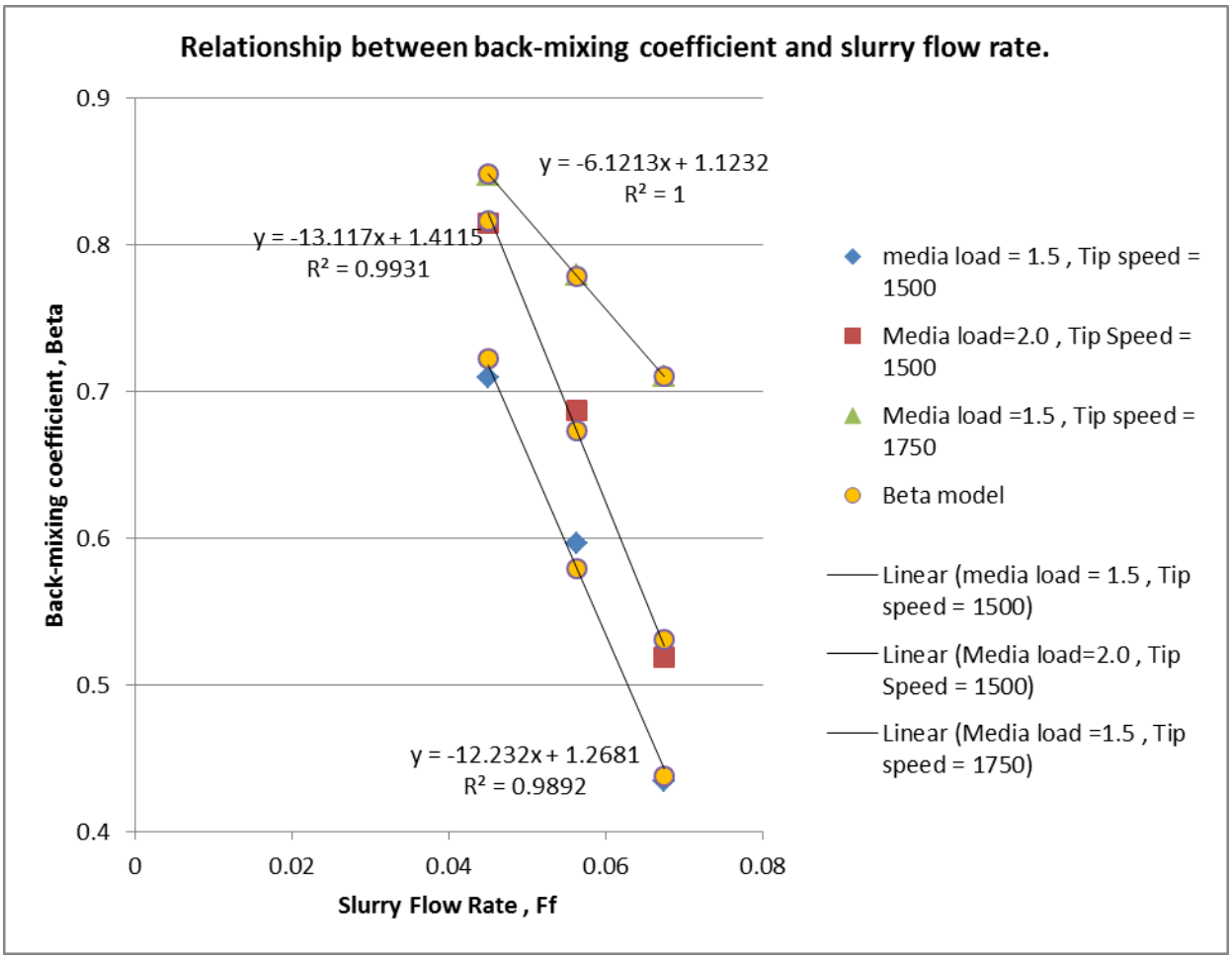

Fig 6.13: Effect of slurry flow rate on the back-mixing coefficient β.

Thus, the back-mixing coefficient decreases with increase in flow rate. This is due to decrease in the backflow as forward flow increases.

Based on the above observed trends, a linear correlation model was developed to describe the inter-relationship between β, mill tip speed, media load and slurry flow rate with slurry flow rate

being the variable under control. From the graphical relationships shown above, the correlation model below was proposed:

$$Beta = a_{Ff}.Ff + a_{ML}.ML + a_{TS}.TS + a_{Ff.TS}.Ff.TS + const$$

where Ff is the feed flow rate, ML is the media load, TS is the mill tip speed, const is a constant term in the linear equation, a_{Ff} is a coefficient of Ff, a_{ML} is the coefficient of ML and $a_{Ff.TS}$ is the coefficient of Ff.TS. the multiplication factors used were to ensure that the values of the variables were in comparable ranges.

The above model was input into an excel spread sheet with the various slurry flow rates while all other mill variables were kept constant at those varying slurry flow rates. Initial values of the coefficients and the constant were assigned and the corresponding β values for the different conditions were then computed. The excel spreadsheet was designed such that there was provision of calculating the square of error between the semi-empirically obtained value of β from each experiment and the correlated value of β.

A solver program was run with the objective being to minimise the sum of the square of errors between the semi-empirically obtained and the mathematically obtained β values. This was obtained subject to changing values of the coefficients and the constant.

The calculated coefficients would then show the relationship between β and the variables under investigation, Ff, TS and ML in the above case.

The data below illustrates the relationship between β and the flow rate under the shown experimental conditions.

Table 6.5: Effect of flow rate on back-mixing coefficient, β

Variation of β with slurry flow rate at various Media Loads and Tip speeds

Expt No.	Ff	Beta	C	P80	Media load	Tip Speed	beta model	dev^2
7	0.045	0.7094	0.09623	67	1.5	1500	0.72262771	0.000175
13	0.0563	0.5961	0	67.83	1.5	1500	0.57943336	0.000278
22	0.0675	0.4341	0	68	1.5	1500	0.43750622	1.16E-05
31	0.045	0.8141	0	57	2	1500	0.81618781	4.36E-06
37	0.0563	0.6872	0	53.5	2	1500	0.67299346	0.000202
46	0.0675	0.5189	0	60.5	2	1500	0.53106632	0.000148
5	0.045	0.84763	0.0625	63.83	1.5	1750	0.84778716	2.47E-08
14	0.0563	0.7788	0.1735	67.5	1.5	1750	0.77856261	5.64E-08
23	0.0675	0.7099	0	61	1.5	1750	0.70995065	2.57E-09
							S^2	0.000819

	Coefficient	Multiplier for
aFf	-51.948061	Feed flowrate
aML	0.1871202	Media Load
aTS	-0.0006776	Tip Speed
const	2.02865345	
aFf.TS	0.026184	Ff x TS

Notes:

(i)The Back-mixing coefficient decreases as the flow rate increases.

$$Beta = a_{Ff}.Ff + a_{ML}.ML + a_{TS}.TS + a_{Ff.TS}.Ff.TS + const$$

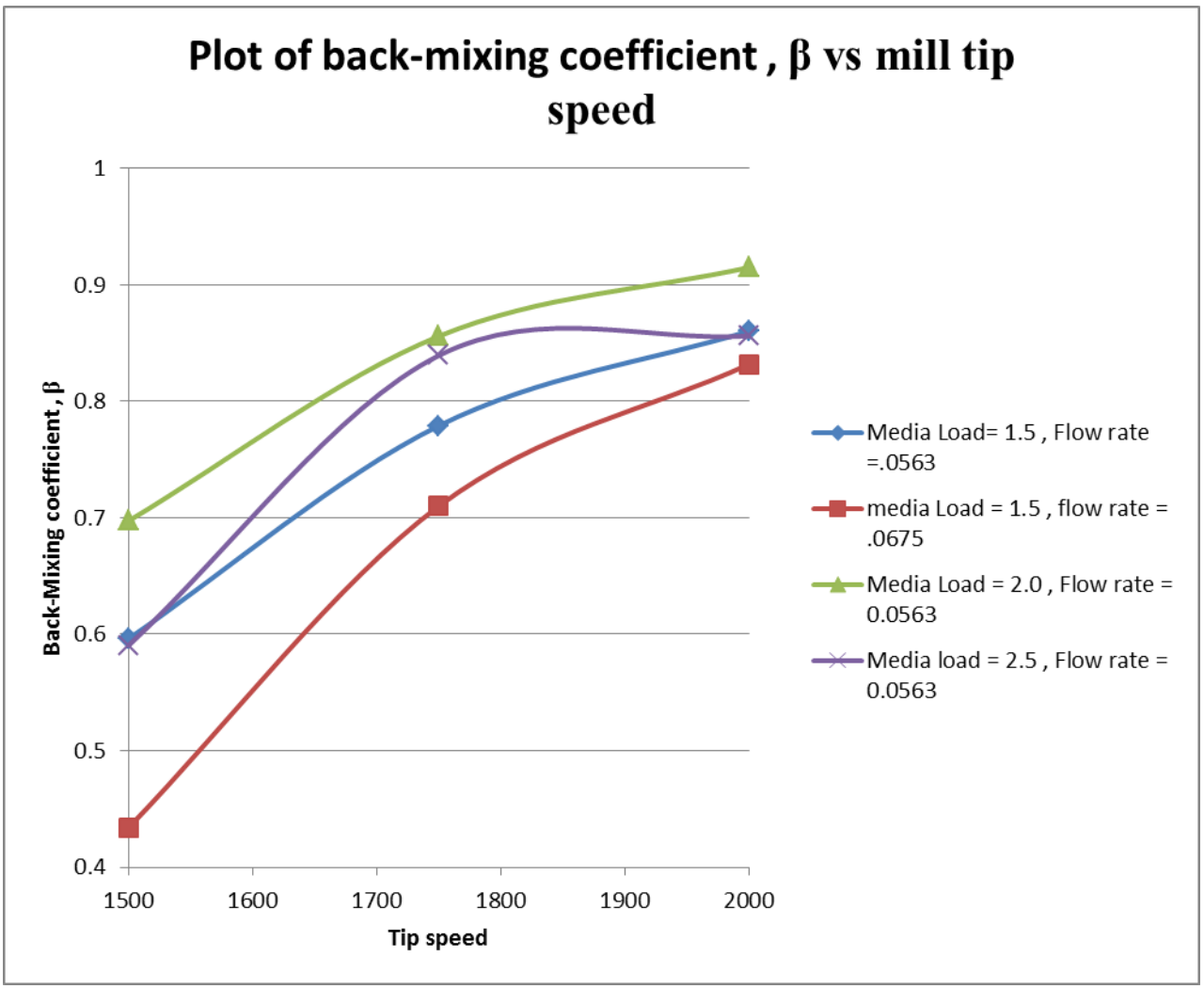

Fig 6.14 : Effect of tip speed on the back-mixing coefficient , β.

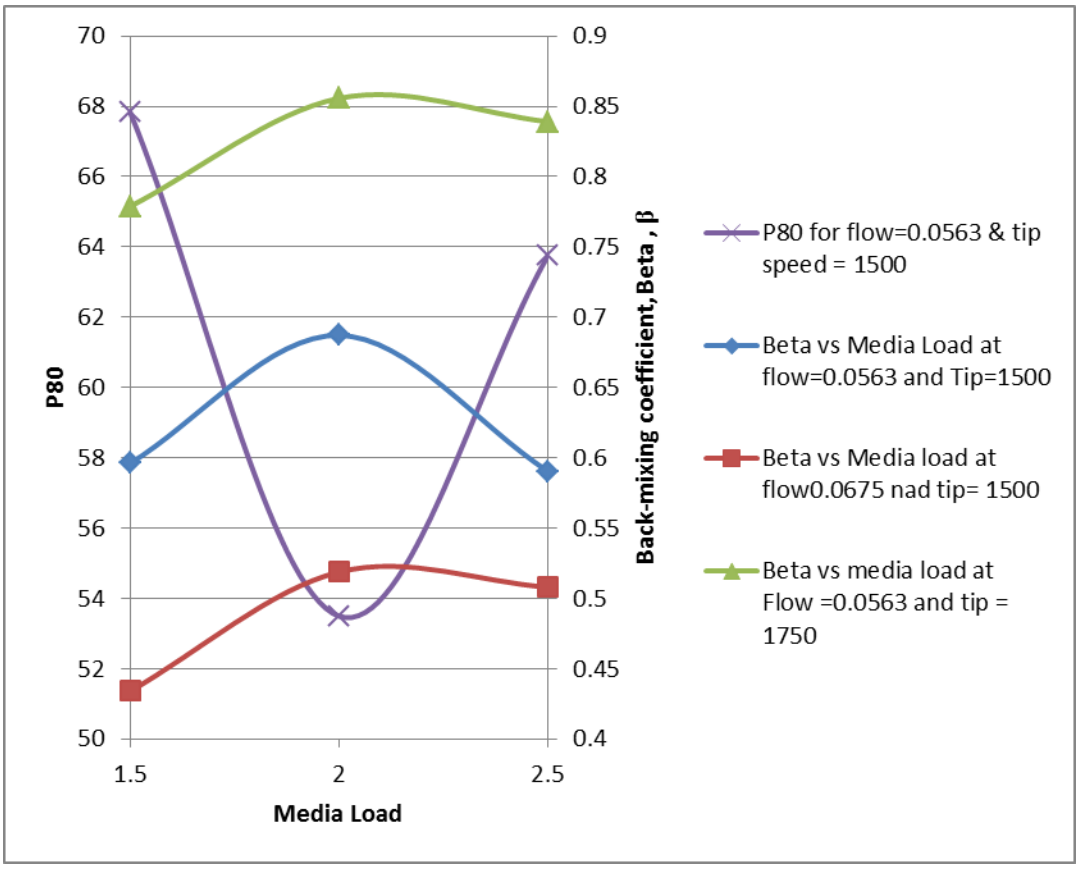

Fig. 6.15 : Effect of media load on back-mixing coefficient as well as on PSD.

The graph below is an extract showing the relationship between the media load and the product particle size distribution.

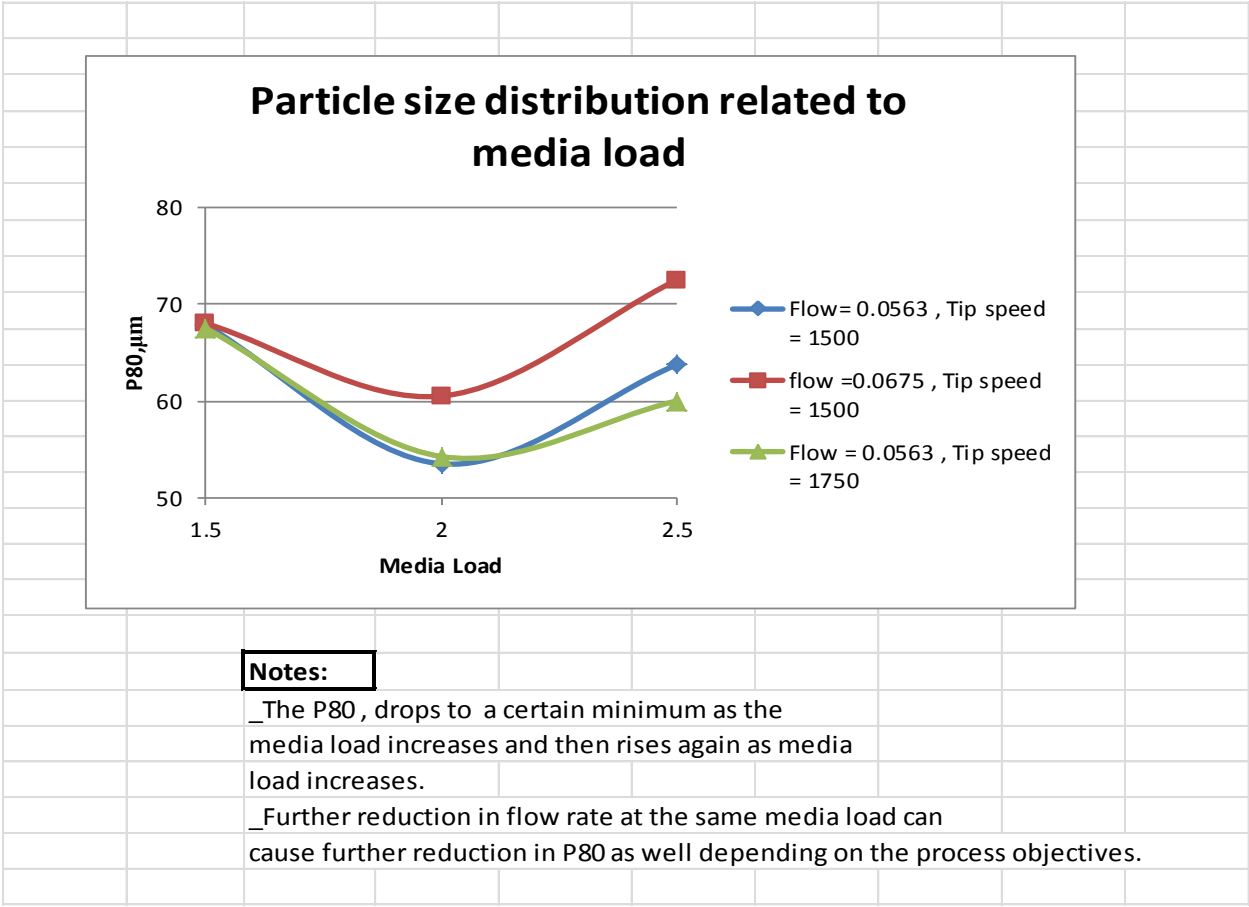

Fig. 6.16: Effect of media load on PSD.

6.5 Summary

The predictive mathematical model was successfully developed and the coefficients of the model were determined to show how the back-mixing coefficient, β is related to the mill operating variables, tip speed, flow rate and media load.

CHAPTER 7: CONCLUSIONS, RECOMMENDATIONS AND REFERENCES

7.1 Conclusions

From the experimental work done using the UG2 ore from Amandebult, South Africa, it has been found that the flow pattern of slurry within an M4 IsaMill can be indirectly measured by using temperature profiles along the mill length. Temperatures inside the mill could be measured indirectly by use of Resistance Temperature Devices (RTD). The temperature profiles along the length of the mill showed that the net flow of slurry in the mill is partially plug flow with superimposed axial mixing

The degree of back-mixing within the mill was denoted by a model parameter, β, and it was noted that the value of this back-mixing coefficient could be controlled by adjusting the values of the mill operating variables , flow rate , mill tip speed and the media load while factoring the desired product particle size distribution. The value of β ranges from 0-1 and the lower this value is, the closer the flow is to plug flow. Plug flow in the mill is an indicator of mill efficiency as measured by the fineness of the particle size distribution.

The developed mathematical models (Chapter 6) could relate the back-mixing coefficient to the mill operating variables, thus giving useful information for mill control. The temperature-displacement plots (Chapter 5 and Chapter 6) obtained when the model was optimised against the measured temperatures indicate a good degree of correlation between model and experimentally determined values.

It has been shown that β decreases with increase in flow rate, increases with tip speed and increases to a maximum level and the decreases with media load.

The model temperatures under the various mill operating conditions may be considered the standard temperature profiles for those conditions. When the model prediction is integrated with a computer program that can show the current mill temperature under similar conditions it can be used to compare the outcome with the model-predicted temperatures. This can be a visual plant control tool that can be used to manage plant operation in real time.

7.2 Recommendations

Of all the mill operating variables observed on the model, it was noted that the model was most sensitive to slurry flow rate. Therefore for future experimental work regarding this technique, it is recommended that slurry flow rate be measured in real time or with greater frequency.

The slurry density will also affect the solids balance in model development. Thus, it is recommended that for further work, the system needs to be integrated with a real time density measurement mechanism or the slurry density be measured with increased frequency.

Future work using this technique of using temperature to diagnose mixing in the IsaMill could involve the use varying media types as well as varying media sizes. The resulting temperature profiles and the effect of these variables on the back-mixing coefficient, β would then be charecterised.

For full characterisation of the temperature-displacement response of the M4 IsaMill on UG2 ore, it is recommended to have runs with several samples of ore from different sections of the mine site to make the charecterisation as representative as possible.

Changes in the disc structure and shape will affect the degree of back-mixing in the mill. Thus, there is potential to use this technique for condition-based maintenance planning as the disc condition may be observed by observing changes in the temperature profile. For future application of this technique it is recommended that similar tests could be done possibly with a faulty disc in the middle of the mill or with one disc missing and the results compared with the results obtained with the mill running with a full set of discs or with all new discs. This real-time monitoring of mill condition could save on down time incurred due to maintenance shut down as maintenance will now be done on a need basis.

For scale up purposes and commercialization of the technique, probe design could be improved and the model could be validated by carrying out more experiments.

It is worth noting that there is a lot of scope for future work on the above technique as indicated on the recommendations. The ultimate plant control decision will depend on the process objective like required particle size distribution or throughput.

7.3 References

1. Burford, B.D., Clark, L.W. www.isamill.com/Isamill Technology used in efficient Grinding Circuits: 08/05/2013).

2. Curry, D., Johnson,N.W., Pease, J. , Young, M.F. , 2010. Improving Fines Recovery by Grinding Finer. Mineral Processing and Extractive Metallurgy, Volume 119, Number 4, 2010: 216-222.

3. Farber, B.Y, Bedesi, N. , Durant , B. Minerals Engineering , Volume.24 , No.3-4, 2011.

4.Gao, M., and Weller, K. Review of Alternative Technologies for finer grinding 1993.

5. Haselton, H.T. , Hemingway Jr, B.S. , Robie ,R.A. American Mineralogist : 1984 Vol69, Low-temperature heat capacities of glass and pyroxene and thermal expansion of pyroxene ,p481.

6. http://amrita.vlab.co.in/?sub=1&brch=194&sim=354&cnt=1: 11/06/201.

7. http://hyperphysics.phy-astr.gsu.edu/hbase/tables/thrcn.html: 07/07/2012.

8. http://www.xstratatechnology.com/EN/Publications/IsaMillbrochure.pdf:23 Dec 2012.

9. http://www.xstratatechnology.com/EN/Publications/IsaMillbrochure.pdf: 23 Dec 2012.

10. Jankovic,A., 2002: www.metsopower.se/miningandconstruction/mct_service/044.pdf: 17/04/2012.

11. Jayasundara, C.T., PhD Thesis 2007: Numerical and Experimental Studies of Granular Dynamics In Isamill.

12. Jayasundara, C.T. , Yu, A.B. , Curry, B. , Prediction of disc wear in a model IsaMill and its effect on the flow of grinding media. Minerals Engineering volume 24, Issue 14, November 2011 :1586-1594.

7.3 References

13. Jayasundara, C.T., Yang, R.Y., and Yu, A.B., Discrete Particle Simulation of Particle Flow in the IsaMill Process Ind. Eng. Chem. Res. 2006 :6349-6359.

14. Kwade, A., Schwedes, J.,2007. Wet Grinding in Stirred Media Mills. Handbook of Powder Technology, Volume 12 ISSN 0167-3785: 251-382.

15. Levenspiel, O., 1999. Chemical Reaction Engineering. Third edition. New York: John Wiley and Sons.

16. Makokha, A.B. and Moys, M. H.,PhD Thesis 2011. Measuring, Characterisation and Modeling of Load Dynamic Behaviour in a Wet Overflow Discharge Ball Mill.

17. Metzger, M.J PhD Thesis 2011. Numerical and Experimental analysis of breakage in a mill using the Attainable Region approach.

18. Moys, M.H., and van Nierop., 2001. Axial mixing of slurry in an autogeneous grinding mill. International Journal of Mineral Processing,Volume 65, Number 3, July 2002 : 151-164(14).

19.van der Westhuizen, A.P.,Govender , I., Mainza, A.N.,Rubenstein, J.,2011.Tracking the motion of media particles inside an IsaMill using Positron Emission Particle Tracking. Minerals Engineering, 2011.

20. Wills, B. A. Mineral Processing Technology, 5th Edition; Pergamon Press: Oxford, U.K., 1992.

21. www.cmmp-france.com/chromitegb.html:18/03/2013,

22. www.electronicscooling.com/2001/11/the thermal conductivity of rubber-elastomers: 20/03/2013.

23. www.engineeringtoolbox.com/thermal-conductivity-d_429.html : 17/07/2012.

24. www.peaksensors.co.uk/technicalinfo.html: 05 /07/2012.

25. www.spiraxsarco.com/resources/steam engineering: 05/07/2013.

26. www.spiraxsarco.com/resources/steam-engineering:05/07/2013)

27. www.webmineral.com/data/Albite.shtml:18/03/2013):

28. Young, Y. and Forssberg, E. , 2003. International Overview and Outlook on Comminution Technology. Swedish Mineral Processing Research Association.

APPENDIX A: SUMMARY OF EXPERIMENTAL RESULTS

APPENDIX A : Summary of experimental results

TEST	FEED RATE	MEDIA	TIP S	MEDIA	Tamb	Tf	T1	T2	T3	T4	T5	T6	Td	ΔT(Feed-	POWER	PRESSURE	F50	F80	P50	P80	β	C	Comment on
No.	L/min	Load(L	(rpm)	(mm)	Ambier	Feed	Cell1	Cell2	Cell3	Cell4	Cell5	Cell6	Dischar	°C	(KW)	(Bar)	µm	µm	µm	µm			Temp. profile
7	2	1.5	1500	3	27.827	32.07	34.58	35.29	36.26	35.72	37.32	37.088	37.879	5.81	1.7	0.50	46	88	46	67			Steady
AVG	**2**	**1.5**	**1500**	**3**	**27.827**	**32.07**	**34.58**	**35.29**	**36.26**	**35.72**	**37.32**	**37.088**	**37.879**	**5.81**	**1.7**	**0.50**	**46**	**88**	**46.0**	**67.0**	**0.7094**	**0.0962**	
2	2	1.5	1750	3	31.289	33.9	38.82	39.25	40.13	39.21	40.03	40.694	40.852	6.95	2.1	-	46	88	28	56			Steady
5	2	1.5	1750	3	29.068	31.26	36.56	37.47	38.5	38.28	40.09	39.796	40.467	9.2	2.2	0.60	46	88	34	67			Steady
8	2	1.5	1750	3	28.251	31.41	36.88	37.58	38.47	38.3	40.08	39.843	40.394	8.98	2.2	0.65	46	88	34	68.5			Steady
AVG	**2**	**1.5**	**1750**	**3**	**29.536**	**32.19**	**37.42**	**38.1**	**39.03**	**38.59**	**40.07**	**40.111**	**40.571**	**8.38**	**2.2**	**0.63**	**46**	**88**	**32**	**63.8**	**0.8476**	**0.0625**	
10	2.5	1.5	1500	3	28.451	30.84	32.75	33.4	34	33.73	34.95	35.363	36.018	5.18	1.6	0.50	46	88	34	70			Steady
13	2.5	1.5	1500	3	31.801	32.91	34.65	35.01	35.41	35.41	36.26	36.731	37.914	4.94	1.6	0.50	46	88	34	67			Steady
16	2.5	1.5	1500	3	32.193	32.2	34.33	34.68	35.05	35.02	35.96	36.534	37.602	5.4	1.6	0.50	46	88	33	66.5			Steady
AVG	**2.5**	**1.5**	**1500**	**3**	**30.815**	**31.98**	**33.91**	**34.36**	**34.82**	**34.72**	**35.72**	**36.209**	**37.178**	**5.17**	**1.6**	**0.50**	**46**	**88**	**33.7**	**67.8**	**0.5961**	**0.0000**	
11	2.5	1.5	1750	3	29.112	31.09	35.15	35.82	36.48	36.37	37.76	38.029	38.589	7.5	2.1	0.65	46	88	36	70			Steady
14	2.5	1.5	1750	3	32.165	32.89	36.81	37.15	37.65	37.76	38.87	39.203	40.365	7.48	2.1	0.65	46	88	33	65			Steady
AVG	**2.5**	**1.5**	**1750**	**3**	**30.638**	**31.99**	**35.98**	**36.49**	**37.07**	**37.07**	**38.31**	**38.616**	**39.477**	**7.49**	**2.1**	**0.65**	**46**	**88**	**34.5**	**67.5**	**0.7788**	**0.3400**	
12	2.5	1.5	2000	3	29.505	31	38.34	38.78	39.6	39.65	41.29	41.357	41.755	10.76	2.8	0.85	46	88	33	65			Steady
15	2.5	1.5	2000	3	32.491	32.89	40.02	40.36	41	41.27	42.59	42.788	43.76	10.87	2.8	0.90	46	88	29	60			Steady
AVG	**2.5**	**1.5**	**2000**	**3**	**31.00**	**31.95**	**39.18**	**39.57**	**40.3**	**40.46**	**41.94**	**42.073**	**42.758**	**10.815**	**2.8**	**0.88**	**46**	**88**	**31.0**	**62.5**	**0.8601**	**0.4578**	
22	3	1.5	1500	3	32.00	31.33	32.68	33.14	33.4	33.63	34.21	34.828	35.951	4.62	1.6	0.50	46	88	33	68			Steady
AVG	**3**	**1.5**	**1500**	**3**	**32.00**	**31.33**	**32.68**	**33.14**	**33.40**	**33.63**	**34.21**	**34.83**	**35.95**	**4.62**	**1.6**	**0.50**	**46**	**88**	**33**	**68**	**0.4341**	**0.0000**	
23	3	1.5	1750	3	32.283	31.8	34.51	34.94	35.24	35.55	36.2	36.652	37.885	6.08	2.0	0.65	46	88	31	61			Steady
AVG	**3**	**1.5**	**1750**	**3**	**32.28**	**31.80**	**34.51**	**34.94**	**35.24**	**35.55**	**36.20**	**36.65**	**37.88**	**6.08**	**2.0**	**0.65**	**46**	**88**	**31**	**61.0**	**0.7099**	**0.0000**	
21	3	1.5	2000	3	31.982	31.65	36.82	37.32	37.72	37.99	38.99	39.333	40.379	8.72	2.7	0.85	46	88	30	64			Steady
24	3	1.5	2000	3	32.814	32.29	37.32	37.72	38.17	38.56	39.34	39.686	40.791	8.5	2.6	0.80	46	88	30	60			Steady
AVG	**3**	**1.5**	**2000**	**3**	**32.40**	**31.97**	**37.07**	**37.52**	**37.95**	**38.27**	**39.16**	**39.51**	**40.58**	**8.61**	**2.7**	**0.83**	**46**	**88**	**30**	**62**	**0.8316**	**0.0000**	
31	2	2	1500	3	31.786	33.05	36.19	36.4	36.79	36.59	37.27	37.494	38.974	5.92	1.6	0.5	46	88	28	57			Steady
AVG	**2**	**2**	**1500**	**3**	**31.786**	**33.05**	**36.19**	**36.4**	**36.79**	**36.59**	**37.27**	**37.494**	**38.974**	**5.92**	**1.6**	**0.5**	**46**	**88**	**28**	**57**	**0.8141**	**0.0000**	
37	2.5	2	1500	3	33.483	32.93	35.14	35.73	35.93	36.43	36.73	37.24	38.395	5.46	1.7	0.5	46	88	-	48			Steady
40	2.5	2	1500	3	32.545	33.49	35.56	35.62	36.02	35.82	36.61	36.701	38.411	4.92	1.6	0.5	46	88	27	59			Steady
AVG	**2.5**	**2**	**1500**	**3**	**33.014**	**33.21**	**35.35**	**35.68**	**35.98**	**36.12**	**36.67**	**36.97**	**38.403**	**5.19**	**1.65**	**0.5**	**46**	**88**	**27**	**53.5**	**0.6872**	**0.0000**	
38	2.5	2	1750	3	29.504	31.38	35.44	36.07	36.54	36.26	36.95	37.103	38.54	7.16	2.2	0.6	46	88	32	62			Steady
41	2.5	2	1750	3	33.252	33.26	37.15	37.43	37.88	37.55	38.21	38.43	39.982	6.73	2.0	0.6	46	88	_	46.5			Steady
AVG	**2.5**	**2**	**1750**	**3**	**31.378**	**32.32**	**36.3**	**36.75**	**37.21**	**36.91**	**37.58**	**37.766**	**39.261**	**6.95**	**2.1**	**0.6**	**46**	**88**	**32**	**54.3**	**0.8554**	**0.0000**	
39	2.5	2	2000	3	30.116	31.96	39.37	39.78	40.29	40.27	41.17	41.224	42.222	10.26	2.8	0.9	46	88	_	45			Steady
42	2.5	2	2000	3	33.662	33.72	40.89	41.04	41.61	41.52	42.32	42.446	43.598	9.87	2.7	0.9	46	88	_	44			Steady
AVG	**2.5**	**2**	**2000**	**3**	**31.889**	**32.84**	**40.13**	**40.41**	**40.95**	**40.89**	**41.74**	**41.835**	**42.91**	**10.065**	**2.75**	**0.9**	**46**	**88**		**44.5**	**0.9147**	**0.1374**	
46	**3**	**2**	**1500**	**3**	**30.582**	**31.83**	**33.1**	**33.49**	**33.83**	**33.62**	**34.23**	**34.551**	**36.083**	**4.25**	**1.6**	**0.5**	**46**	**88**	**30**	**60.5**	**0.5189**	**0.0000**	Steady
55	**2**	**2.5**	**1500**	**3**	**32.865**	**34.35**	**36.07**	**37.29**	**38.9**	**38.46**	**39.15**	**39.339**	**40.793**	**6.45**	**1.7**	**0.5**	**46**	**88**	**_**	**34**	**0.5996**	**0.0000**	Steady
56	**2**	**2.5**	**1750**	**3**	**32.27**	**34.43**	**38.78**	**40.35**	**41.91**	**41.51**	**42.33**	**42.45**	**43.489**	**9.05**	**2.1**	**0.65**	**46**	**88**	**_**	**43**	**0.7899**	**0.2380**	Steady
64	2.5	2.5	1500	3	31.5	36.41	37.06	38.7	39.7	39.39	40.34	40.229	41.542	5.13	1.7	0.5	46	88	29	60			Steady
67	2.5	2.5	1500	3	-	34.13	36.49	36.68	37.32	37.04	37.82	37.959	39.385	5.26	1.7	0.5	46	88	32	67.5			Steady
AVG	**2.5**	**2.5**	**1500**	**3**		**35.27**	**36.78**	**37.69**	**38.51**	**38.22**	**39.08**	**39.094**	**40.464**	**5.20**	**1.7**	**0.5**	**46**	**88**	**30.5**	**63.8**	**0.5904**	**0.0000**	
65	2.5	2.5	1750	3	37.08	34.98	39.71	40.07	40.89	40.81	41.91	41.785	42.847	7.87	2.2	0.65	46	88	29	60			Steady
AVG	**2.5**	**2.5**	**1750**	**3**		**34.98**	**39.71**	**40.07**	**40.89**	**40.81**	**41.91**	**41.785**	**42.847**	**7.87**	**2.2**	**0.65**	**46**	**88**	**29**	**60**	**0.8391**	**0.0546**	
66	2.5	2.5	2000	3	38.31	34.57	43.12	43.6	44.7	44.56	45.8	45.602	46.329	11.76		0.85	46	88	-				Steady
69(C	2.5	2.5	2000	3	39.3	34.21	39.98	41.99	43.48	43.09	43.92	44.082	45.02	10.81	2.8	0.75	46	88	-	43			steady
69(d)	2.5	2.5	2000	3	35	34.02	39.76	42.01	43.2	42.79	43.58	43.463	44.7	10.68				88	_				steady
AVG	**2.5**	**2.5**	**2000**	**3**	**37.537**	**34.27**	**40.95**	**42.53**	**43.79**	**43.48**	**44.43**	**44.382**	**45.35**	**11.083**	**2.8**	**0.8**	**46**	**88**		**43**	**0.8558**	**0.4773**	
73	**3**	**2.5**	**1500**	**3**	**37.08**	**34.04**	**35.33**	**35.92**	**36.47**	**36.23**	**37.09**	**37.266**	**38.686**	**4.65**	**1.7**	**0.5**	**46**	**88**	**36**	**72.5**	**0.5081**	**0.0000**	Steady
75	**3**	**2.5**	**2000**	**3**	**38.16**	**33.74**	**39.74**	**40.08**	**40.86**	**40.72**	**41.75**	**41.684**	**42.987**	**9.25**	**2.9**	**0.85**	**46**	**88**	**_**	**51**	**0.8776**	**0.0000**	Steady

Legend

Test- Experiment number
Feed Rate- Slurry feed rate to IsaMill
Mill Tip- Tip speed of the IsaMill(rpm)
Media L- Volume of media in IsaMill
Media- Size of media particles
T0:Shell No- Measured temperature of mill shel:Shell channel No. along shell length
T1- Measured room temperature of the pilot plant
T2- Slurry feed temperature to the mill
T3-T12 Temperatures from first point into the mill to the discharge point
ΔT- Difference in temperature between feed and discharge temperatures.
Power- Power drawn by the mill

Pressure- Pressure inside the mill
F50 µm- 50% of the feed is les than or equal to the given particle size
F80 µm- 80% of the feed is less than or equal to the given particle size
F95 µm- 95% of the feed is less than or equal to the given particle size
P50µm - P95µm - 50% to 95% of the of the product are less than or equal to the given particle sizes
_- Not recorded
Records in bold for experimental numbers indicate that there is only one run under those experimental process conditions: no duplicate or triplicate runs.
AVG indicates the average of values of duplicate or triplicate runs in the rows above the AVG row.

APPENDIX B: CHARTS OF MODEL VS MEASURED TEMPERATURES ALONG MILL LENGTH.

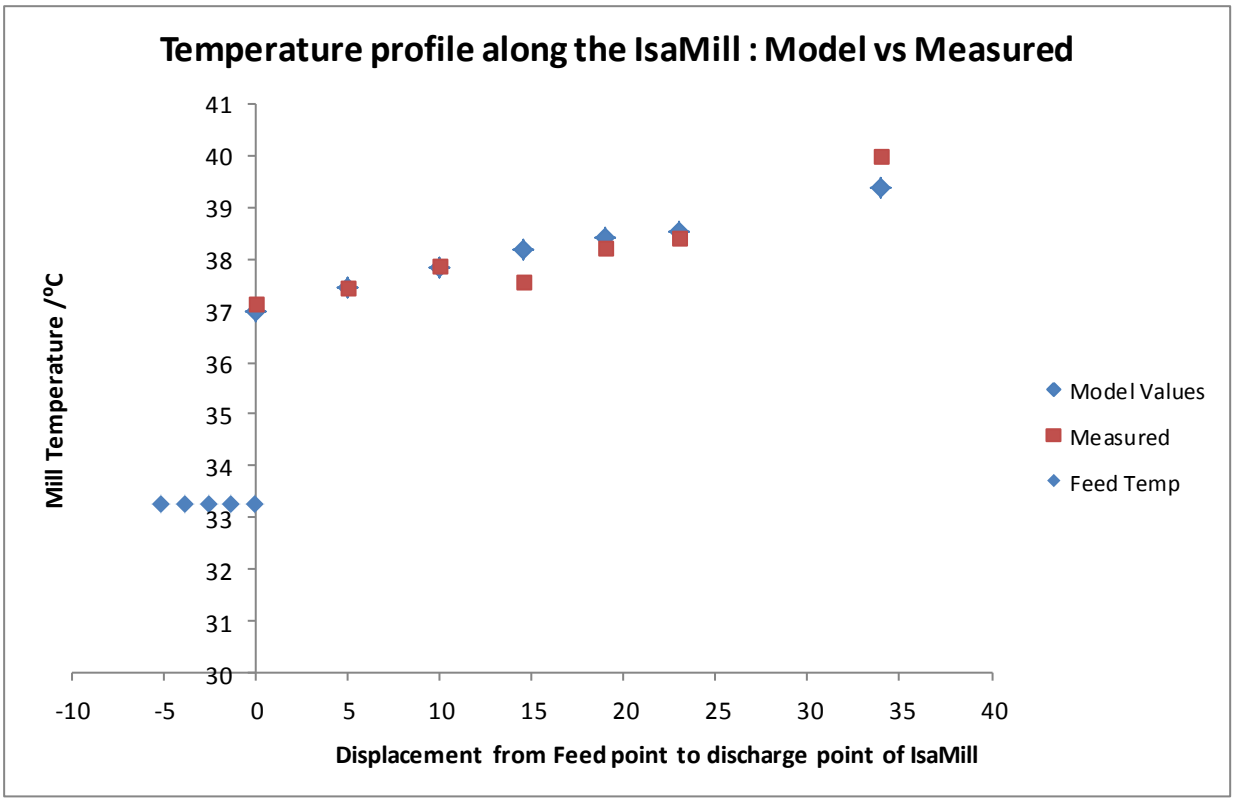

Fig B.1: Expt. 41 Model Vs Experimental results.

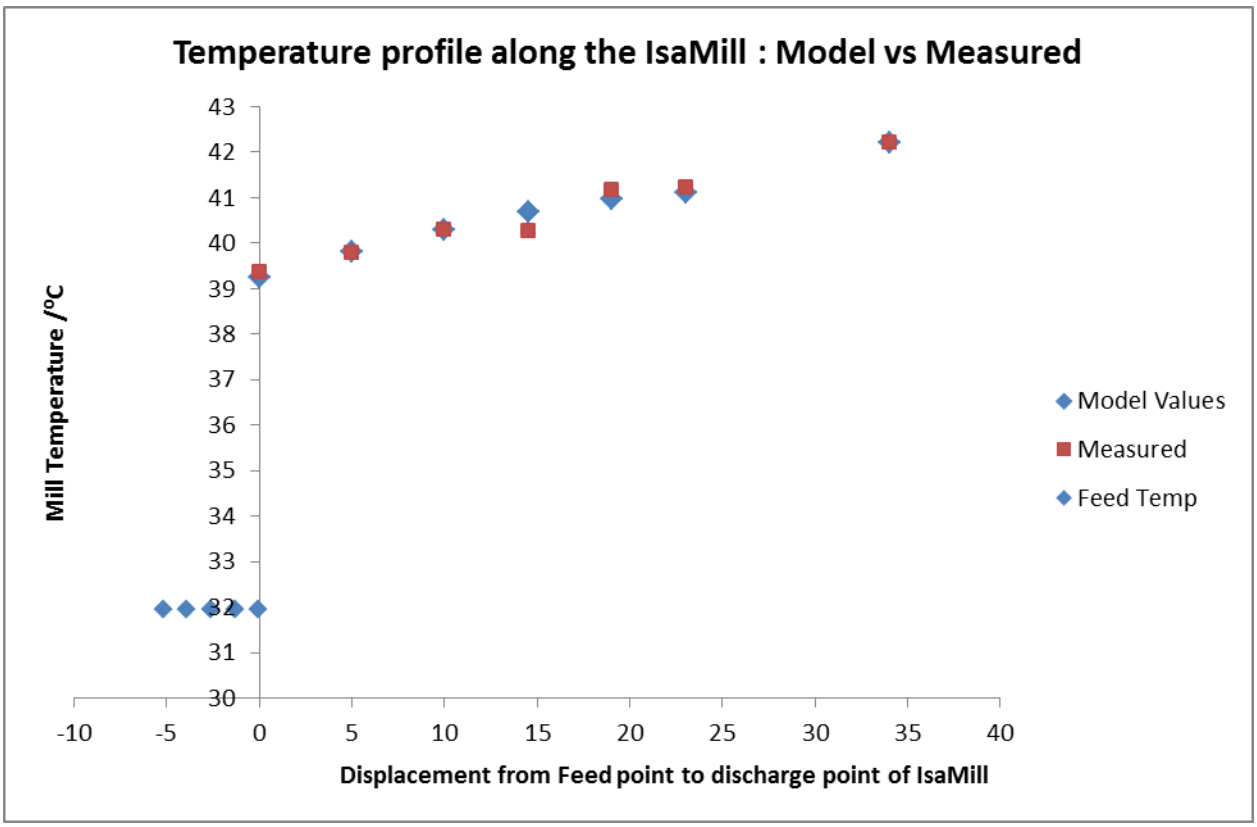

Fig B.2: Expt. 39 Model Vs Experimental results.

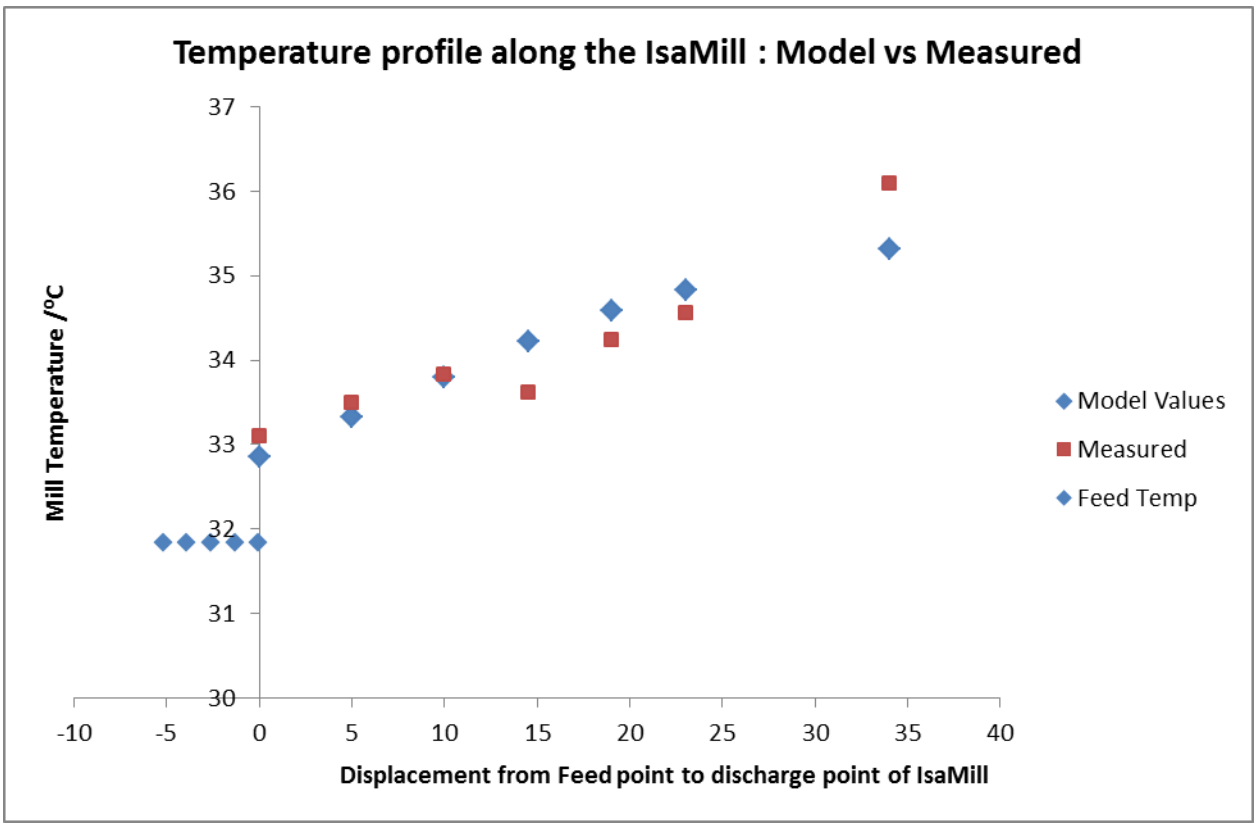

Fig B.3: Expt. 46. Model Vs Experimental results.

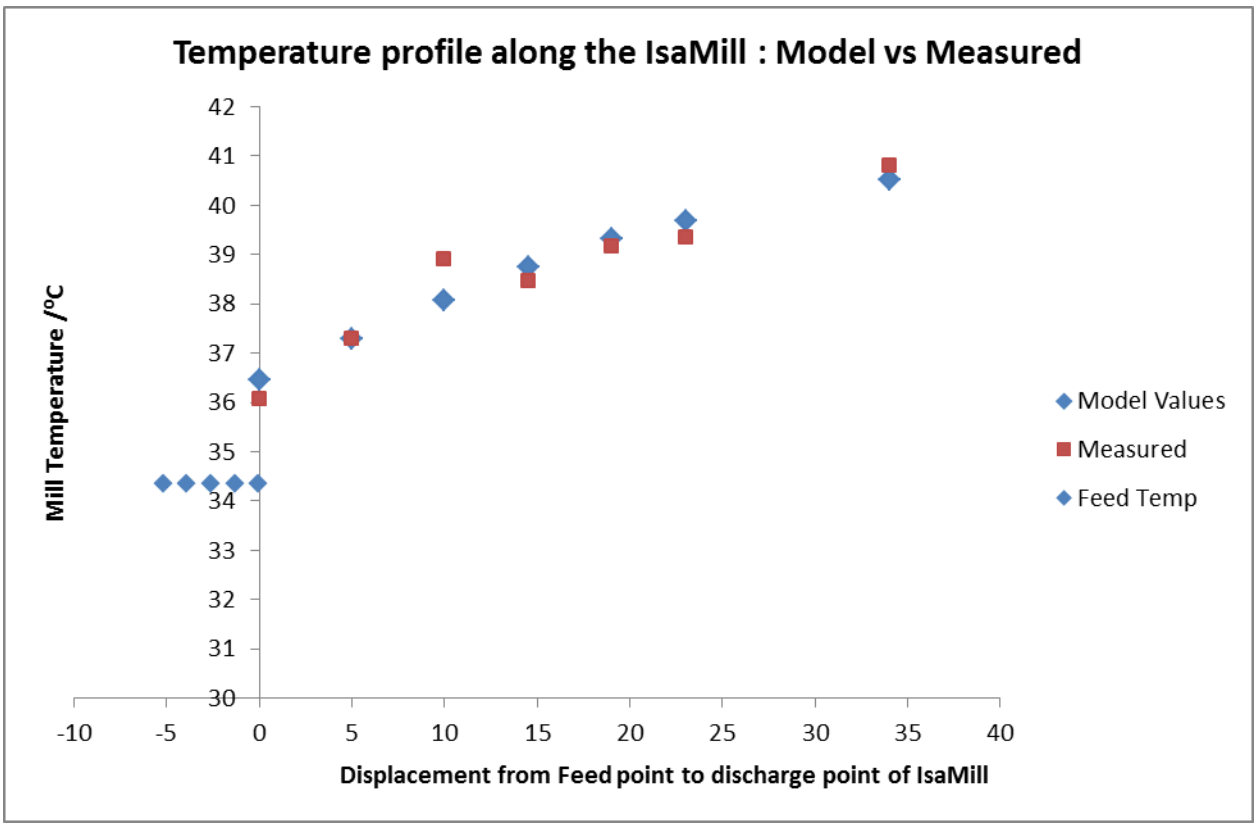

Fig B.4: Expt. 55. Model Vs Experimental results.

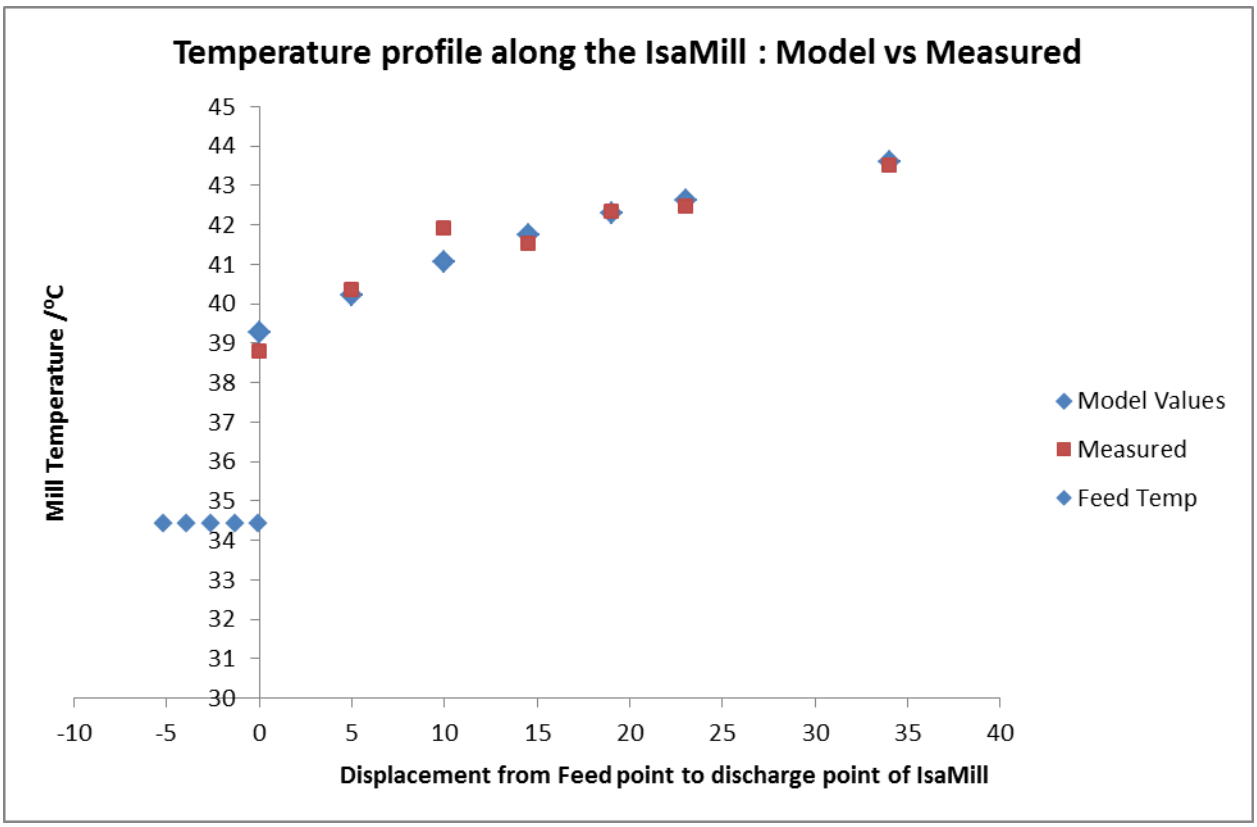

Fig B.5: Expt. 56. Model Vs Experimental results.

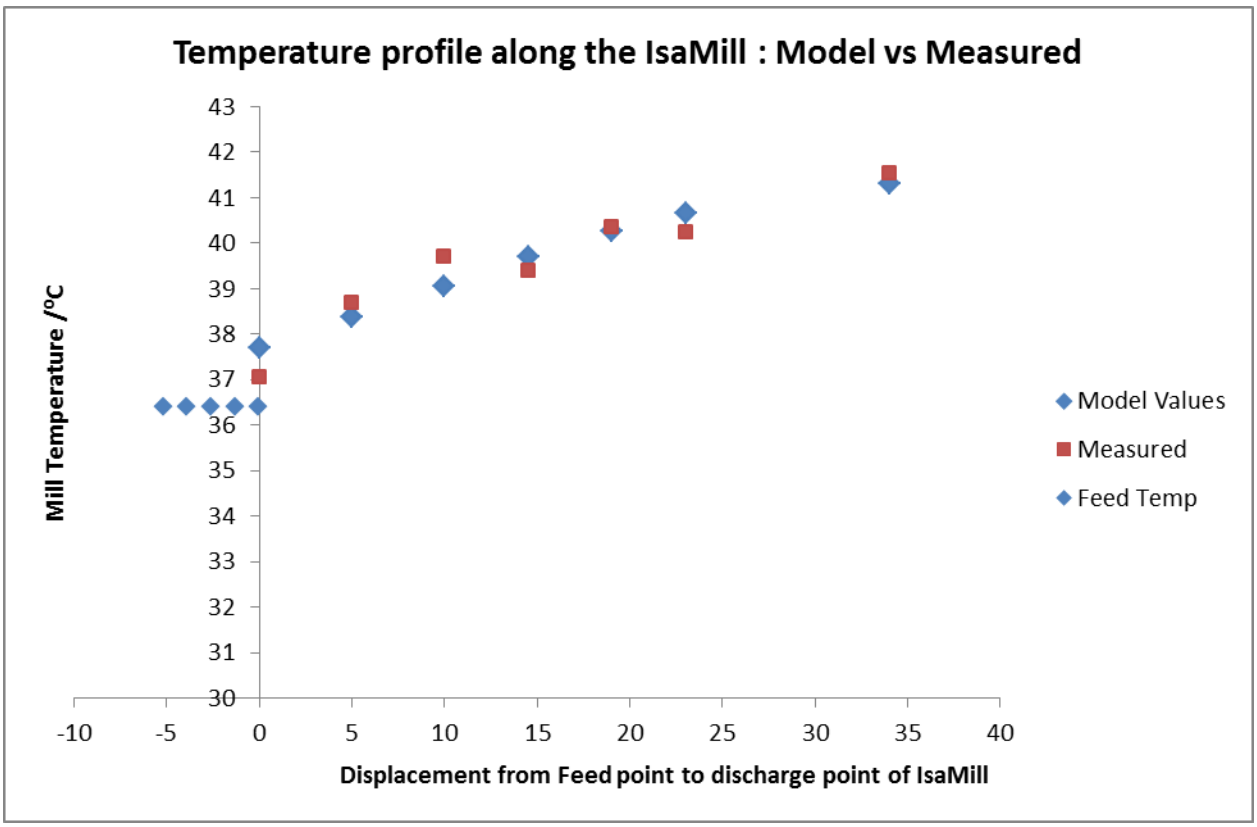

Fig B.5: Expt. 56. Model Vs Experimental results.

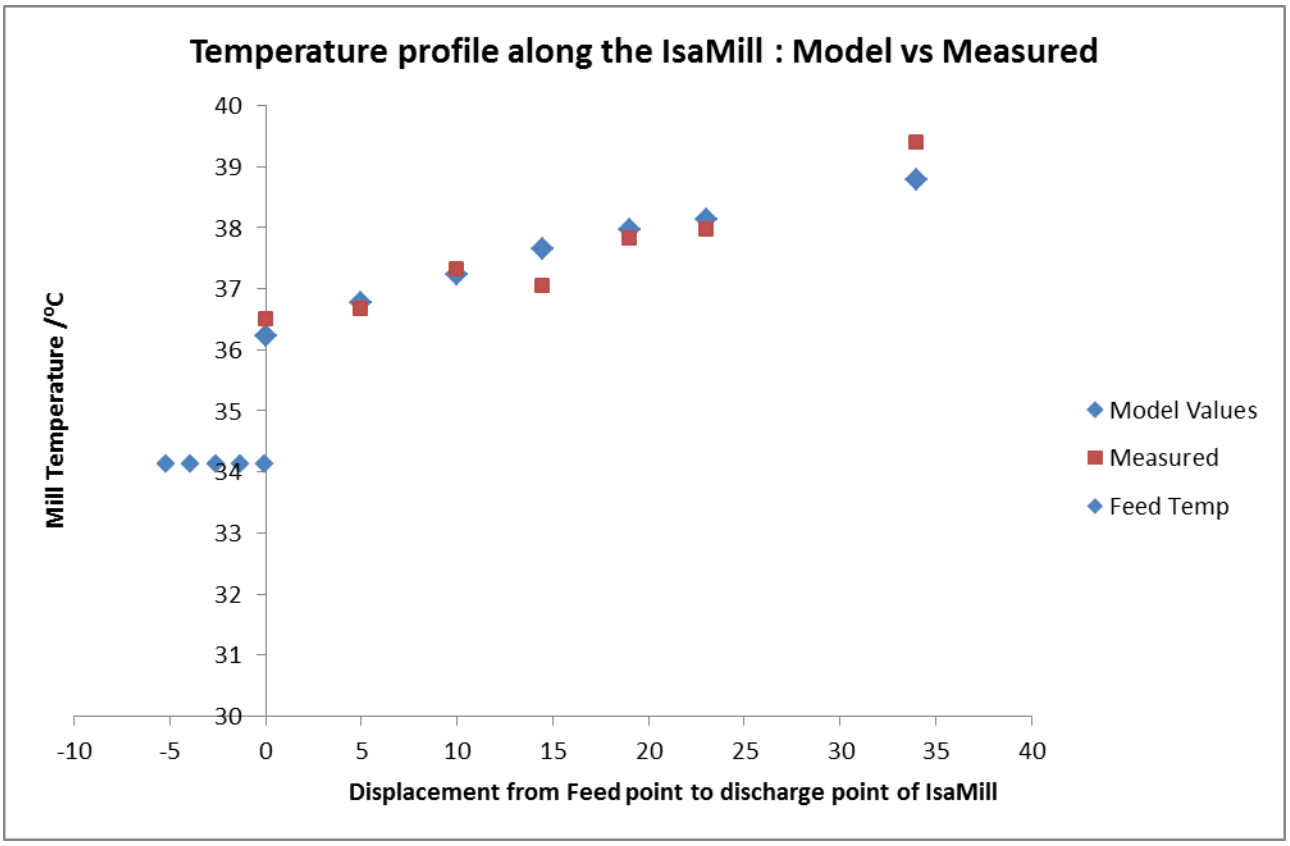

Fig B.5: Expt. 56. Model Vs Experimental results.

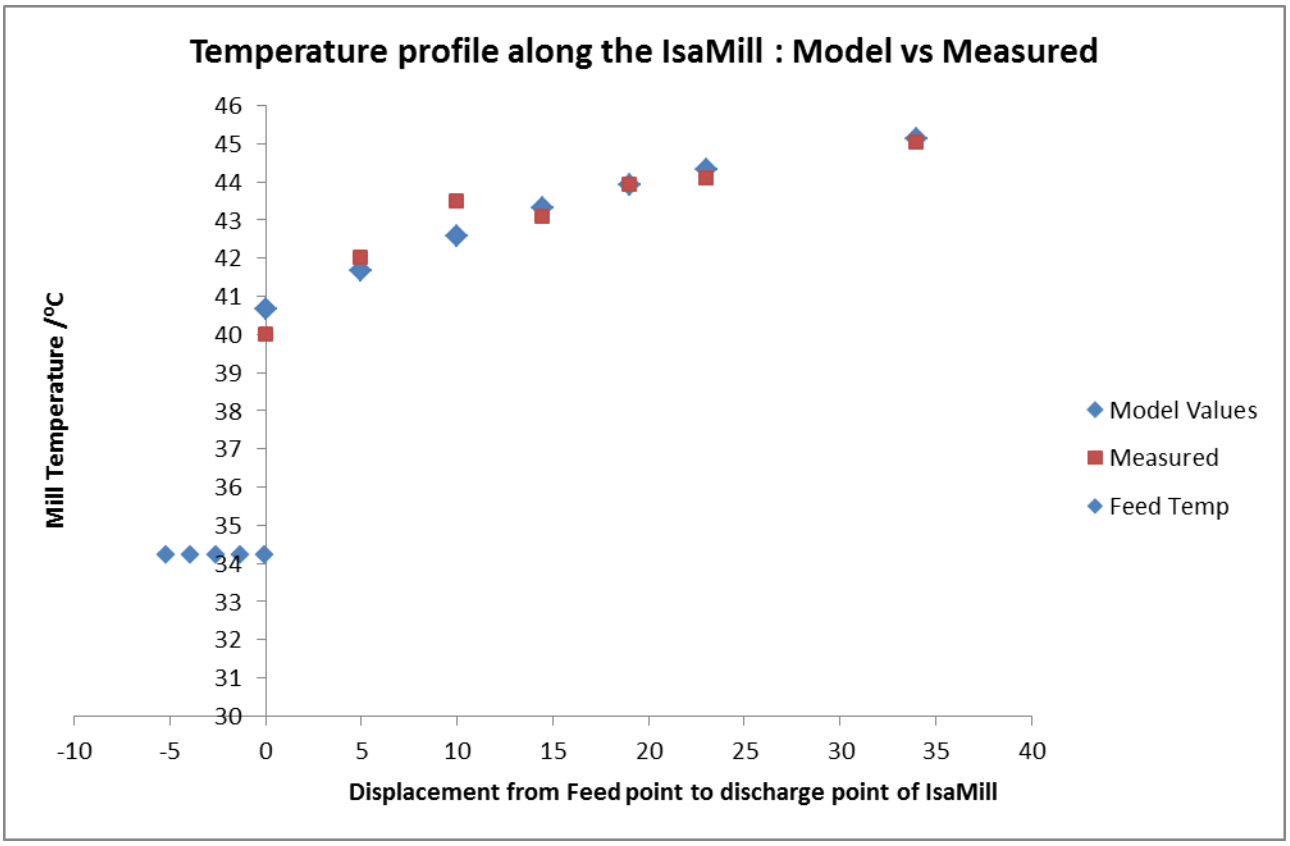

Fig B.6: Expt. 69. Model Vs Experimental results.

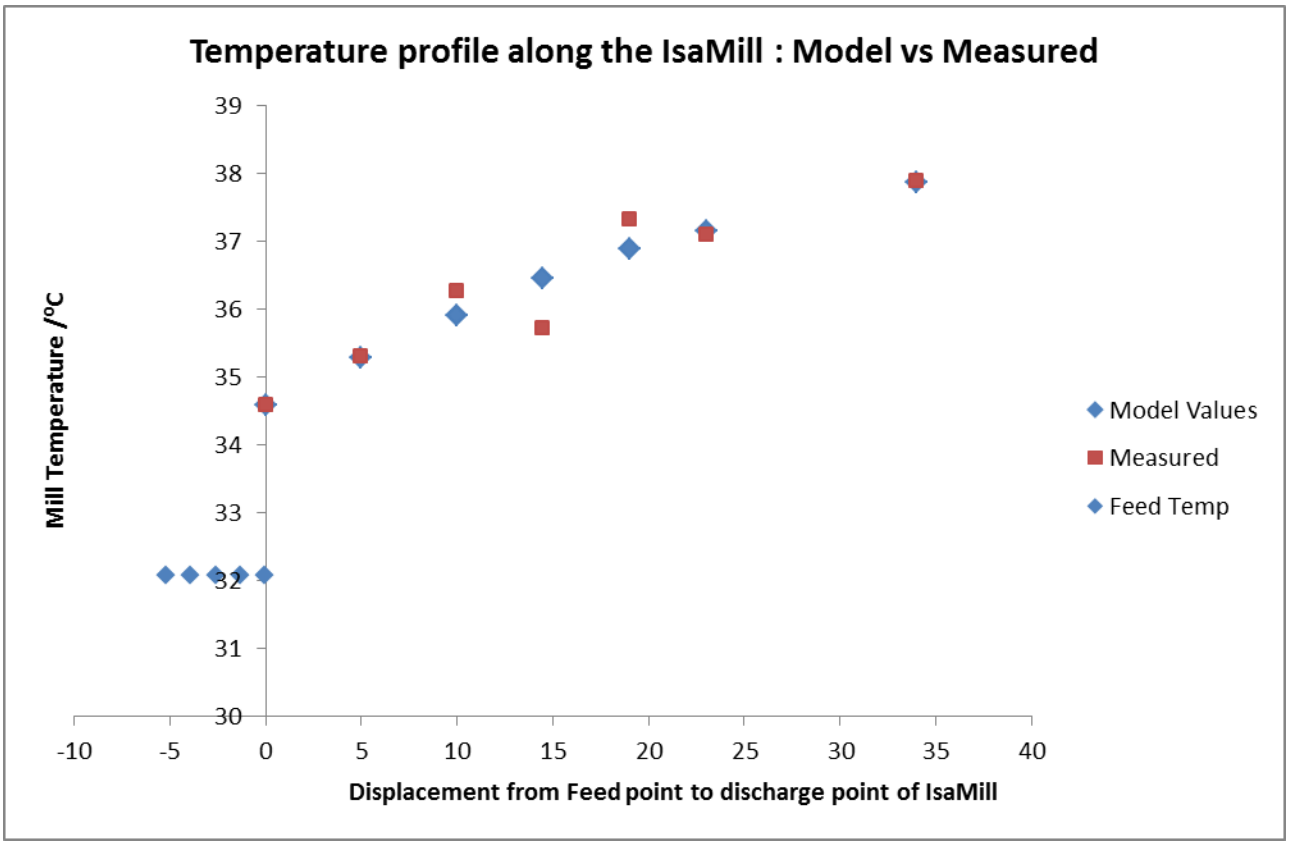

Fig B.7: Expt. 7. Model Vs Experimental results.

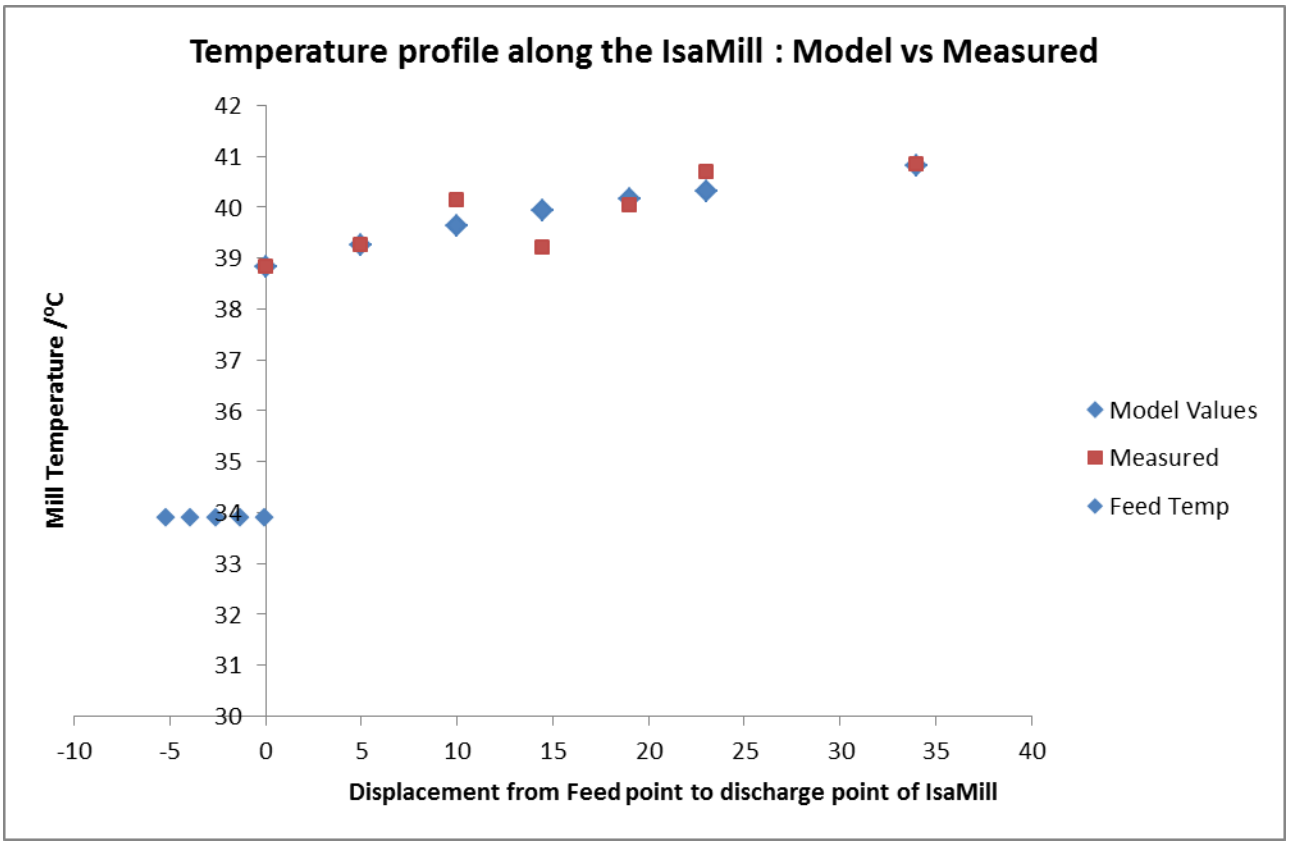

Fig B.8: Expt. 2. Model Vs Experimental results.

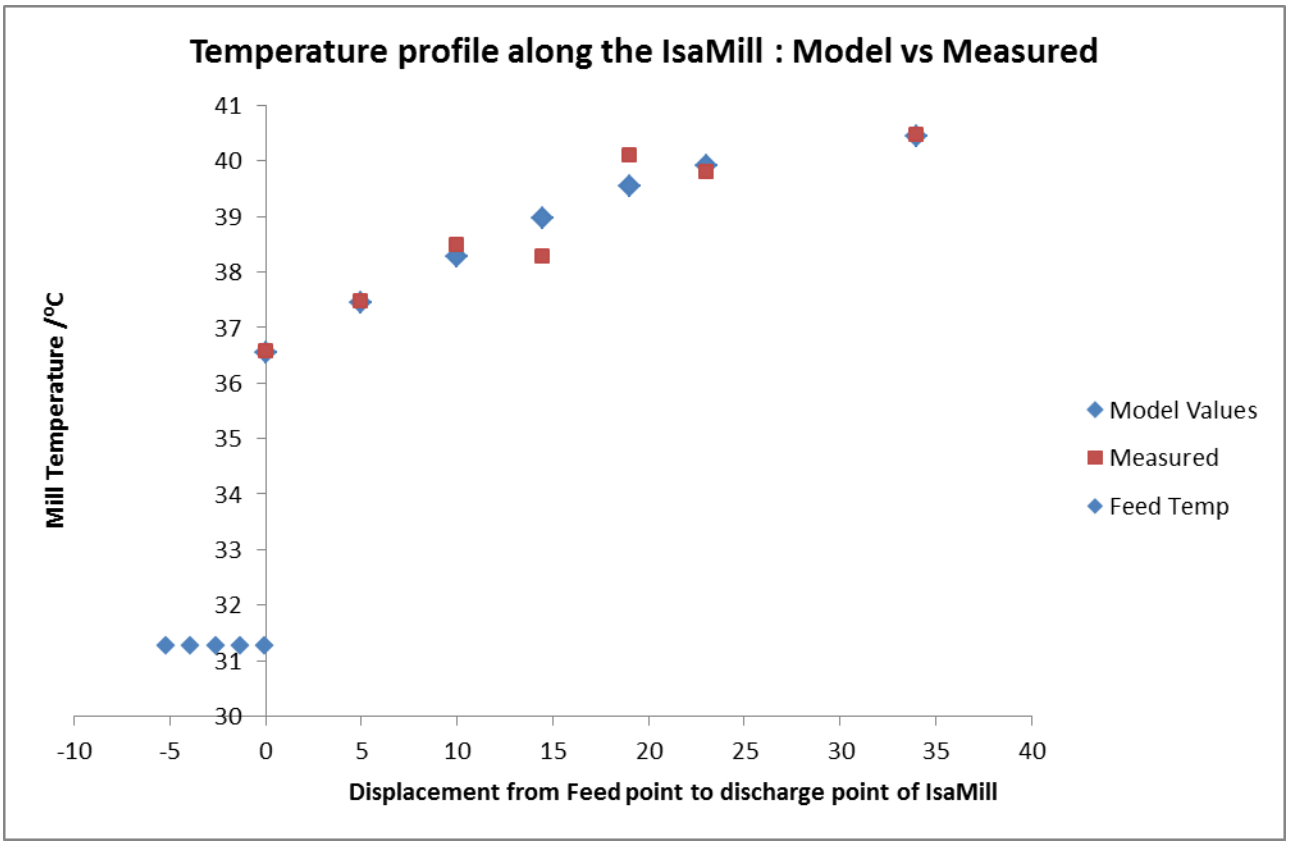

Fig B.9: Expt. 5. Model Vs Experimental results.

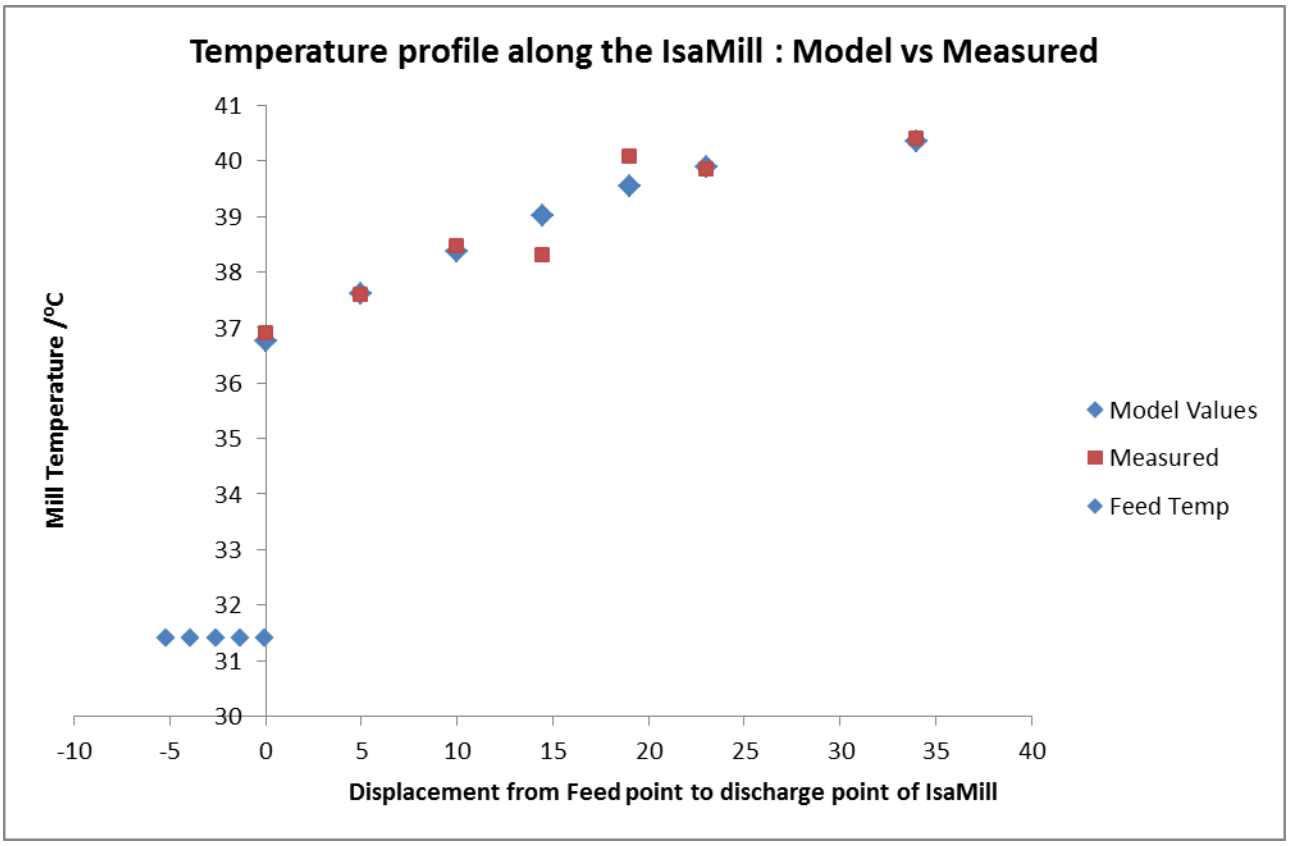

Fig B.10: Expt. 8. Model Vs Experimental results.

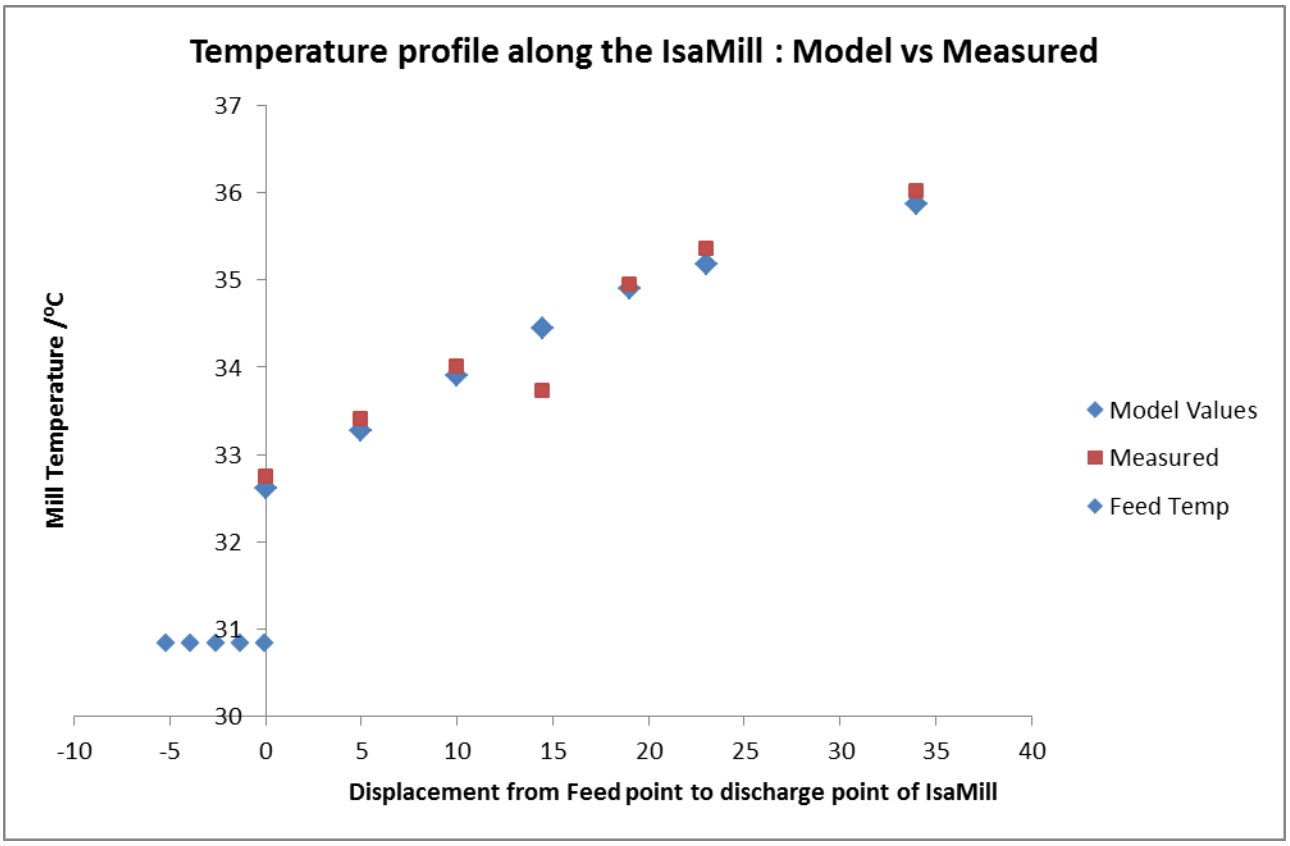

Fig B.11: Expt. 10. Model Vs Experimental results.

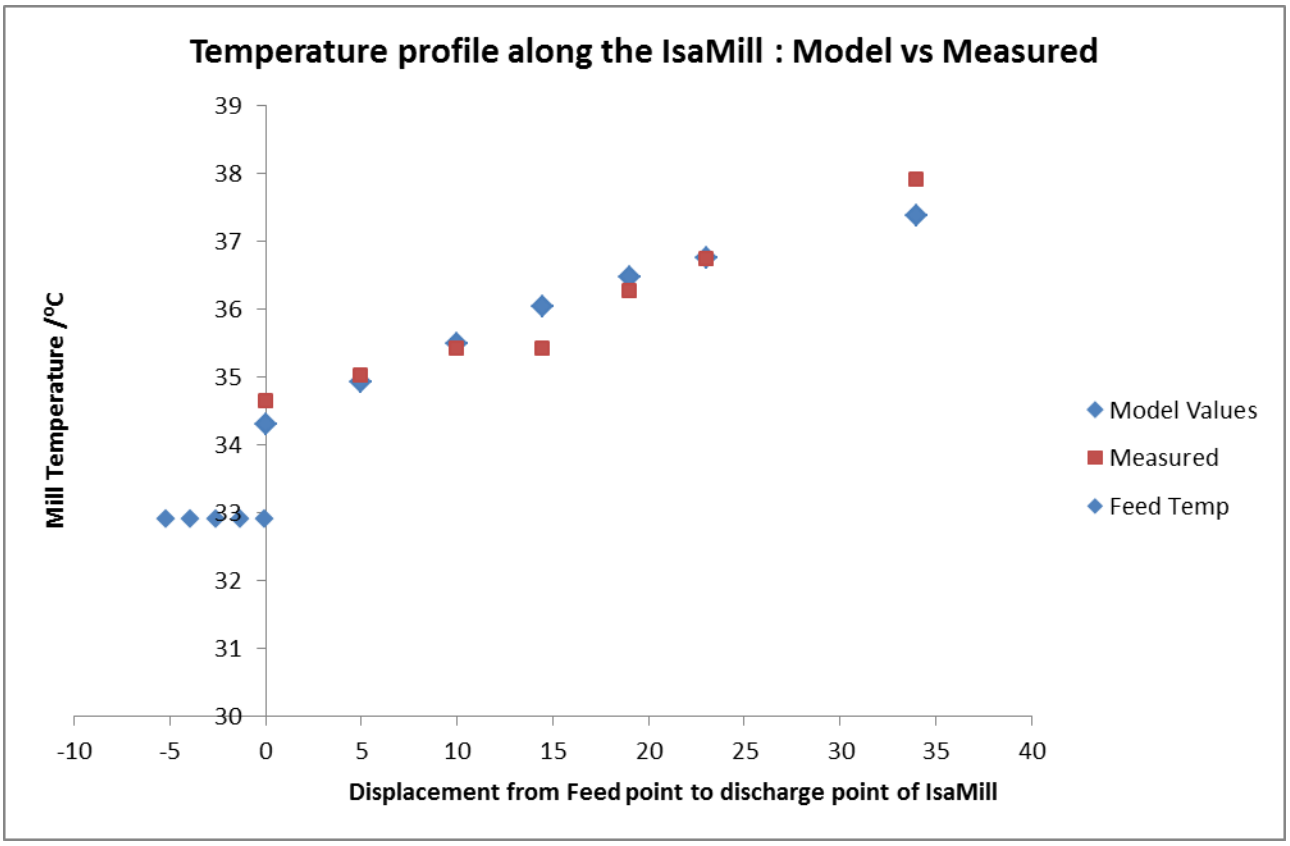

Fig B.12: Expt. 13. Model Vs Experimental results.

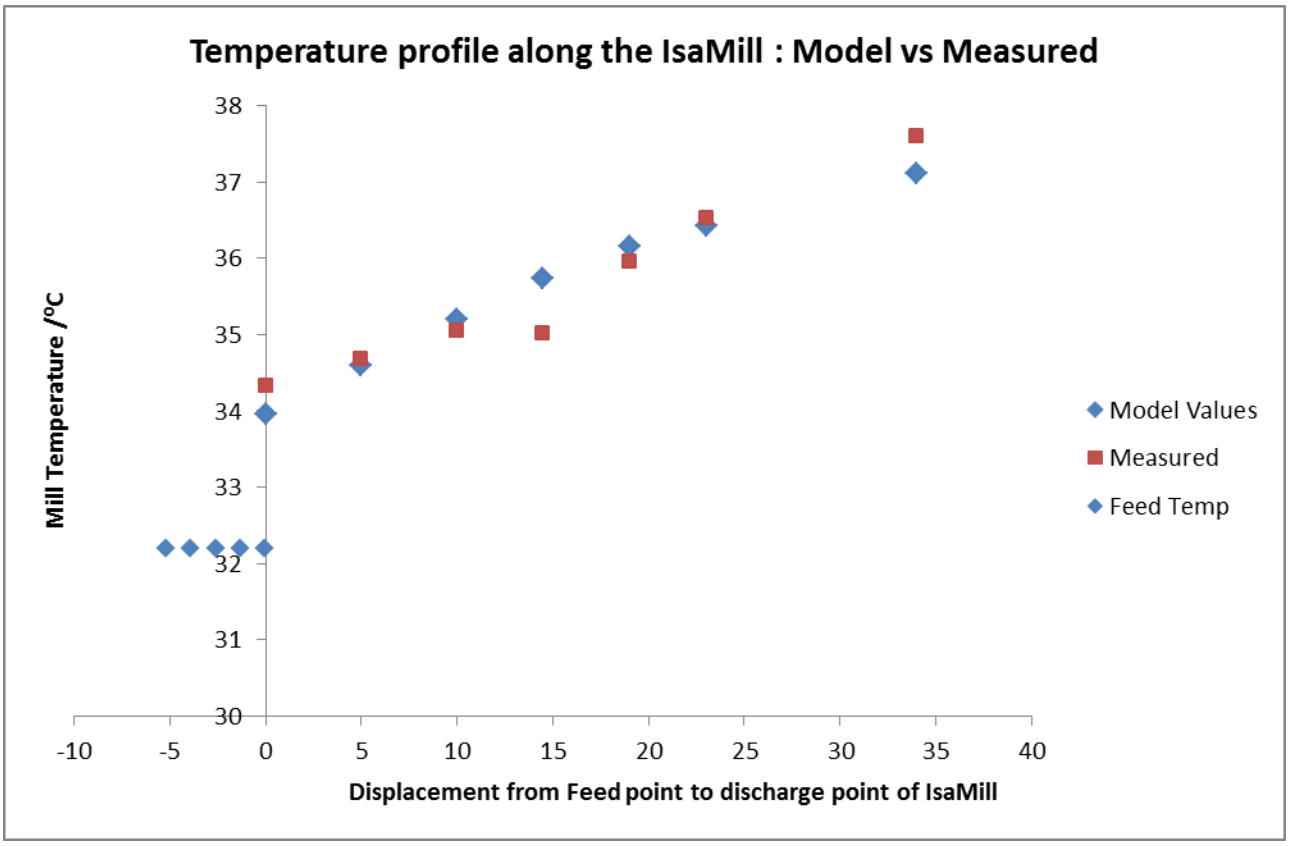

Fig B.13: Expt. 16. Model Vs Experimental results.

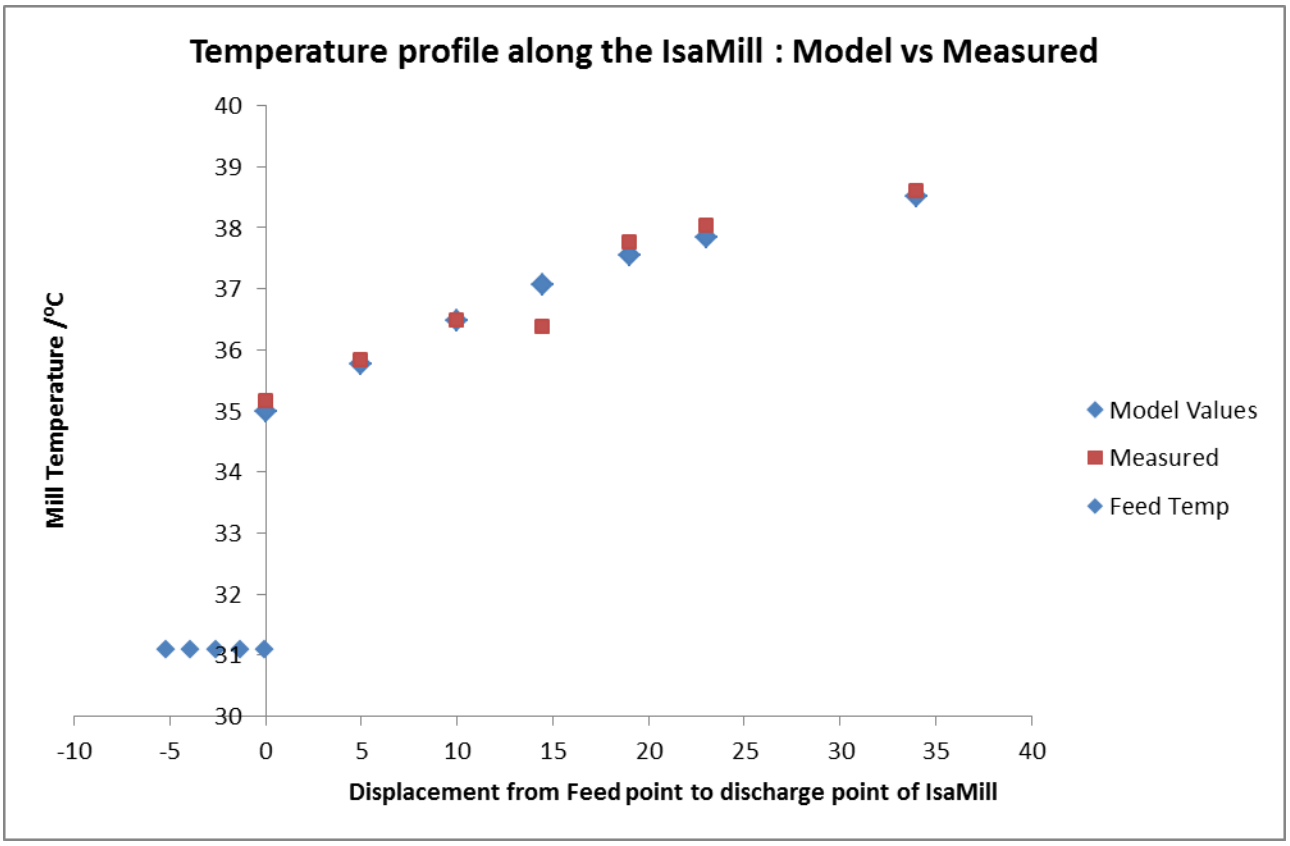

Fig B.14: Expt. 11. Model Vs Experimental results.

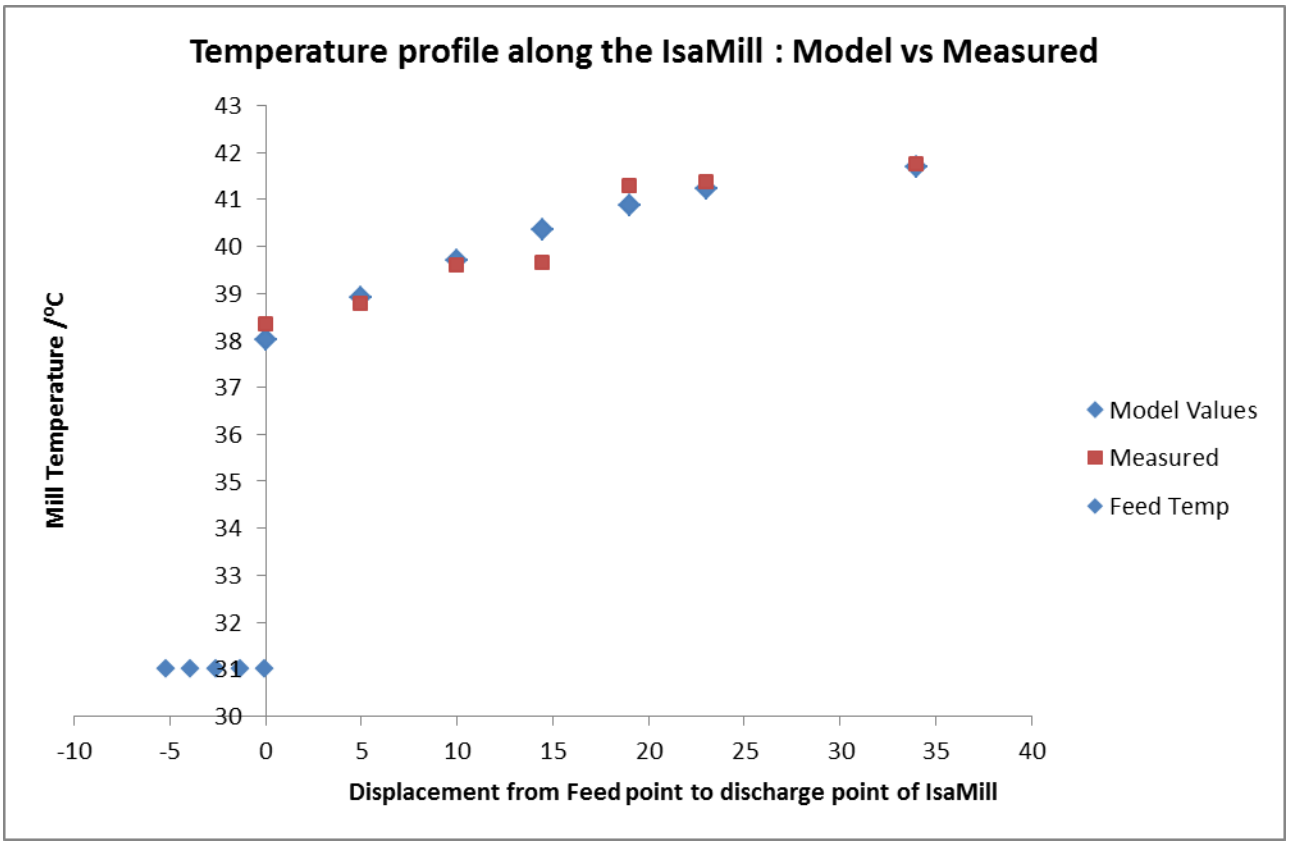

Fig B.15: Expt. 12. Model Vs Experimental results.

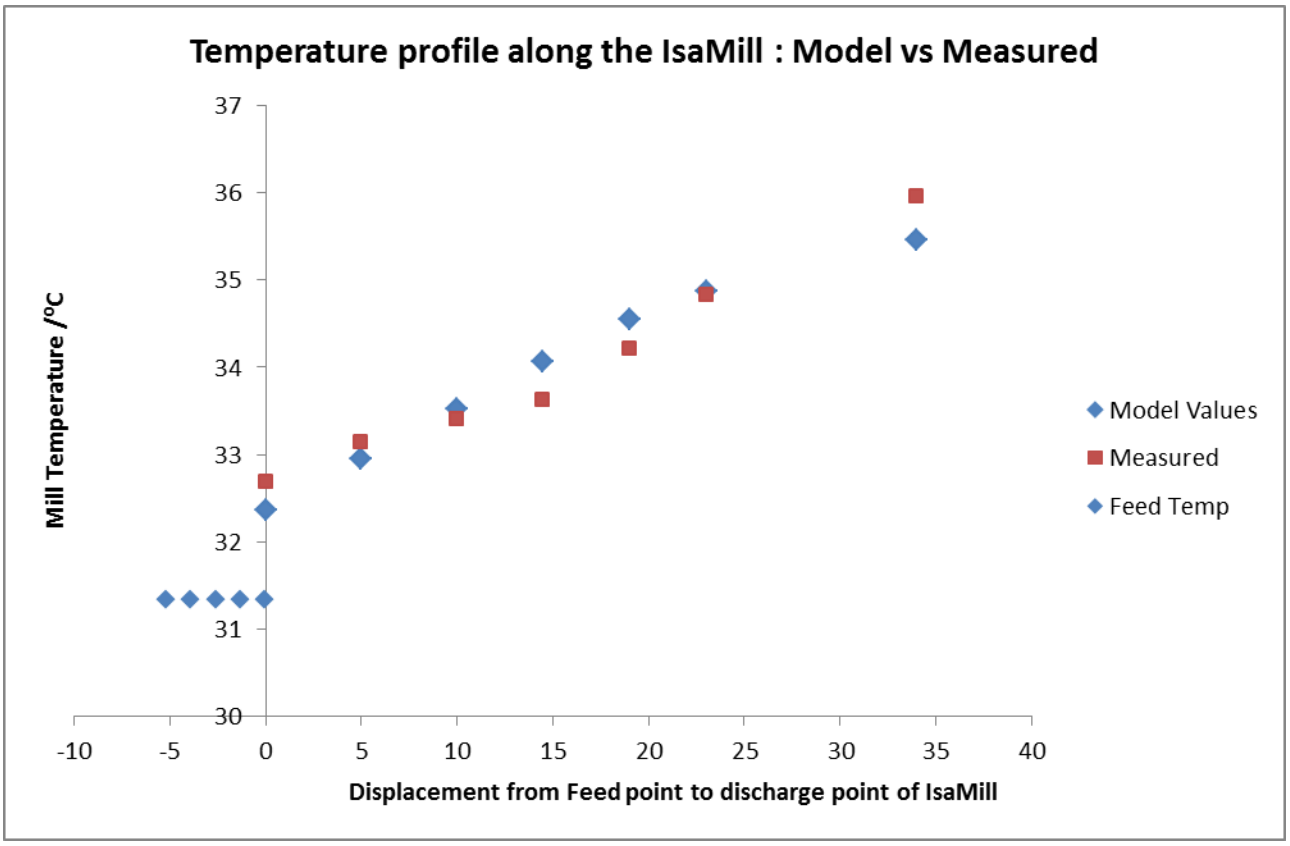

Fig B.16: Expt. 22. Model Vs Experimental results.

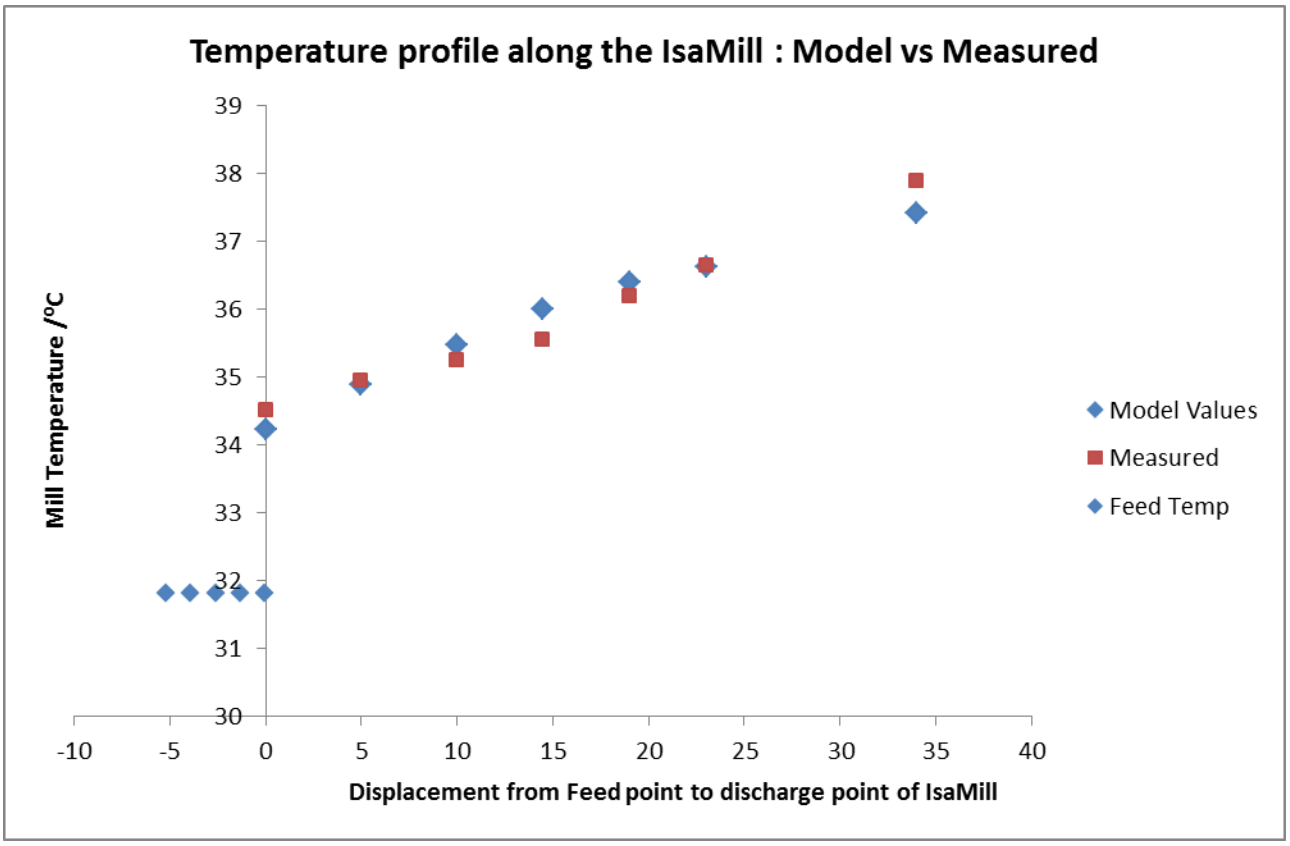

Fig B.17: Expt. 23. Model Vs Experimental results.

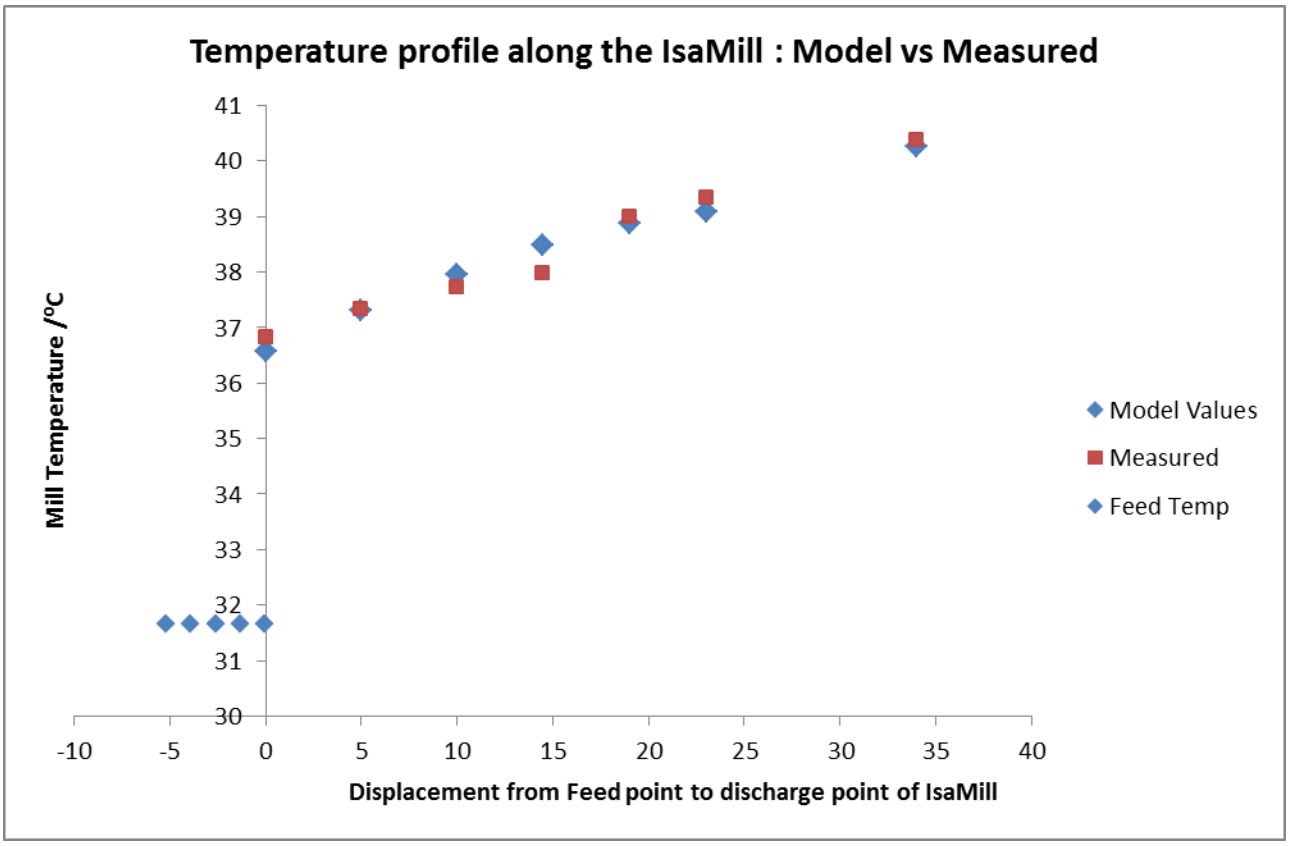

Fig B.18: Expt. 21. Model Vs Experimental results.

APPENDIX C: MODEL MATRIX INVERSION PROGRAMME

	Cp	h	A1-A6	A7	Tf	Tamb	P	Ff	α	θ	β	C
	2.95	0.0384	0.02	0.053	31.328	32	1.6	0.126	0.767	0	0.434	0

Cells in yellow to be filled in manually

Minus((1+N6)*M6*F6+G6*H6)

Equals(0.03*L6/7)-(G6*H6*K6)-M6*F6*J6-(L6/7)

B16 :H22 represents matrix **A**
I16:I22 represents column vector **x**
J16:J22 represents column vector **b**

A

	T1	T2	T3	T4	T5	T6	T7		**b**
T1	-0.65944	0.285957	0	0	0	0	0	T1	-11.92
T2	0.658673	-0.9454	0.285957	0	0	0	0	T2	-0.246
T3	0	0.658673	-0.9454	0.285957	0	0	0	T3	-0.246
T4	0	0	0.658673	-0.9454	0.286	0	0	T4	-0.246
T5	0	0	0	0.658673	-0.95	0.286	0	T5	-0.246
T6	0	0	0	0	0.659	-0.659	0	T6	-0.246
T7	0	0	0	0	0	0.3727	-0.375	T7	-0.287

{equalsMINVERSE(B16:H22)}

A'[Inverse of matrix A]

T1 =	-2.67335	-1.15826	-0.50185	-0.21746	-0.09	-0.041	0
T2 =	-2.66794	-2.67106	-1.15732	-0.50149	-0.22	-0.094	0
T3 =	-2.66266	-2.66576	-2.67022	-1.15706	-0.5	-0.217	0
T4 =	-2.65763	-2.66073	-2.66518	-2.67022	-1.16	-0.502	0
T5 =	-2.6532	-2.65629	-2.66073	-2.66576	-2.67	-1.158	0
T6 =	-2.65011	-2.6532	-2.65763	-2.66266	-2.67	-2.673	0
T7 =	-2.63572	-2.63879	-2.6432	-2.6482	-2.65	-2.659	-2.668

{equalsMMULT(B26:H32,J12:J18)}

	Tcalc	Tmeasur	ΔT^2	(Error/Ra	Displacement(cm)	
Tf	31.328	31.33	0	0	-5.2	
Tf	31.328	31.33	0	0	-3.9	
Tf	31.328	31.33	0	0	-2.6	
Tf	31.328	31.33	0	0	-1.3	cells in yellow to
Tf	31.328	31.33	0	0	-0.03	to be filled in
T1 =	32.369	32.68	0.1	-7.54	0	manually.
T2 =	32.952	33.14	0	-4.58	5	
T3 =	33.522	33.4	0	3.013	10	
T4 =	34.064	33.63	0.2	10.53	14.5	
T5 =	34.542	34.21	0.1	7.986	19	
T6 =	34.876	34.83	0	1.105	23	
T7 =	35.452	35.95	0.2	-12.1	34	
		sum	0.7	2.243		

Fig. C.1: Excel Matrix Inversion and Temperature Computations

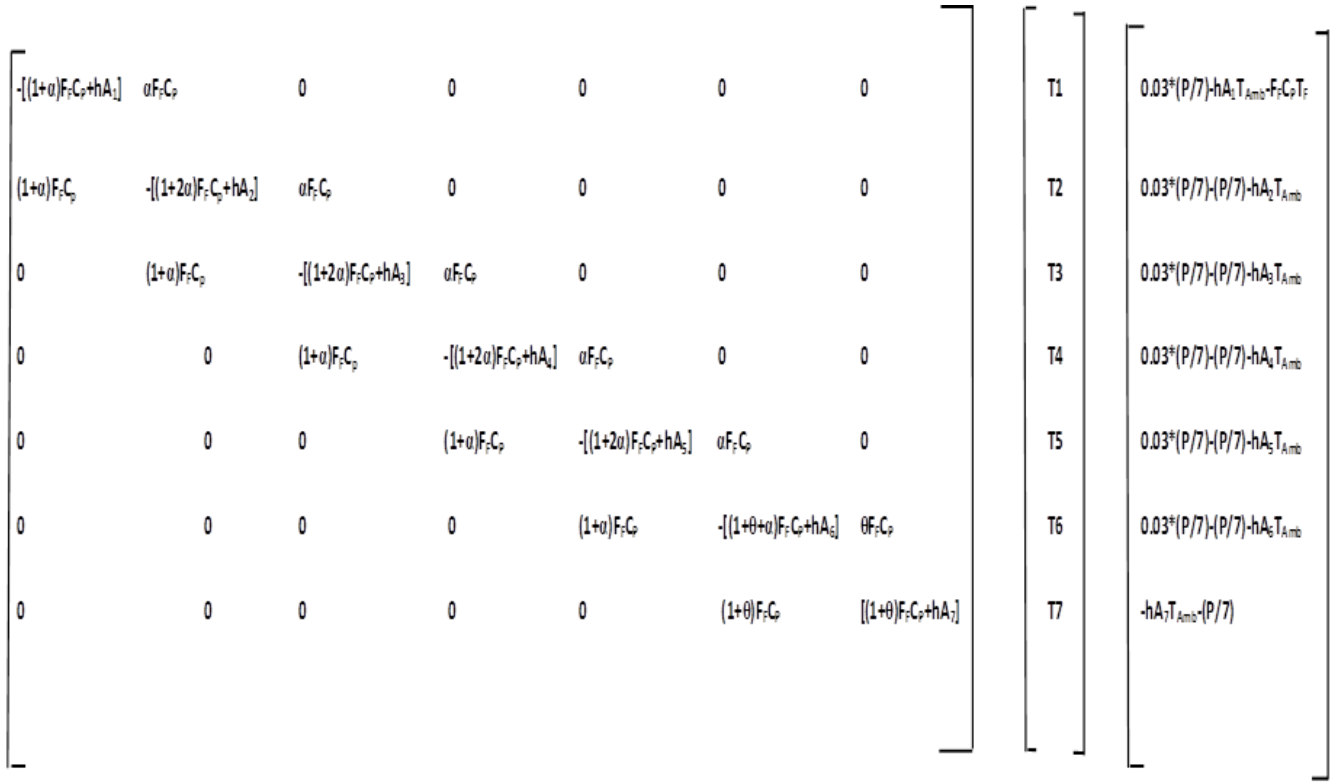

$-[(1+\alpha)F_FC_p+hA_1]$	αF_FC_p	0	0	0	0	0	T1	$0.03*(P/7)-hA_1T_{Amb}-F_FC_pT_F$
$(1+\alpha)F_FC_p$	$-[(1+2\alpha)F_FC_p+hA_2]$	αF_FC_p	0	0	0	0	T2	$0.03*(P/7)-(P/7)-hA_2T_{Amb}$
0	$(1+\alpha)F_FC_p$	$-[(1+2\alpha)F_FC_p+hA_3]$	αF_FC_p	0	0	0	T3	$0.03*(P/7)-(P/7)-hA_3T_{Amb}$
0	0	$(1+\alpha)F_FC_p$	$-[(1+2\alpha)F_FC_p+hA_4]$	αF_FC_p	0	0	T4	$0.03*(P/7)-(P/7)-hA_4T_{Amb}$
0	0	0	$(1+\alpha)F_FC_p$	$-[(1+2\alpha)F_FC_p+hA_5]$	αF_FC_p	0	T5	$0.03*(P/7)-(P/7)-hA_5T_{Amb}$
0	0	0	0	$(1+\alpha)F_FC_p$	$-[(1+\theta+\alpha)F_FC_p+hA_6]$	θF_FC_p	T6	$0.03*(P/7)-(P/7)-hA_6T_{Amb}$
0	0	0	0	0	$(1+\theta)F_FC_p$	$[(1+\theta)F_FC_p+hA_7]$	T7	$-hA_7T_{Amb}-(P/7)$

Fig 6.5 : Matrix representation of the material and energy balance equations.

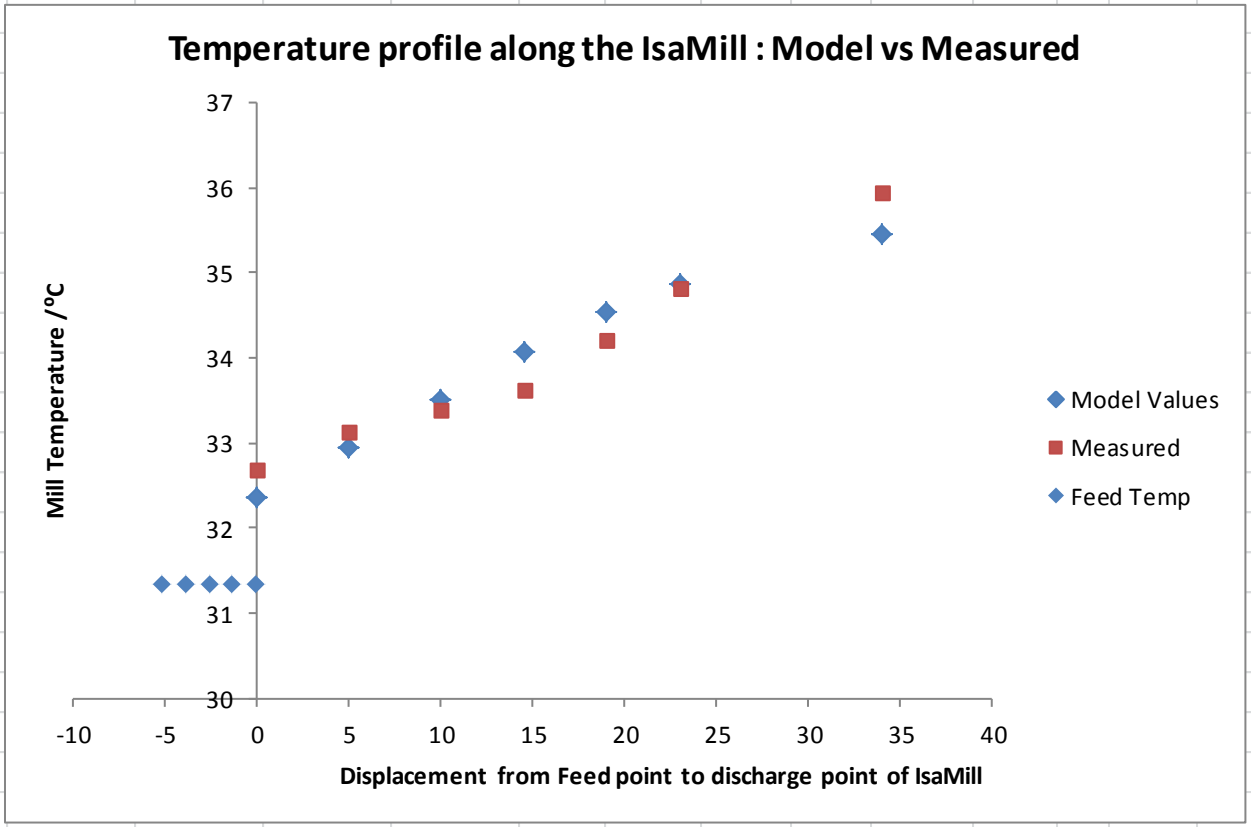

Fig. C.3 Meassured Vs Model values from excel computations